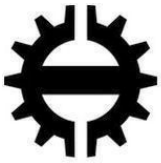

TAMPERE UNIVERSITY OF TECHNOLOGY
International Master's Degree Programme in Biomedical Engineering

ANDREI DANIEL JAKAB

DEVELOPMENT OF A PORTABLE AND EASY-TO-USE EEG SYSTEM TO BE EMPLOYED IN EMERGENCY SITUATIONS

Master of Science Thesis

Examiners: Prof. Jari Hyttinen
Dr. Pasi Kauppenen
Examiners and topic approved in the Science and Environmental Engineering Faculty Council meeting of 08.12.2010

Abstract

TAMPERE UNIVERSITY OF TECHNOLOGY
Master's Degree Programme in Biomedical Engineering
Jakab, Andrei Daniel: Development of a Portable and Easy-to-Use EEG System to be Employed in Emergency Situations
Master of Science Thesis, 115 pages, 18 Appendix pages
April 2011
Major: Medical Instrumentation
Examiners: Prof. Jari Hyttinen, Dr. Pasi Kauppinen
Keywords: electroencephalography, EEG, stat EEG, emergency medicine, measurement system, measurement software, wireless, portable device, easy-to-use, aEEG, quick-application electrode cap.

This thesis describes the development and evaluation of two portable devices intended for the recording of the electroencephalogram (EEG) in emergency situations. The topic originated from the EEG in Emergency Medicine (EEGEM) project, which seeks to develop the necessary technology and methodology that will help reduce the cost, the preparation time, and the overall complexity associated with EEG nowadays. The work contained herein builds upon the results obtained during previous Master theses that were completed in this project in order to obtain two systems that can be used in to investigate the feasibility and clinical value of EEG in emergency medicine (EM).

Before starting the work, a thorough investigation of the EEG signal, which included its origins and its diagnostic potential, was carried out. Existing instrumentation was analyzed as well as factors that influence the quality of the recording. Since the EEG is an established diagnostic tool, it was necessary to follow existing recording guidelines. The recording guidelines of the American Clinical Neurophysiology Society (ACNS) were summarized and employed in the design stages of this study. A review

of commercial EEG recorders and quick application EEG caps revealed the absence of an integrated solution for recording this signal in EM.

Two systems were developed, one that is able to measure 1 channel of EEG while the other can measure six. The 1-channel system's particularity is that it allows a person's EEG to be displayed on a standard electrocardiogram (ECG) monitor. It features a high input impedance, low noise amplifier that increases the EEG signal's amplitude in order to allow it to be displayed on an ECG monitor. The amount of amplification is dynamically adjusted depending on the peak-to-peak amplitude of the EEG signal. After every gain change, the EEG recording is temporarily interrupted and a sinusoidal signal with an amplitude equivalent to $100\,\mu$V at the current gain level is outputted. The user interface is made up of a red, green and blue (RGB) light-emitting diode (LED) unit and a capacitive button that starts/stops the recording.

The 6-channel system interfaces with a computer and consists of three parts: a wireless EEG (WEEG) recording device, a quick-application cap, and recording software that runs on a computer. The WEEG device is able to measure 6 channels of EEG and tri-axial acceleration for the identification of movement artefacts. The recorded data is transmitted to a measurement computer by means of a 2.4 GHz wireless protocol. The author worked with the group from the Department of Automation Science and Engineering (ASE) that developed the previous versions of the device in order to reduce the size of the system and to improve its integration with the measurement computer.

An initial prototype of a quick-application electrode cap for out-of-hospital measurements that can be performed by non-EEG specialists was designed by M.Sc. Salmi. It was made up of easily sterilizeable materials that were also elastic. Due to its many straps and adjustment points as well as the floating electrode leads, the band was not easy to apply. This study reports a simplified version of the cap that possesses only two attachment points and can be easily applied even with the patient in the supine position. Also, in the present version, the electrode leads are firmly attached to the cap.

The past version of the recording software, which was developed by M.Sc. Pänkälä, had only basic functionality. It displayed the EEG signals, stored them, and allowed the WEEG device to be configured and patient information to be saved. Digital low-pass filtering of the displayed data, the ability to control the vertical sensitivity as well as the time scale, automatic uploading of the recorded file, and an implementation of the aEEG algorithm were added during this thesis. Also, information about the recording can now be stored together with the recorded signals. Furthermore, the

software's usability was improved by means of a simple graphical user interface (GUI), which makes all functions easily accessible.

During the evaluation of the two prototype systems, the electrical and software performance were ascertained. In the electrical tests, the operating time of the device, the common mode rejection (CMR), the frequency response, the noise level, and the signal to noise ratio (SNR) of the two systems were measured. In order to assess the reliability of the software of the two systems, both static and functional tests were conducted.

The results obtained from the testing of the systems indicate that they offer similar performance to those offered by commercial EEG recording systems. This demonstrates that they can be used to investigate the clinical indications of EEG in EM.

Preface

The work presented in this thesis was performed at the Department of Biomedical Engineering, Tampere University of Technology (TUT), from 2008 to 2011. I would like to acknowledge the support received from the Finnish Funding Agency for Technology and Innovation (Tekes) through the EEG in emergency medicine project. Furthermore, I gratefully acknowledge the one year grant that I was awarded in 2010 by the Instrumentatium Foundation.

I owe my deepest gratitude to my supervisors, Dr. Pasi Kauppinen and Professor Jari Hyttinen, for making this Finnish adventure possible, for supporting me every step of the way, and for allowing me considerable latitude in choosing the direction of my work. Also, I am heartily thankful to Soile Lönnqvist, our wonderful department secretary, without whose help I would've surely drowned in a sea of red tape.

I would like to thank my colleagues and collaborators for their invaluable input and our stimulating discussions: Dr. Antti Kulkas, Timo Salpavaara, MSc, Ville-Pekka Seppä, MSc, Alper Cömert, MSc, Ashkan Bonabi, BSc. I would especially like to thank Dr. Ville Jäntti for inspiring me with every conversation that we have.

To my dearest friends Katrina Wendel, Piotr Mitoraj, and the whole INTO family: thank you for being there for me and keeping me afloat when times got rough. I also wish to thank Masha and her family for standing behind me over the years.

To my wonderful family: Mulţumesc pentru toate sacrificiile pe care le-aţi făcut pentru mine, darurile pe care mi le-aţi acordat, şi încrederea care o aveţi în mine. Fără voi nu aşi fi ajuns unde sunt acum. Vă iubesc!

Last but certainly not least, my amazing Ags. I am at a loss for words trying to describe the influence you've had on me. Hence, I offer this quote to you: "Oboje sa przekonani, że połaczyło ich uczucie nagłe. Piekna jest taka pewność, ale niepewność jest piekniejsza."

Andrei Daniel Jakab
Tampere, Finland, March 2011

Contents

Acronyms and Symbols

3D	three dimensional
AA	anti-aliasing
abEEG	abbreviated EEG
ABS	acrylonitrile butadiene styrene
aEEG	amplitude integrated EEG
ACNS	American Clinical Neurophysiology Society
ADC	analog-to-digital converter
Ag/AgCl	silver-silver chloride
ANC	adaptive noise canceller
AR	autoregressive
ASIC	application-specific integrated circuit
BDF	BioSemi data format
BIS	bispectral index
BP	bandpass
BR	bandreject
BTH	behind-the-head
CF	CompactFlash
CFM	cerebral function monitor
CIU	computer interface unit
CMR	common-mode rejection
CMRR	common-mode rejection ratio
CPU	central processing unit
DAC	digital-to-analog converter
dB	decibels
DC	direct current
ECG	electrocardiogram
EDF	European data format
EFE	EDF File Editor

EEG	electroencephalogram
EEGEM	EEG in Emergency Medicine
EEPROM	electronically erasable programmable read-only memory
EM	emergency medicine
emEEG	emergency EEG
EMG	electromyography
EMI	electromagnetic interference
EMT	emergency medical technician
EOG	electrooculogram
ER	emergency room
FEM	finite element modeling
FDA	Food and Drug Administration
FIR	finite impulse response
FSM	finite-state machine
GDF	general data format for biosignals
GDT	gas-discharge tube
GUI	graphical user interface
HDD	hard disk drive
HP	high-pass
HR	heart rate
IA	instrumentation amplifier
IC	integrated circuit
ICU	intensive care unit
ICT	Instrument Control Toolbox
IDE	integrated development environment
IFCN	International Federation of Clinical Neurophysiology
ISM	industrial, scientific and medical
I/O	input/output
I^2C	Inter-Integrated Circuit
JTAG	Joint Test Action Group
LCD	liquid crystal display
LED	light-emitting diode
LP	low-pass
LSB	least significant bit
MFB	multiple-feedback
MCU	microcontroller

Mini PCIe	PCI Express Mini
NCSE	nonconvulsive status epilepticus
OR	operating room
OS	operating system
OTH	over-the-head
PC	personal computer
PCB	printed circuit board
PCM	protection circuit module
PGA	programmable gain amplifier
PMU	portable measurement unit
PP	peak-to-peak
PSG	polysomnography
PTT	pulse transit time
PWM	pulse-width modulation
qEEG	quantitative EEG
RAM	random access memory
RGB	red, green and blue
RMS	root mean square
SAR	successive approximation
SNR	signal-to-noise ratios
SPI	Serial Peripheral Interface
SpO_2	oxygen saturation level
SRAM	static random access memory
SSH	Secure Shell
stEEG	stat EEG
TI	Texas Instruments
USART	universal asynchronous receiver/transmitter
USB	Universal Serial Bus
VGA	variable gain amplifier
WEEG	wireless EEG
WLAN	wireless local area network
UDP	User Datagram Protocol
XML	Extensible Markup Language

A_{CM}	common-mode gain
A_D	differential-mode gain

f_c	cut-off frequency

List of Figures

List of Tables

Chapter 1

Introduction

The human brain is a highly complex and delicate organ. Although it is protected by many evolutionary defenses, it is highly susceptible to many types of damages and diseases. No matter what the underlying etiology is, brain disorders need to be detected as quickly as possible to limit the amount of permanent damage and to increase the chances of the patient making a full recovery.

The electroencephalogram (EEG) is the most common diagnostic procedure used to study the function and the activity of the brain and consists of the recording of the electrical activity of the brain. It can help a physician distinguish among different types of unconsciousness and it is unmatched as a diagnostic tool for the detection of nonconvulsive status epilepticus (NCSE), which is a life-threatening situation that is under-diagnosed due to its subtle symptoms [1]. The EEG has also been applied to the investigation of strokes, head trauma, and intracranial haemorrhages [2, 3].

Despite the existence of abundant literature that discusses the indications and usefulness for the application of EEG in the emergency department [2, 4, 5, 6, 7, 8, 9], this diagnostic method remains underused in this setting [1]. In order to obtain a quality recording, an experienced nurse must apply the measurement electrodes, a process that can take up to one hour. Once the signals are recorded, only a trained neurophysiologist can interpret the data, as an unprocessed EEG is unintelligible to the untrained eye. These reasons together with the lack of standards regarding how and when the EEG should be employed in emergency situations restrict the use of this valuable tool. Furthermore, many small emergency centers do not possess any type of EEG recording capabilities since the required investment in infrastructure and training is deemed to be unjustified. This situation is in stark contrast to the electrocardiogram (ECG). Nowadays, ECG monitors can be found in medical centers large and small as well as in ambulances. Moreover, the signal can be easily interpreted not only by

doctors but also by nurses and emergency medical technicians (EMTs).

1.1 The "EEG in Emergency Medicine" Project

This thesis is a part of the EEG in emergency medicine (EEGEM) project, whose aim is to develop the necessary technology and methodology that will help reduce the cost, the preparation time and the overall complexity associated with EEG nowadays. In turn, this will make it possible for any medical unit in the world to harness the diagnostic power of the EEG in emergency situations. Although many portable EEG recording systems are available commercially, they are intended for long-term ambulatory monitoring and thus are not suitable for emergency use since they share many of the shortcomings of traditional recorders (see chapter 2).

Two avenues of research are currently being pursued in the EEGEM project: the first is centered on the novel concept of allowing the EEG to be recorded using the same infrastructure that is currently used for the recording of the ECG; the second explores the suitability of a 6-channel wireless recording system that interfaces with a portable computer.

The main objective of this work was to build on the results obtained so far in this project so as to obtain two EEG systems that can be used to investigate the feasibility and clinical value of EEG in emergency medicine. Hence, the systems must be portable, lightweight, and user friendly while at the same remaining rugged enough to survive the rigors of hospital- and ambulance-use. Furthermore, the preparation time of both systems should be minimal so that the recording of the EEG can be started quickly. A secondary objective was to investigate the amplitude integrated EEG (aEEG), a signal processing method that could facilitate the analysis of the recorded EEG data by compressing hours worth of EEG into a signal that can be displayed on a single screen.

The work carried out for this thesis was multifaceted and extensive. First, the shortcomings of the previous adapter version were investigated and a new electronics board was designed. The Altium Designer software package was used for designing the circuit and creating the printed circuit board (PCB). Second, the components of the 6-channel system, i.e., the recording software, the quick-application cap, the and wireless EEG (WEEG) device, were analyzed and improved. Many features were added to the recording software to increase its usefulness, including an implementation of the aEEG algorithm. With the help of a seamstress, the quick-application cap was redesigned to make it more versatile and easier to apply. Also, a smaller WEEG device was created

in collaboration with the Department of Automation Science and Engineering. The final step of the work consisted of testing both systems in the electronics laboratory of the department, first with an oscilloscope and a signal generator, and then with the department's Neuroscan EEG monitor.

1.2 Thesis Overview

The remainder of the thesis is organized in the following way. Chapter 2 presents background information about the EEG, including clinical uses as well as recording principles and guidelines. The aEEG algorithm is also described and a number of commercial EEG recorders are introduced. Chapter 3 covers the design of the new 1-channel EEG-to-ECG adapter and the upgrades that were made to the components of the 6-channel system. The measurement electrode selection, the implementation of the aEEG algorithm, and the testing methodology that was used to evaluate the performance of both systems are also explained. In chapter 4 the results of the work are shown while chapter 5 compares them to the goals set out at the beginning of the project and also to the commercial alternatives presented in the background chapter. Afterward, future avenues of research are suggested. The last chapter summarizes the work that has been accomplished.

Chapter 2

Theoretical Background

2.1 Introduction

Chapter two provides an overview of the background knowledge that was required for the successful completion of this thesis. Section 2.2 introduces the electroencephalogram (EEG) and its use in medicine. An overview of the technical requirements and challenges associated with the recording of the EEG is provided in section 2.3. Section 2.4 briefly summarizes two ACNS guidelines regarding EEG recordings. Section 2.5 presents the aEEG algorithm, which allows the time- and amplitude-compression of an EEG signal. Finally, a number of commercial products are reviewed in section 2.6.

2.2 EEG Overview

The electrical activity of the brain, also known as "brain waves" in common language, was first recorded in 1924 by Hans Berger, who named this type of recording the electroencephalogram. [10]

The origin of the EEG lies at the neuronal level. More precisely, the sources of the electrical activity that is measured as EEG are ionic currents generated by biochemical sources at the cellular level. In the case of EEG recorded from the scalp, it is believed that almost all of the activity stems from the postsynaptic potentials of a large number of synchronously activated pyramidal neurons. There are two reasons why EEG signals are believed to consist only of postsynaptic potentials and not any other membrane potentials such as action potentials. First, the membrane potential variation created by action potentials is small and is only present over a small section of the membrane at any one time. On the other hand, a postsynaptic potential extends over a larger portion of the membrane and as a result generates a larger potential.

Second, since action potentials have a short duration, they tend to overlap less, as opposed to postsynaptic potentials that can last between 10 and 250 ms. [11]

The neuronal population believed to be most responsible for the signal that is recorded as scalp EEG are pyramidal neurons. These types of neurons are located in layers IV and V of the cerebral cortex and are the most common type of neuronal cell present in the cortex [12]. When a number of pyramidal neurons are simultaneously activated, extracellular currents will flow in proximity to their dendrites. The longitudinal components of these currents will add while the transverse components will tend to cancel out [11]. Since the apical dendrites of these neurons are long and perpendicular to the cortex, the longitudinal components of the extracellular current create electrical dipoles between the dendrite and the soma. It is these electrical dipoles that create the signal which is recorded as scalp EEG.

In humans, the amplitudes of the scalp EEG lie mostly in the 10–100 μV range. However, for adults, the range is usually reduced to 10–50 μV [13]. It is important to note that EEG amplitudes are normally measured from peak to peak [13]. In the frequency domain, it is possible to differentiate among α-, β-, δ- and θ-waves. Time-domain examples of these waves together with their associated frequency bands and the anatomical region where they are best recorded are shown in Figure 2.1.

In traditional EEG recordings, the delta wave is the slowest type of brain wave activity with a frequency range of 0.5–4 Hz[1]. This type of activity is normal in the EEG of infants and of sleeping adults. It is believed that delta waves originate solely within the cortex and do not depend on any activity in the deeper brain regions. Theta waves, which are located in the 4–8 Hz range, play a dominant role in the childhood but are present only in small amounts in the EEG of adults, usually when the subject is drowsy or sleeping. The designation "theta" alludes to the brain wave's possible thalamic origin. Alpha waves have a frequency band of 8–13 Hz. This type of activity is best recorded occipitally when the subject is awake, relaxing, and has their eyes closed. This rhythm can be temporarily blocked by mental activities, or by opening one's eyes. Contrary to the outdated theory which stated that thalamocortical feedback loops are responsible for generating the alpha rhythm, it is now believed that the cortex is the sole source of this rhythm. The fourth and final of the normal rhythms is the beta rhythm. Its designated frequency range is from 13 until 30 Hz and can be recorded mainly over the frontal, parietal and central regions of the head. This rhythm is present in the EEG of nearly all healthy adults and is associated with intense mental activity and tension. [14]

[1] In full-band EEG recordings, the slowest components are DC-level changes.

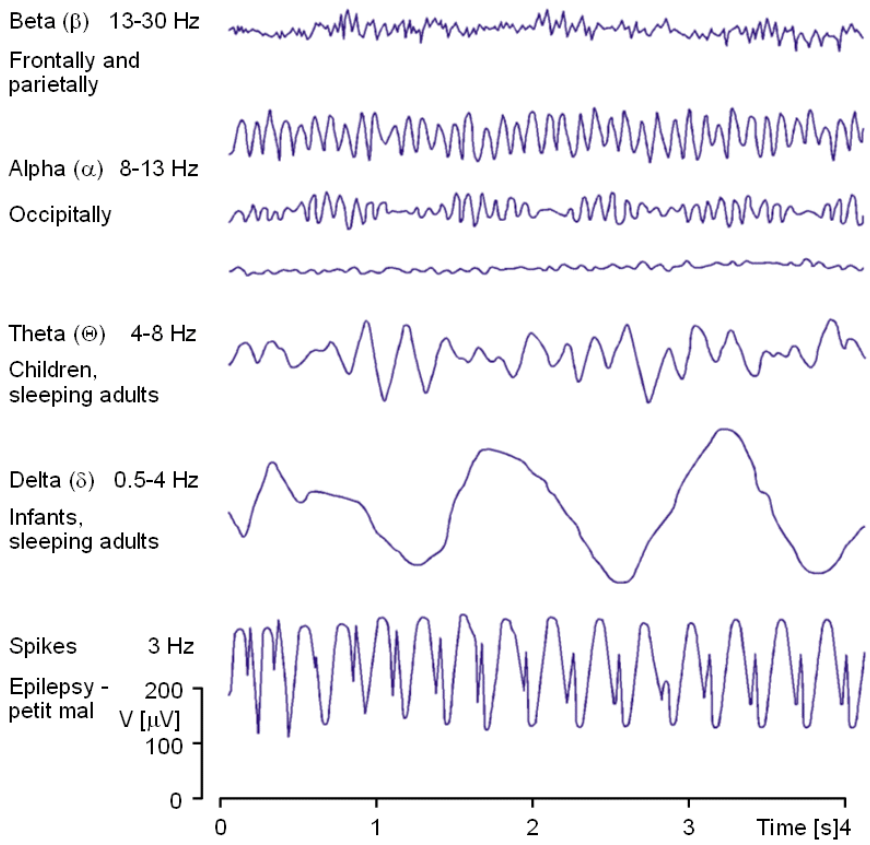

Figure 2.1: EEG wave examples. *Reproduced from* [10].

2.2.1 EEG as a Diagnostic Tool

Even though modern neuroimaging techniques have reduced the clinical indications associated with it [15], due to its relatively low cost, short examination time, lack of risk and personnel requirements [16], the EEG continues to be one of the most commonly used tests for the clinical evaluation of neurologic disorders [17]. It can be used to make a diagnosis, contribute to an already established diagnosis, or rule-out a diagnosis [18]. Furthermore, the EEG is useful for determining the severity of the disorder and in predicting the outcome, especially in cases where the etiology is known [17].

The EEG is an important test in the assessment of patients with altered mental states and coma [17]. This is especially true in cases where an imaging examination would be normal, e.g., exogen intoxication [16]. In comatose patients, the EEG can help distinguish among different forms and depths of coma [1]; increasingly, the EEG is being used to help diagnose cerebral death in patients with irreversible comas, particularly when the organs can be salvaged for transplantation [17].

Another important area of application of EEGs is in the detection and evaluation

of epilepsy, which is a group of related disorders whose common characteristic is the increased probability of recurrent seizures [19]. The power of EEG in this application lies in the fact that in a high proportion of patients, the EEG presents specific changes both during a clinical seizure but also in the period of time between seizures [17]. An epileptic condition for which the EEG it is unmatched as a diagnostic tool is the detection of nonconvulsive status epilepticus (NCSE), which is a life-threatening situation that is under-diagnosed due to its subtle symptoms [1].

A further application of the EEG is in the detection of encephalopathies, which are disturbances, either temporary or permanent, of the normal functioning of the brain. In particular, the EEG is decisive for the diagnosis, prognosis and therapy monitoring of hepatic encephalopathy [16]. While it is impossible to distinguish between the different types of encephalopathies using this test, the severity of the EEG changes, the severity of the encephalopathy, and the clinical state of patient are correlated [17].

Finally, the EEG is valuable for the diagnosis of strokes, head trauma, and intracranial haemorrhages [2, 3, 20].

2.2.2 Current Use and Protocols in Emergency Medicine

Currently, continuous EEG monitoring from the site of the emergency until and including the emergency room (ER) does not exist. Instead, upon the patient's arrival in the ER, assuming that the receiving facility possesses the necessary equipment and staff, the attending physician can request an emergency EEG (emEEG), also known as a stat EEG (stEEG) [8], which usually lasts 20 minutes. Another option is to perform an abbreviated EEG (abEEG), where the patient's EEG is measured for a short amount of time, e.g., 5 minutes [1].

There are three main problems with the aforementioned approach. In some institutions, only neurologist can approve emEEGs [21], while in others, the emEEG measurement must be performed in the laboratory of neurophysiology [16]. Furthermore, in order to obtain a quality recording, an experienced nurse or technician must apply the measurement electrodes, a process that can take from minutes up to 1 hour [22]. Once the signals are recorded, only a trained neurophysiologist can interpret the data, as an unprocessed EEG is nearly impossible to understand by untrained personnel. All of these delays contribute to the fact that the mean response time from approval to the interpretation of the emEEG is roughly 3 hours in the USA [21]. Such a long delay is clearly unacceptable given that a patient's prognosis deteriorates with time, e.g., the mortality rate of untreated NCSE increases by 1–2% per hour [23].

The second problem pertains to the length of the emEEG recording. It is widely

agreed upon that the EEG must be recorded for 24 h in order to detect seizures in noncomatose patients, with longer periods (48 h) being required for comatose patients [18]. Hence, a 20 minute recording cannot be assumed to be completely indicative of the patient's true condition [24]. While recording the EEG for 24 to 48 h is impossible in an emergency situation, starting the recording of the EEG as soon as the patient is picked up by the paramedics would provide the attending physician with valuable additional data. Also, continuing the recording for days would allow the physician to analyze trends and slow changes that can help with determining the patient's prognosis.

Finally, two common situations are possible in facilities that offer the possibility to perform emEEG 24 h/day. Either this service may remain underused in the emergency setting [1], or it may be abused, e.g., by ordering emEEGs as a prerequisite to discharging a patient [8]. Both of these situations have one root cause: there is a lack of literature and guidelines available that describe the appropriate use of EEG in an emergency setting [1, 8]. While in France there has been an effort to compile such a set of guidelines [25, 20, 4], a global consensus on the use of the EEG in the ER has yet to emerge. In the United States, Dr. Kenneth Jordan, who for many years has advocated the importance of electrophysiological monitoring after acute brain injuries, suggests that emEEG is valuable for the detection of the following conditions: general slowing due to intoxication, concussions or encephalitis; seizures; asymmetries, which are caused by brain damage due to vascular accidents, concussions, etc. [26, 23].

2.3 Recording Principles

Bioelectric signals are challenging to record owing to their small amplitudes, high source impedances and the relatively high-amplitude noise sources that are usually superimposed on the signal. Amplifiers that have been specially designed in order to amplify such signals are called biopotential amplifiers, or bioamplifiers. The general characteristics of a biopotential amplifier are discussed in section 2.3.1 while the building blocks of an EEG bioamplifer are described in section 2.3.2. Finally, some factors that can negatively affect the recording of an EEG signal are detailed in section 2.3.3.

2.3.1 Biopotential Amplifier Characteristics

Similarly to other types of amplifiers, bioamplifiers have long lists of characteristics and specifications. However, the following seven attributes are considered to be the most important ones for typical medical applications [27].

Gain. Due to their very small amplitude (1 μV – 100 mV), bioelectric signals must be amplified so that they can be interfaced with recorders, converters, displays, etc. Hence, large gains on the order of 1000 or greater are common in bioamplifiers [28]. It is typical for the bioamplifier's gain to be expressed in decibels (dB). The amplifier's voltage gain can be translated into decibel form by means of the following formula:

$$\text{Gain(dB)} = 20 \log_{10}(\text{Voltage Gain}) \tag{2.1}$$

Frequency response. Bioelectric signals usually have a limited bandwidth and therefore bioamplifiers should only amplify the frequencies associated with the bioelectric signal of interest without attenuation while rejecting components outside of the signal's typical bandwidth [29]. The amplifier's bandwidth is defined as the difference between the upper cutoff frequency f_H and the lower cutoff frequency f_L, which are also known as the half power points. At the cutoff frequencies, the amplifier's gain has decreased to 70.7 % of the passband gain. If the gain response of the amplifier is normalized to the passband gain, these points are also known as the -3 dB points, since $20 \log_{10}(\frac{70.7}{100}) = -3$ dB.

Common-mode rejection. Typical bioamplifiers are differential, which means that only differential signals, i.e., signals that appear between the two inputs, are amplified while common mode signals that appear at both inputs are attenuated [29]. Power line interference is the most common source of common mode noise in bioelectric recordings and therefore a strong rejection of common mode signals is a fundamental property of biopotential amplifiers [30]. The common-mode rejection ratio (CMRR) of a bioamplifier is defined as the ratio of the differential gain A_D over the common-mode gain A_{CM} and is an indication of the amplifier's capability of rejecting common-mode signals. The common-mode rejection (CMR) is the CMRR expressed in decibels:

$$\text{CMR(dB)} = 20 \log_{10}(\text{CMRR}) = 20 \log_{10}(\frac{A_D}{A_{CM}}) \tag{2.2}$$

Input impedance. A bioamplifier must have a sufficiently large input impedance so that the measured bioelectric signal is not attenuated due to the potential divider created by the amplifier's input impedance and the potentially large impedance of the electrode-skin interface. It can be shown that the relative drop in recorded signal amplitude caused by the electrode impedances is given by $(Z_1 + Z_2)/(Z_{in} + Z_1 + Z_2)$, where Z_{in} = input impedance of the differential amplifier, Z_1 = impedance of electrode 1, Z_2 = impedance of electrode 2 [31].

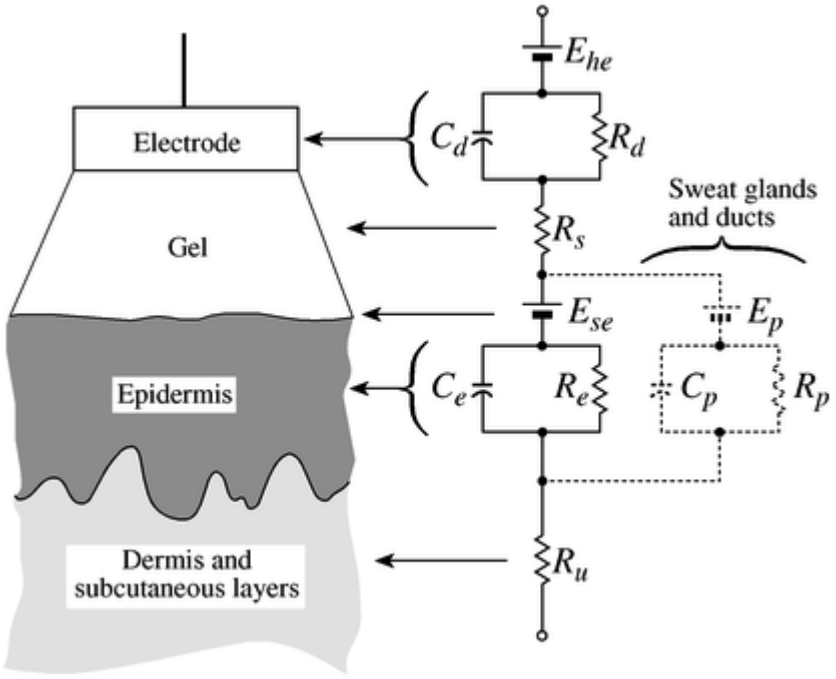

Figure 2.2: Electrode-tissue interface. E_{he}: electrode half-cell potential, E_{se}: skin potential. *Reproduced from* [33].

To illustrate this issue, an electronic model of the electrode-tissue interface is presented in Figure 2.2. While the impedance of the electrode, the gel and the dermis are relatively small, the impedance of the epidermis may have values from kilohms to hundreds of kilohms depending on scalp condition and preparation as well as the amount and quality of electrode paste [32]. Nevertheless, this problem can be easily overcome nowadays since modern amplifiers have very large input impedances. For example, assuming that the bioamplifier has an input impedance of 10 MΩ and the impedance of the two electrodes is equal to 50 kΩ, the measured signal will only be attenuated by approximately 1%.

Noise and drift. Noise and drift are unwanted signal components introduced into the biopotential signal by the biomplifier's electronics. Noise is defined as undesirable components above 0.1 Hz while drift refers to components below the aforementioned frequency, i.e., slow baseline changes. [27]

Noise can either be expressed numerically in microvolts peak to peak ($\mu V_{p\text{-}p}$), or microvolts root mean square (RMS) over a given frequency band, or displayed graphically as noise density graphs, where the noise power density is plotted as a function of frequency. Due to its low frequency, drift is typically expressed as a peak-to-peak (PP) value. [27]

Recovery. Certain transient signals such as large electrode offset voltages and defibrillation pulses cause the bioamplifier to go into saturation and stop operating normally. After the end of the saturating signal, the bioamplifier will remain in saturation for a finite amount of time, after which it will drift back to its original baseline. The time that it takes for the bioamplifier to return to normal operation after the end of the transient is termed the recovery time. [27]

Effect of electrode polarization. When an electrode is placed in contact with skin, a galvanic half-cell is created at the electrode/electrolyte interface due to the ion-electron exchange that takes place [34]. Since similar electrodes at separate locations will develop slightly different half-cell potentials, the difference of the two potentials will generate a differential DC signal at the input of the bioamplifier [27]. Moreover, this offset voltage usually varies slowly over time resulting in a low-frequency drift [34]. Hence, the front end of a biopotential amplifier must be designed to withstand a certain amount of electrode-offset voltage, usually by keeping the gain low and stable; otherwise, this noise signal will saturate the bioamplifier and thus obstruct the measurement of the desired bioelectric signals.

2.3.2 EEG Bioamplifier Structure and Properties

Although various EEG devices have different internal structures depending on their intended usage, the front end that couples to the patient consists of the same basic building blocks. The structure of a typical EEG recording channel is presented in Figure 2.3. The functions and properties of each block are expanded upon in the following paragraphs.

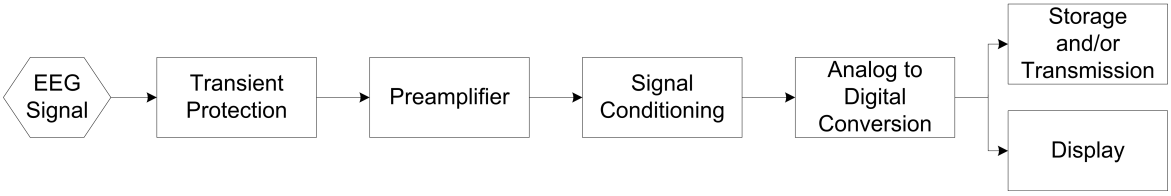

Figure 2.3: Schematic design of the main stages of a typical EEG recording channel.

EEG signal. The EEG is recorded from the scalp by means of bioelectrodes, which act as transducers that convert the ionic currents in the body into electronic current that can be recorded by the bioamplifiers. Ideally, the electrode impedances should

be less than 10 kΩ in order to ensure that a quality signal is recorded. This is especially difficult to achieve on the scalp due to the presence of hair, which also impedes the stable attachment of the electrode. Methods of overcoming these two challenges include the use of conductive electrode paste, which lowers the impedance and also helps with the adherence of the electrodes, the immobilization of the electrodes by means of gauze and contact cement, the slight abrasion of the scalp and the taping of measurement leads to the subject. It is considered good practice to measure electrode impedance prior to the start of a measurement since high electrode impedances can cause distortions that can be indistinguishable from the EEG signal. [12]

Transient protection. High-voltage transients such as those created by defibrillators can permanently damage the electronics of a bioamplifier unless its inputs are adequately protected. Voltage-limiting devices connected between each input and the power rails, as shown in Figure 2.4, ensure that the voltage at the preamplifier's inputs does not exceed a pre-defined threshold V_T. At input voltages below V_T, such a device conducts very little current and therefore appears as an open circuit. Once the voltage drop across it exceeds V_T, the device start conducting enough current such that the voltage drop across the resistor R maintains the input voltage below V_T. [29]

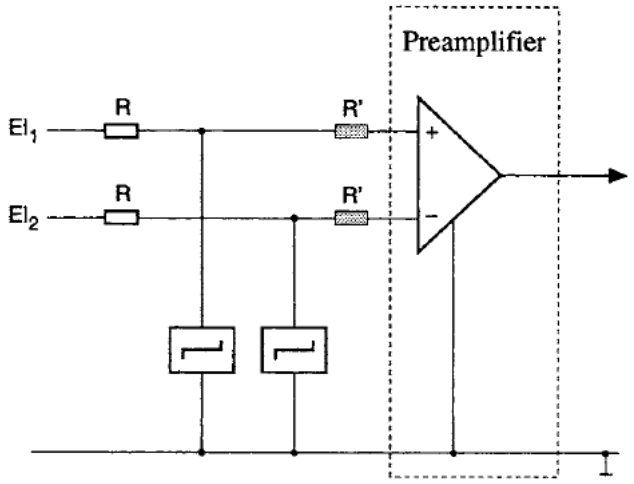

Figure 2.4: Protection of the amplifier input against high-voltage transients. *Reproduced from* [29].

Three types of protection circuits are commonly employed: silicon diodes, back-to-back Zener diodes, and gas-discharge tubes. Silicon diodes limit the input voltage to that of their forward voltage drop, which is usually about 600 mV. However, because of the slow transition from non-conducting to conducting state, input signal distortions are possible starting at approximately 300 mV. Although the PP amplitude of scalp

EEG never reaches this level, it is possible that the electrode offset causes a shift of this magnitude in the input voltage. A higher threshold voltage can be obtained by employing two Zener diodes connected back to back. Such a configuration possesses a break-down voltage in the 3–20 V range and a voltage-current characteristic that is sharper than that of the silicon diodes. [28]

The preferred transient protection device in bioamplifiers is the gas-discharge tube (GDT). Prior to reaching its breakdown voltage, which is typically in the 50–90 V range, the resistance of such a device is practically infinite. Once the tube switches to the conducting state, it will maintain a voltage across it that is a few volts less than its breakdown voltage. Although this level is still too high for most electronic devices, the input voltage can be further decreased by placing resistor in series with the amplifier's inputs, as indicated in Figure 2.4 by resistors R'. Miniature neon lamp GDTs are favored in biomedical applications due to their low price and symmetric characteristic. [28]

Preamplifier. The preamplifier is crucial to the quality of the acquired signal since it must amplify the low EEG signal while rejecting common mode noise, usually in the presence of electrode polarization overpotentials. As discussed in section 2.3.1, the preamplifier must have extremely high input impedance ($> 10\,\mathrm{M}\Omega$), high CMR (≥ 80 dB), as well as a low (≈ 10), accurate and stable gain [31]. Due to these reasons, an instrumentation amplifier (IA) is often the fundamental element of the preamplifier block since an IA possesses all of the before-mentioned properties and is particularly well suited for amplifying low-level signals with large common-mode components [35].

Signal conditioning. In this block, the preamplified signal is band limited and further amplified so that it can be used by subsequent blocks. First, the electrode half-cell potentials, which limited the gain of the preamplifier stage, are removed by means of a high-pass (HP) filter with a long time constant. Typical time constant values are 0.1, 0.3, 1 and 3 sec, which correspond to cut-off frequencies of 5, 1.6, 0.5, 0.16 and 0.05 Hz [31].

Then, the EEG signal is amplified so as to bring the signal magnitude into the range of volts. Practically, this means that the overall gain of a typical EEG systems is 10000–20000. In some systems, the amplification circuitry consists of a variable gain amplifier (VGA) or a programmable gain amplifier (PGA), both of which allow the gain of the system to be adjusted, either manually or automatically, based on the characteristics of the input signal so as to make the best use of the dynamic range of

the analog to digital converter (ADC).

The last part of this block is a low-pass (LP) filter. This step serves the double purpose of reducing the noise components outside the bandwidth of interest, therefore reducing aliasing during the sampling step, and of reducing the noise-bandwidth of the system. Although most of the information content lies in the frequency bands below 40 Hz [12], typical EEG bioamplifiers have an upper cut-off frequency of 100 Hz [28].

Analog to digital conversion. The ADC transforms the analog EEG signal into a digital form by sampling and quantizing it. Sampling is the process of converting the continuous-time signal into a discrete-time version, which consists of data samples taken at discrete sampling intervals, but with continuous amplitude values [36]. In systems with a fixed sampling frequency, in order to ensure that the sampled signal is an accurate representation of the continuous-time version, the minimum sampling frequency f_s must satisfy the Shanon-Nyquist theorem:

$$f_s \geq 2 \times f_h \tag{2.3}$$

where f_h = highest frequency component occurring in the signal [Hz]. If a signal component with frequency $f > f_s$ exists in the signal to be sampled, it will create a spurious component in the discrete-time signal with frequency $f_s - (f - f_s)$, a phenomenon which is known as aliasing [31]. As mentioned previously, one of the purposes of the LP filter located in the signal conditioning block is to significantly attenuate high-frequency component so as to prevent aliasing. In this case, the LP filter is also known as an anti-aliasing filter.

Due to the slow roll-off of analog filters and the variability of filter characteristic caused by component variations, it is usually preferable to keep the analog bandwidth large and sample the signal with a higher frequency than required by the Shanon-Nyquist theorem. Nowadays, sampling frequencies in the 100–2000 Hz range are common. Once the signal has been digitized, digital finite impulse response (FIR) filters with linear phase, which have a higher performance than analog filters, are applied in order to reduce the signal bandwidth. Subsequently, the sampling rate can be reduced by decimation. For example, if the cut-off frequency of the anti-aliasing filter is 100 Hz, the EEG signal is typically sampled at 256 Hz [31].

The second step of the digitizing process is quantization, which maps the continuous amplitude value of each data sample into one of the possible 2^N levels, where N is the resolution of the ADC [37]. Current commercial EEG systems typically sample with resolutions up to 22 bits but store the data with a smaller precision, e.g., 16 bits [31].

The choice of the ADC resolution is mainly a trade-off between the input amplitude range that can be digitized and the least significant bit (LSB), which is the minimum detectable signal level and is defined as:

$$LSB = \frac{V_{FSR}}{2^N} \tag{2.4}$$

where V_{FSR} = full-scale input amplitude range of the ADC [V] [37]. The speed of the conversion process and the cost of the hardware are also factors in determining the resolution, since the higher the number of bits, the slower the conversion process and the more expensive the ADC will be.

Data display. Depending on the intended use of the EEG system, a display may or may not be present. In clinical systems, the display is an essential sub-system since it allows the operator to visualize the EEG in real-time and make various annotations on the data. Older systems employed galvanometers that moved ink-fed pens in order to continuously write the EEG traces on z-folded paper [32]. In modern systems, the pen-writer units have been replaced by high-resolution computer screens [31]. If desired, the EEG traces can be printed out by means of conventional inkjet or laser printers.

Portable systems on the other hand must be small, lightweight and power-efficient. Therefore, a means to display the acquired signal is usually not included. It is typical for the device either to transmit the EEG data to a measurement server or to store it onboard for later retrieval.

Storage and/or transmission. Certain EEG recorders, which possess on-board memory devices (e.g., solid-state memory, optical media, magnetic media), have the possibility to store the recorded signal. In such devices, it is generally recommended that the raw data should be stored without any processing [31]. Patient information, technical data about the recording and event markers should also be saved together with the EEG data for easy access. Specialized file formats have been developed by various groups in order to facilitate the storage of biosignals and to improve interoperability, e.g., European Data Format (EDF) [38], BioSemi Dataformat (BDF) [39], General Data Format for Biosignals (GDF) [40].

Portable systems often have a means to transmit the measurement data to a master device. The transmission can be accomplished either with a wireless module (e.g., Wi-Fi™, Bluetooth, ZigBee) or by using traditional wired interfaces (e.g. USB, Serial, Firewire).

2.3.3 Factors that Affect the Quality of EEG Recordings

Due to its low amplitude, the EEG signal is easily corrupted by noise. Based on their origin, noise sources can be broadly classified either as physical artefacts[2], or biological artefacts, or electronic noise. Physical artefacts originate outside of the patient while biological artefacts originate within the patient. On the other hand, electronic noise arises within the measurement device itself. The following sections provide some examples of these sources of noise and how to handle them.

Physical Artefacts

Almost any source that can radiate a strong enough electric or magnetic field in the vicinity of the EEG measurement site will create artefacts in the recording due to the phenomenons of electrostatic and magnetic coupling. Examples include faulty X-ray machines, hospital call systems, and the switching on of a fibrillator. Even changes in the ambient electrostatic field caused by the movement of the patient or the technician can cause artefacts. A more exhaustive list of possible physical artefacts can be found in [31] and [14].

Two of the most common physical artefacts are the mains artefact and the movement artefact. The mains artefact is characterized by a peak at 50/60 Hz in the power spectrum and periodic, small-amplitude peaks in the time-domain "riding" on top of the EEG signal. Sometimes harmonics are present at integral multiples of the line frequency. Normally, this type of artefact is caused by poor electrode impedance [31]. Motion artefacts are created by the movement of the electrodes relative to the patient and/or by the mechanical contraction of the skin. This movement disturbs the electrode-electrolyte-skin interface and/or the double layer of charge that exists between the tissue layers. As long as the movement continues, the half-cell potential will fluctuate. Once the movement ceases, the half-cell potential will stabilize and the artefact will disappear. On an EEG record, this change in half-cell potential causes the well-known base-line drift artefact.

The best way to deal with physical artefacts is to make sure that they do not disturb the EEG recording in the first place. This can be accomplished by turning off possible interference sources, such as faulty X-ray machines, and by having a good recording setup, which serves to minimize the effects of such artefacts. As explained in the previous section, the essential component of a good recording setup is a differential amplifier with a high CMRR. However, patient preparation is also extremely impor-

[2] Artefacts are interfering signals that arise from another source than the electrophysiological source that is being monitored.

tant. Finally, shielding the leads and the measurement circuitry, as well as keeping the leads as short as possible, also helps to prevent the appearance of these artefacts. If shielded leads are not a possibility, twisting the lead wires together and keeping them close to the body helps to prevent magnetic-field pickup [28].

Even with the precautions and preparations described in the previous paragraph, physical artefacts, especially mains artefacts, inevitably appear in EEG recordings. When this occurs, the only remaining recourse is filtering. For a normal EEG recording, the bandwidth of interest is usually 0.16–100 Hz [32]. Thus, high- and low-frequency artefacts outside of this range can be easily removed by means of low- and high-pass filters, respectively. Artefacts with a frequency that is inside of this range, such as the mains artefact, are more problematic. The usual course of action is to employ a comb filter, which is a type of filter that exhibits an almost flat frequency response with deep notches at the frequencies that need to be removed. Another option is to employ an adaptive noise canceller (ANC). However, this method requires that the original interfering signal be recorded at the same time as the noisy EEG, something that is rarely the case [41].

Biological Artefacts

Biological artefacts are by far the most common type of artefact present in EEG records and the hardest to deal with. Common interference sources are electrocardiogram (ECG), electrooculogram (EOG), breathing, and electromyography (EMG) signals [42]. In addition, spontaneous EEG is considered as noise when recording evoked potentials.

Biological artefacts are not always considered a nuisance. They can have practical use and they may convey important clinical information about the patient. For example, EOG artefacts in an EEG can be used as an inbuilt calibration signal to check the recording setup. Also, consistent occurrence of EOG or muscle activity may indicate subclinical epileptic seizures. In the ICU, the presence of EEG artefacts may indicate emergence from a coma or from anaesthesia. Therefore, the definitions of signal and noise are relative to the phenomenon being investigated. [43]

Similarly to physical artefacts, it is best to prevent the appearance of biological artefacts rather than having to deal with them in the measured signal. This is especially true of EOG and EMG signals, which can be controlled by a conscious patient. Thus, it is important to inform the patient that they should sit as still as possible and limit their eye movement. However, the appearance of biological artefacts is also inevitable, especially since certain interference sources such as breathing and ECG

cannot be controlled. Due to the reasons mentioned in the previous paragraph, the best way to deal with biological artefacts in a clinical setting is to identify, classify, and annotate them but preferably not remove them from the EEG record [43]. However, if filtering must be performed, it is imperative to retain a copy of the raw data. On the other hand, when performing EEG research, the type of signal being sought is usually known and thus filtering does not pose as a big a challenge as in the clinical setting. Thus, LP filters can be employed to remove most types of EMG interference, provided that the frequency of the interference does not overlap with that of the EEG, and HP filters can be applied to remove breathing and baseline drift artefacts. More problematic are ECG and EOG artefacts since their power spectrum usually overlaps that of the EEG. In such cases, the two options are either to use an ANC, as described in the previous section, or to simply discard the parts of the EEG signal that are corrupted by this type of noise.

Electronic Noise

Even after the external physical noise sources have been eliminated or reduced, noise will be introduced by the bioamplifier circuitry itself. This type of noise, which is known as internal or inherent noise, has a random character since it is caused by random phenomena, e.g., random generation and recombination of electron-hole pairs in semiconductors [44]. Two types of inherent noise, thermal noise and integrated circuit (IC) noise, will now be discussed.

All passive resistive elements, including stray resistances and electrode impedances, exhibit thermal noise, which is also known as Johnson noise [44]. Thermal noise increases with the size of the resistance and with temperature but is unaffected by the passage of current through the resistive element. Its magnitude can be calculated with the following equation:

$$E_{R_{RMS}} = \sqrt{4kRT\Delta f} \tag{2.5}$$

where $E_{R_{RMS}}$ = root-mean-square value of the noise voltage [V], k = Boltzmann's constant [$1.3806503 \times 10^{-23} J/K$], R = resistance value [Ω], T = temperature [K], Δf = bandwidth over which the noise energy is calculated [Hz] [45].

Since it is located at the beginning of the measurement chain and thus subject to all of the bioamplifier's gain stages, the total source resistance, which includes the electrode impedance and all of the intermediary resistances to the bioamplifier input, places in theory a boundary on the smallest signal that can be recorded due to the

Johnson noise it introduces. In a bandwidth of 0.1–100 Hz at 25 °C:

$$E_{R_{RMS}} \approx 1.3 \times 10^{-3}\sqrt{R_e}\ \mu\text{V} \tag{2.6}$$

where R_s = total source resistance [Ω]. However, in practice, such a low noise level cannot be achieved since the electrode drift raises the noise floor of the measurement. [34]

ICs also exhibit inherent noise, which consist of two frequency-dependent components, a voltage noise source and a current noise source. Both noise sources are a mixture of white noise[3] and 1/f noise[4]. At low frequencies, the 1/f noise dominates while at high frequencies the noise is predominantly white. The borderline frequency between the two noise regions is called the corner frequency. Analytically, the noise spectral densities are expressed as

$$e_n^2 = e_{nw}^2(\frac{f_{ce}}{f} + 1) \quad i_n^2 = i_{nw}^2(\frac{f_{ci}}{f} + 1) \tag{2.7}$$

where e_n = voltage noise power density [V^2/f], e_{nw} = voltage noise white-noise floor [V^2/f], f_{ce} = voltage noise corner frequency [Hz], i_n = current noise power density [A^2/f], i_{nw} = current noise white-noise floor [A^2/f], f_{ci} = current noise corner frequency [Hz] [44]. Modeling the bioamplifier as one IC and combining Equations 2.6 and 2.7, an expression can be obtained for the total input noise of the system. Due to the random nature of the noise, the summation of the two noise types must be performed in a in the square-power sense:

$$E_{RMS}^2 = \int_{f_2}^{f_1} e_{nw}^2(\frac{f_{ce}}{f} + 1)\, df + R_s^2 \int_{f_2}^{f_1} i_{nw}^2(\frac{f_{ci}}{f} + 1) + 4kRT\Delta f \tag{2.8}$$

where $\Delta f = f_2 - f_1$.

Prevention is the best way to deal with electronic noise. Care must be taken during the design stage in order to select components with low electronic noise levels. Also, the size of the resistors should be minimized wherever possible.

[3]White noise has a uniform spectral density. [44]

[4]The spectral density of 1/f noise is inversely proportional to frequency. [44]

2.4 EEG Recording Guidelines

In an effort to homogenize the practice of clinical neurophysiology and to foster high standards in the profession, the International Federation of Clinical Neurophysiology (IFCN) released in 1999 an updated version of its book of recommendations for the practice of clinical neurophysiology, which includes two sections regarding the use of EEG [46]. Another set of guidelines pertaining to the recording of EEG in various settings was published by the American Clinical Neurophysiology Society (ACNS) in 2006 and are available from the society's website [47].

Given that the author was not able to obtain access to the IFCN recommendations, the ACNS guidelines were used in this thesis. The relevant parts of the following guidelines will be briefly summarized in subsequent sections:

- Minimum Technical Requirements for Performing Clinical Electroencephalography [48]
- Guidelines for Recording Clinical EEG on Digital Media [49].

2.4.1 Minimum Technical Requirements for Clinical EEG

Equipment

Number of channels. The minimum number of channels required in order to detect whether an area produces normal or abnormal EEG activity is 16.

Shielding. Electrical shielding of the patient and of the recording equipment is not required under normal clinical conditions.

Electrodes

Types. EEG electrodes must be of the low-noise, low-drift type and should not significantly attenuate signals in the 0.5–70 Hz range. Silver-silver chloride (Ag/AgCl) or gold disk electrodes immobilized with non-flexible collodion[5] are recommended.

Locations. All 21 electrodes of the international 10-20 System (Figure 2.5) should be employed[6]. A smaller number of electrodes than specified by the 10-20 system can be used in special circumstances but such recordings are not considered to be

[5]Collodion is a strongly adhesive solution composed of pyroxylin in ether with a varying proportion of alcohol. [50]

comprehensive. A ground electrode should always be used except in cases where there is a risk of double-grounding, e.g., intensive care unit (ICU), operating room (OR).

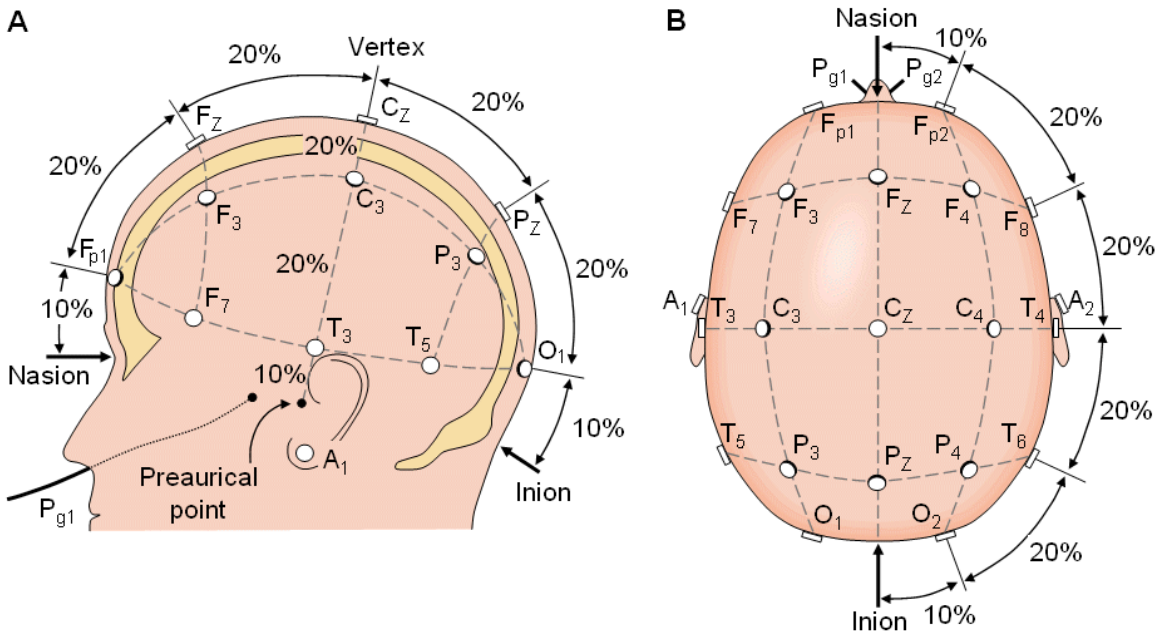

Figure 2.5: The electrodes of the 10-20 System. *Reproduced from* [10].

Impedance. Interelectrode impedances must be checked prior to the start of the recording and should not be larger than 5 kΩ. If patterns that may be artifactual in origin appear during the recording, the impedance should be rechecked.

Recording

Montages. In digital systems, the initial recording should be made in a referential montage in order to allow reformatting to be performed at a later time. Since the reference electrode should not be one of the standard 10-20 electrodes, an additional electrode is commonly placed between the C_Z and P_Z locations for this purpose.

Calibration. Calibration is an essential part of the recording process since it gives the interpreter a reference signal whose scale the EEG signal can be compared against and it provides information about the system's sensitivity, its high- and low-frequency response as well as the noise level. The first calibration step consists of a standard square-wave calibration which allows all channels to be adjusted so that they respond

[6] In addition to the electrodes of the 10-20 System, intermediate 10% electrodes, which have been standardized by the American Electroencephalographic Society, can also be applied. [10]

identically to the calibration signal. A biological calibration step during which all channels are connected to the same pair of electrodes can follow afterward, but this step is uncommon when modern digital EEG recorders are employed.

If a system does not make provisions for any calibration methods, the technologist should carefully observe the first 30 sec of the recording in a referential montage.

Sensitivity. Digital systems must include clear scale markers as part of their display since the physical units of μV/mm used in paper systems have no meaning.

Filters. In order to prevent information loss, for standard recordings, the cut-off frequency of the HP filter should not be higher than 1 Hz, while that of the LP filter should not be lower than 70 Hz. The use of 50/60 Hz notch filters is discouraged except when all other measures against power line interference has failed, since this type of filter can attenuate spikes.

Digital display length. A digital page of EEG data should be 10 seconds long for routine recordings. In special conditions, a longer length of 20 sec/page can be used.

2.4.2 Recording of EEG on Digital Media

Patient and recording information. Patient- and recording-related information such as the name and date of birth, the date and time at which measurement was done as well as relevant patient and laboratory identification numbers must be recorded. While this information must be entered at the time of the recording, it should be possible to correct errors and omissions after the recording is complete.

Recording of information. Instrumental, and bio-calibration if necessary, should be carried out at the beginning and at the end of the recording, with the resulting signal(s) being included in the recorded data.

It must be possible to store annotations along with the EEG data. This feature can be used to record the technologist's comments and event codes, even after the recording has ended. Additional information about the recording settings, e.g., filter settings, gain, montage selections, should be stored automatically at the onset of the measurement and as soon as changes are made during recording.

Technical specifications. The EEG must be sampled with a rate that is at least three times higher than the cut-off frequency of the LP filter, with even higher sampling

frequencies being preferred, e.g., pattern recognition requires a sampling frequency that is at least seven times the cut-off frequency. The system must have a resolution of at least 0.5 μV and detect signals up to several millivolts without clipping. The CMR must be 80 dB or higher for each channel, and the interchannel crosstalk should be 40 dB or better. Finally, the noise level must not exceed 2 μV PP in a 0.5–100 Hz bandwidth.

Recording media. Digital EEG data should be stored on widely supported storage media, e.g., CD-ROM, DVD-ROM, in a non-proprietary/publicly available data format.

Display. The display of the EEG on a screen should approximate the temporal and spatial resolution of traditional paper systems while the available montages should be in line with ACNS guidelines. Horizontal and vertical scales should be indicated on the display. Although appropriate channel spacing between the baselines of different channels must be provided, occasional overlap of data between channels is acceptable.

2.5 aEEG Algorithm

To the untrained eye, an EEG recording resembles noise. Hence, only a neurophysiologist that has been trained to interpret EEGs can visually analyze the signal and, based on his experience, offer a diagnostic. Moreover, EEG recordings may span many hours, making their interpretation time-consuming and tedious. It is for these reasons that efforts are being made to develop signal processing methods that can aid physicians in the interpretation of the EEG. The bispectral index (BIS) [51], the Datex-Ohmeda entropy algorithm [52], both of which are used to measure depth of anesthesia, and the quantitative EEG (qEEG) [53] are examples of such signal processing methods. The aEEG, which is also such a method, was used in this work and is described in more detail below.

The aEEG algorithm can be thought of as a software implementation of the cerebral function monitor (CFM), a device that was designed in 1969 by Maynard et al. in order to simplify the recording and interpretation of long-term EEG recordings [54]. In the CFM, the EEG signal was measured from a pair of electrodes located near the vertex, amplified and then filtered with a special type of band-pass filter, whose purpose was to flatten the spectrum of the EEG signal, thus countering its 1/f character. It had a lower and upper cut-off frequencies of 2 Hz and 15 Hz, respectively, and a pass-band

slope that approximated the inverse of the spectrum of a normal EEG with no alpha or beta wave activity. After filtering, the signal's amplitude was semi-logarithmically compressed to make it possible for the device to handle a wide range of EEG levels without the need for gain adjustment. The final step of the process was the PP detector and rectifier block. At its output, the signal was a line drawn through the peaks of the compressed and rectified EEG. When this output signal was printed out on heat-sensitive paper at a slow-speed (2.5–36 cm/hour), the level and width of the trace were a function of the mean amplitude and variation of the cerebral activity [55].

The usefulness of aEEG in a clinical setting has been demonstrated by a multitude of studies. It can help to measure the recovery or deterioration following brain damage or a drug induced coma and to monitor the cerebral function after cardiorespiratory resuscitation [54, 55, 56]. Also, it can be used to monitor the incidence of epileptiform discharges [57]. More recently, the aEEG has been shown to be a valuable addition in the clinical assessment of patients with metabolic disorders [58]. Furthermore, slow EEG trends and burst suppression patterns are easily visible in the aEEG. Although nowadays the aEEG is being used extensively for the monitoring of neonates suffering from a variety of ailments, this topic will not be expanded upon here since it is unrelated to the present work.

A common conclusion among many of the recent aEEG studies is that an aEEG trace should be displayed simultaneously with the raw EEG that was used to generate it. This increases the method's sensitivity and specificity by allowing the caregiver to easily determine if a sudden change in the aEEG is of a physiological or of an artefactual nature. Modern CFM monitors, such as the Natus Olympic CFM 6000 and the GE Healthcare BrainZ Neonatal Brain Monitor, already possess this functionality.

2.6 Review of Commercial Products

In this section, the state-of-the-art in portable EEG recording systems will be reviewed. As stated previously, no EEG recording system exists at the time of this writing that combines a quick-application EEG cap with a portable, wireless recording unit and that is specifically intended for use in emergencies. Hence, portable EEG devices and quick-application caps will be reviewed separately.

2.6.1 Portable EEG Systems

An Internet search using the `eeg portable OR ambulatory` query yielded numerous hits. Additional products were found by searching through the websites of the manufacturers listed in the overview of ambulatory physiological monitoring devices published by Yucha et al. [59]. From these results, products from non-reputable companies and devices that have not received regulatory approval were discarded. Devices intended for biofeedback or polysomnography (PSG) studies as well as products without datasheets were also removed. Finally, if a manufacturer had more than one offering that met these criteria, the product with the smallest dimensions was chosen for this review.

As it can be appreciated from the next pages, due to the lack of technical information provided by the manufacturers, it is difficult to determine whether these devices follow the ACNS guidelines described in section 2.4. In particular, the noise properties of a given device are especially hard to analyze since the manufacturers either omit the noise figures completely, or provide them as RMS values without specifying the frequency ranges over which they were calculated. The only exception is the NicoletOne ambulatory EEG system, which clearly infringes the ACNS guidelines since its noise level is $3\,\mu V_{P\text{-}P}$ in a 0.16–70 Hz range.

Although the following systems are portable and have many advantages over non-portable ones, they also have a number of shortcomings that make their use in emergency medicine challenging. First, the devices are voluminous (average volume: $254\,cm^3$) and heavy (average weight: 415 g). Second, most require a carrying system, e.g., pouch, lanyard, that would impede the work of medical personnel. Finally, since they were not designed as quick-application devices, some of the systems need to be assembled prior to use.

TREA® Ambulatory EEG System

Figure 2.6: TREA® 27-channel system - 16 monopolar EEG channels, 5 monobipolar EEG/PSG channels, and 5 Pulse Oximeter channels (SpO_2, HR, PLETH, PTT, HR PTT). *Reproduced from* [60].

Table 2.1: Characteristics of the TREA® ambulatory EEG system.

Parameter	**Value**
Manufacturer	Grass Technologies (West Warwick, USA)
No. EEG channels	21
Sampling frequency (Hz)	200, 400, 800, 1600
Storage frequency (Hz)	200, 400, 800, 1600
Resolution (bits)	16
Bandwidth (Hz)	0.1–128
CMR (dB)	>94
Input impedance (MΩ)	6.6
Noise (μVrms)	<0.5
Power source	3× AA batteries
Max . operating time (hours)	24–72 (depends on battery type and sampling frequency)
Weight (g)	140 (without batteries)
Dimensions (mm)	130 × 30 × 80
Comments	- Includes TWin EEG recording software
	- Data is stored on internal solid-state memory
	- Possesses LCD screen user interface

This device deserves particular attention since its excellent electrical characteristics and relatively small dimension could make it suitable for emergency use. However, the lack of a quick-application cap means that traditional wired EEG caps, with their associated shortcomings, must be employed. Also, attaching 21 electrodes would require a large amount of time, something that is undesirable for emEEG.

Easy® Ambulatory 2

Figure 2.7: Cadwell Easy Ambulatory 2 components: A) Recorder pouch, B) Amplifier pouch, C) Easy Net® cable, D) Recording electrodes, E) Amplifier, F) Recorder, G)Large limb straps, H) Small chest strap, I) Medium chest strap, J) Small limb straps, K) Large chest strap. *Reproduced from* [61].

Table 2.2: Characteristics of the Easy® ambulatory 2 EEG system.

Parameter	**Value**
Manufacturer	Cadwell Laboratories (Kennewick, USA)
No. EEG channels	21
Sampling frequency (Hz)	3200
Storage frequency (Hz)	200
Resolution (bits)	16
Bandwidth (Hz)	Unknown
CMR (dB)	Unknown
Input impedance (MΩ)	Unknown
Noise (μVrms)	Unknown
Power source	2× C or D batteries
Max . operating time (hours)	24 (C batteries) or 48 (D batteries)
Weight (g)	500
Dimensions (mm)	Unknown
Comments	- Amplifier and recorder are separate units
	- Data stored on CF card

Trackit™ 24

Figure 2.8: Complete Trackit™ 24 system, including recording laptop. *Reproduced from* [62].

Table 2.3: Characteristics of the Trackit™ 24 system for applications in ambulatory EEG.

Parameter	**Value**
Manufacturer	Lifelines (West Warwick, U.K.)
No. EEG channels	24
Sampling frequency (Hz)	1–256
Storage frequency (Hz)	Unknown
Resolution (bits)	16
Bandwidth (Hz)	0.16–70 (-6 dB)
CMR (dB)	>110
Input impedance (MΩ)	Unknown
Noise (μVrms)	Unknown
Power source	3× PP3 Lithium or Canon BP511 Lithium-ion
Max . operating time (hours)	96 (PP3) or 36 (BP511)
Weight (g)	<500
Dimensions (mm)	$97 \times 74 \times 36$
Comments	- Can transmit data to host PC via Bluetooth
	- Data stored on CF card in EDF format

Ambulatory EEG Recorder

Figure 2.9: The PL-EEG Ambulatory EEG option ALPHA-D16. *Reproduced from* [63].

Table 2.4: Characteristics of the ALPHA-D16 ambulatory EEG recorder.

Parameter	**Value**
Manufacturer	Walter Graphtek (Luebeck, Germany)
No. EEG channels	14
Sampling frequency (Hz)	Unknown
Storage frequency (Hz)	Unknown
Resolution (bits)	16
Bandwidth (Hz)	0.5–60
CMR (dB)	77 @ 50 Hz
Input impedance (MΩ)	>100
Noise (μVpp)	1.2
Power source	2× nickel-metal hydride AA batteries
Max . operating time (hours)	60
Weight (g)	170
Dimensions (mm)	$120 \times 65 \times 22$
Comments	- Can be operated by PC via Bluetooth or serial
	- Data stored on CF card

NicoletOne™ Ambulatory EEG

Figure 2.10: The NicoletOne™ ambulatory EEG recorder and patient connection unit. *Reproduced from* [64].

Table 2.5: Characteristics of the NicoletOne™ ambulatory EEG system.

Parameter	**Value**
Manufacturer	Carefusion (San Diego, USA)
No. EEG channels	32
Sampling frequency (Hz)	1, 2, 4, 8, 16, 25, 32, 50, 64, 128, 200
Storage frequency (Hz)	Unknown
Resolution (bits)	16
Bandwidth (Hz)	0.5–60
CMR (dB)	>110
Input impedance (MΩ)	100
Noise (μVpp)	3 @ 0.16–70 Hz
Power source	6× AA batteries, Alkaline or Lithium
Max . operating time (hours)	72
Weight (g)	763 (recorder + patient unit)
Dimensions (mm)	recorder - 146 × 124 × 39
	patient unit - 163 × 60 × 28
Comments	- Includes NicoletOne™ nEEG and Reader software
	- Data stored on CF card in EDF format

ZOOM-100DC

The Brainscope ZOOM-100DC is an 8-channel, hand-held EEG device intended to be used at the initial point of care in order to quickly assess brain function. It can display 5 channels of raw EEG at a time and calculate the standard qEEG parameters. Although the developer of the device has received US Food and Drug Association (FDA) clearance under section 510(k) to market the device in August of 2009, the ZOOM-100DC has yet to go on sale.

Table 2.6: Characteristics of the ZOOM-100DC brain electrical activity data collection system. [65]

Parameter	**Value**
Manufacturer	Brainscope (Bethesda, USA)
No. EEG channels	8
Sampling frequency (Hz)	Unknown
Storage frequency (Hz)	Unknown
Resolution (bits)	Unknown
Bandwidth (Hz)	0.5–4000
CMR (dB)	$\geq$100
Input impedance (MΩ)	$\geq$10
Noise (μVrms)	Unknown
Power source	Lithium-ion battery
Max . operating time (hours)	Unknown
Weight (g)	Unknown
Dimensions (mm)	Unknown
Comments	- Electrode impedance check prior to recording
	- Raw and processed data stored on CF card

2.6.2 Quick Application EEG Caps

The following non-exhaustive list of fast-application EEG caps was compiled using the results obtained from an Internet search with the `eeg electrode fast` query:

- BraiNet® (Jordan NeuroScience)
- StatNet™ (HydroDot)
- Fast'nEasy Cap (Brain Products)
- Quick-Cap (Compumedics)
- WaveGuard™ (Advanced Neuro Technology)

With the exception of the Quick-Cap and the WaveGuard cap, which are very similar to the Fast'nEasy Cap, a brief overview of each of these will be given in subsequent sections.

BraiNet®

The BraiNet by Jordan NeuroScience is a versatile cap that can be used for any type of EEG study, from stat EEG to long term monitoring. Designed under the guidance of Dr. Kenneth Jordan, the cap is compatible with all EEG electrodes and the electrode locations are based on the 10/20 system. Different sizes exist and one is selected based on the circumference of the patient's head. The cap is one-time use only so as to avoid the risk of cross-contamination. According to company literature, the attachment of the BraiNet takes approximately 10–15 minutes. [66, 67]

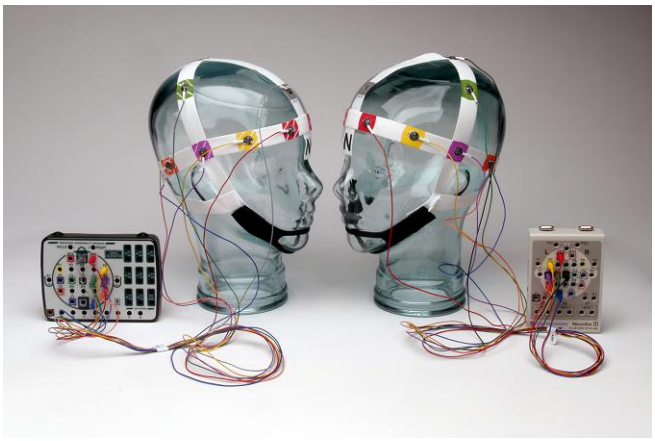

Figure 2.11: BraiNet® EEG template by Jordan NeuroScience. *Reproduced from* [66].

StatNet™

The StatNet is a disposable "peel and stick" EEG headpiece manufactured by Hydrodot Inc. Its soft layered integrated circuit "sandwich" construction embeds pregelled, elongated Ag/AgCl electrodes. The electrical signals are transmitted to two connectors via silver ink tracings embedded into the cap. In the company literature it is advertised that the cap takes an average of 5 minutes to apply with no prior skin preparation. However, from a demonstration video available online, it is clear that if the patient has long hair, the attachment takes significantly longer since the hair under each electrode location must first be moved to the side in order to expose the scalp. Also, the person performing the attachment would need to have extensive experience in order to carry out this action quickly and accurately. [68]

Figure 2.12: StatNet™by Hydrodot Inc. *Reproduced from* [68].

Fast'nEasy Cap

The Fast'nEasy by Brain Products GmbH resembles traditional EEG caps in that it completely covers the patient's head and it is reusable. Depending on the model, it features either 32 or 64 Ag/AgCl pellet pin electrodes. With the help of adapters, the cap can be connected to any commercial EEG amplifier. Many sizes are available, from caps for newborns to caps for adults with large heads. A major shortcoming with this cap is that the electrodes cannot be replaced since they are permanently fastened to the cap. Hence, the whole cap must be thoroughly cleaned after each use. [69]

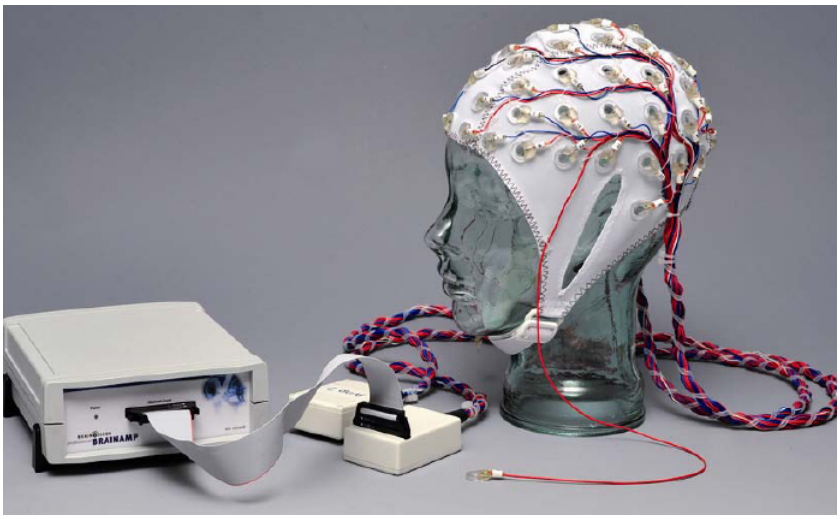

Figure 2.13: Fast'nEasy Cap by Brain Products GmbH. *Reproduced from* [69].

Chapter 3

Research Methods and Material

3.1 Introduction

The main objective of this work was to build on the results obtained during the Master theses of Salmi [70], Pänkälä [71], and Tuomi [72] so as to obtain two working EEG systems that are suitable for investigating the feasibility and clinical value of EEG in emergency medicine. In order to accomplish this goal, both systems must be light, portable, easy-to-use and have a short preparation time. A secondary objective was to investigate the aEEG algorithm and explore potential uses in both systems.

The 1-channel system is described in section 3.2 and the 6-channel system in section 3.3. The electrodes that were used in this study are the subject of section 3.4 while section 3.5 explains how the aEEG algorithm was implemented. Finally, section 3.6 details the tests that were carried out to evaluate the two systems.

3.2 1-channel System

3.2.1 Past Work

As part of the work towards her M.Sc. degree, Tuomi developed the hardware prototype of an EEG-to-ECG adapter, a one channel device that allows a person's EEG to be displayed on a standard ECG monitor [72]. The device featured a high input impedance, low noise amplifier that increased the EEG signal's amplitude in order to allow it to be displayed on an ECG monitor. The amount of amplification was dynamically adjusted depending on the characteristics of the signal. The first version of the prototype device is pictured in Figure 3.1.

The prototype had a number of shortcomings that made it unsuitable for clinical

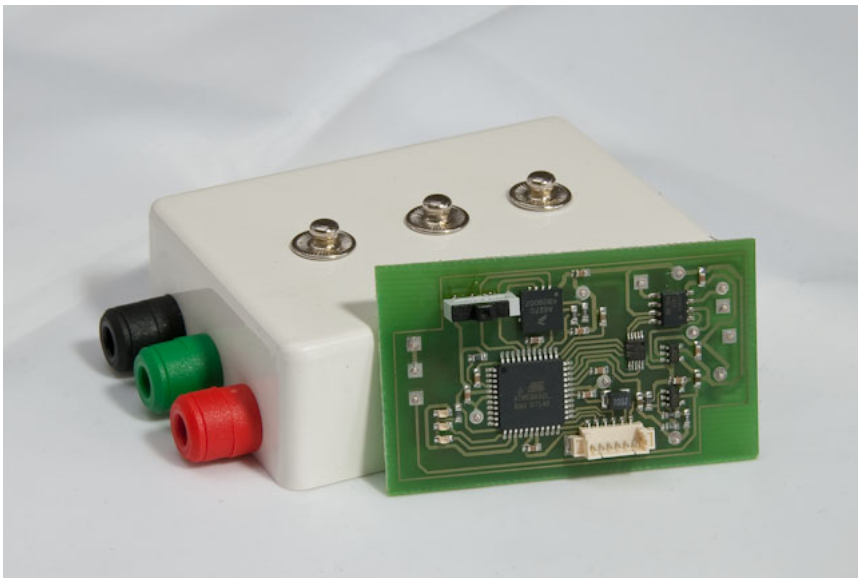

Figure 3.1: First version of the EEG-to-ECG adapter prototype.

use. The PGA circuit was constructed by placing a digital potentiometer in the feedback network of a non-inverting op-amp circuit. Due to the large end-to-end tolerance of a digital potentiometer, which can be up to 25 %, this configuration caused the adapter's gain to also have a large tolerance. Furthermore, whenever the gain was changed, a DC error voltage appeared at the op-amp circuit's output, which made it impossible for the on-board microcontroller (MCU) to sample the amplitude of the EEG signal and dynamically adjust the PGA's gain. The PCB layout of the adapter was not optimal seeing as though the principle of segregation was not respected, a solid ground plane was absent, and the width of the tracks varied along their length. Finally, given that a mechanical slider switch was used to turn the adapter on or off, a hole had to be made in the enclosure, which allowed the slider to be moved, but through which fluids could also enter the device.

3.2.2 Overview of Present Work

In order to overcome the aforementioned shortcomings and to further improve the functionality of the device, the author redesigned the adapter. As a result, the circuit of the new version is substantially different from the previous prototype. The block diagram of the new device is shown in Figure 3.2 while the complete circuit is included in Appendix A.1.

As it can be seen in the block diagram, the adapter is actually a battery-powered embedded system that consists mainly of a one-channel, variable-gain EEG bioampli-

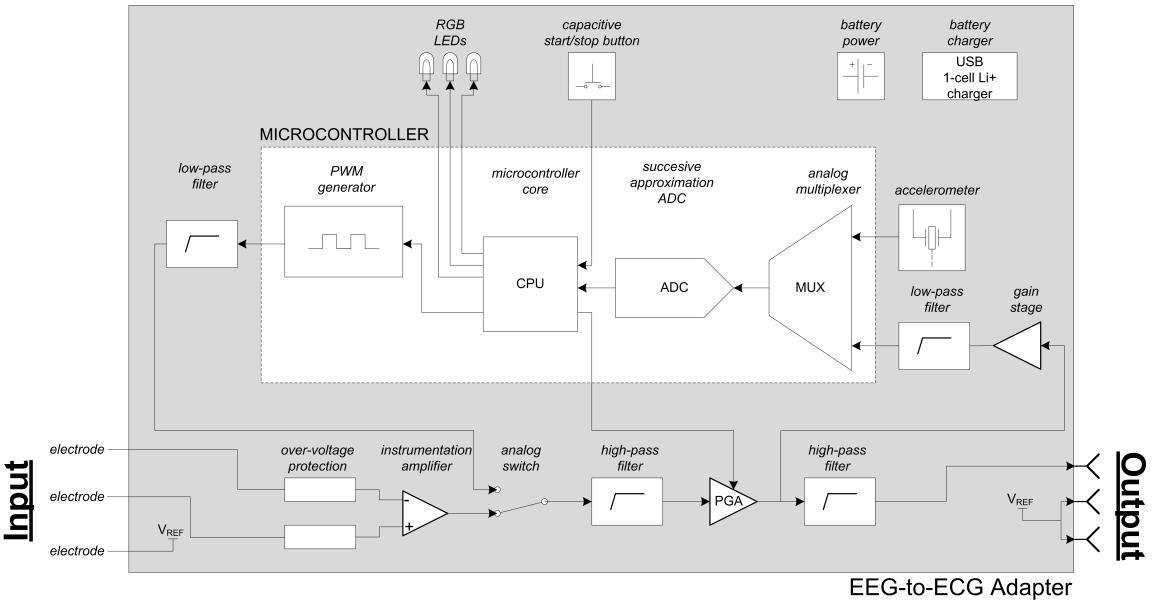

Figure 3.2: Block diagram of the 1-channel system.

fier and an ATmega1284P MCU. The MCU samples the EEG signal in order to determine the appropriate gain in real-time. After every gain change, the EEG recording is temporarily interrupted and a sinusoidal scale-indicator signal with an amplitude equivalent to 100 μV at the current gain level is outputted by a pulse-width modulation (PWM) digital-to-analog converter (DAC). An on-board three dimensional (3D) accelerometer is used to determine whether the adapter is moving excessively. The user interface is made up of a red, green and blue (RGB) light-emitting diode (LED) unit and a capacitive button that starts/stops the recording.

The following sections discuss the hardware and firmware of the adapter in greater detail.

3.2.3 Hardware

Transient Protection

In order to be considered defibrillator-proof, the transient protection network must withstand such a defibrillation pulse as is described in the "Medical electrical equipment - Part 1: General requirements for basic safety and essential performance" standard, which is more commonly known as IEC 60601-1. The standard specifies a defibrillation pulse that is sourced from a 32 μF capacitor charged to 5000 V and then discharged via a 500 μH series inductor [73]. However, the standard also allows for a lower test voltage to be used depending on the intended use of the medical device and

the location of the electrodes on the patient. Since the electrodes of the EEG-ECG adapter are applied to the forehead of the patient, it is logical to assume that the full defibrillation pulse will not appear at the input of the adapter. This reasoning is further validated by the fact that the GE Healthcare Entropy Module, which measures depth of anesthesia from a set of forehead electrodes, is designed to withstand a 3000 V pulse [74]. Therefore, for the purposes of this design, it was assumed that the maximum input voltage caused by a defibrillator is 3 kV.

The silicon diode protection scheme is employed in this design due to its smaller size and lower cost. The Fairchild MMBD1503A small signal diodes (D300 and D301) were chosen given their extremely small reverse-leakage current (0.5 nA at 130 V), which helps minimize any offset errors and other non-idealities induced in the EEG input channels. The minimum value of the voltage limiting resistor was calculated by means of the formula

$$R_{MIN} = \frac{|V_{IN}| - |V_{SUPPLY}| - V_F}{I_{LIMIT}} \tag{3.1}$$

where R_{MIN} = smallest current limiting resistor [Ω], V_{IN} = maximum input voltage [V], V_{SUPPLY} = battery supply voltage [V], V_F = diode forward voltage at the selected forward current [V], and I_{LIMIT} = forward current [A] [75]. Setting I_{LIMIT} to half the maximum diode forward current, i.e. 100 mA, results in $V_F = 0.9$ V. Thus R_{MIN} is equal to:

$$R_{MIN} = \frac{3000 - 3.7 - 0.9}{0.1} = 29954\,\Omega \tag{3.2}$$

The desired resistor had to have a voltage rating of 3 kV, since voltages close to the maximum input voltage could appear across this resistor, and a power rating of 2 W at 25 °C [76]. The most adequate resistor that was found was the 40.2 kΩ Vishay Dale RNX075. At room temperature and assuming that the bandwidth of interest is 100 Hz, the thermal noise induced by the resistor is equal to:

$$E_n = \sqrt{4 \times 1.38 \times 10^{-23} \times 298.15 \times 40200 \times 100} \approx 0.256 \mu V_{RMS} \tag{3.3}$$

Since this value is small compared to the typical range of the human EEG signal, the resistor choice is valid.

Preamplifier

The preamplifier stage consists of the Texas Instruments (TI) INA118 monolithic IA (U300). A monolithic IA has many advantages compared to a custom device constructed from discrete parts. All of the resistors are laser-trimmed at the factory

so that they are closely matched, which affords the device a high CMR. Also, since the resistors are all on the same die, they will stay matched over temperature ensuring an excellent performance over a wide temperature range. Finally, monolithic IAs are available in small, low-cost surface mount packages.

The key characteristics of the INA118 that led to its selection are included in Table 3.1. Among the main reasons are an extremely large input impedance, a large CMR as well as a small gain error and a low input bias current. Furthermore, this IA is a low-power device that can operate in a single-supply configuration with a power supply as small as 2.7 V. Finally, the IA's bandwidth far exceeds that of a typical EEG signal.

The gain of the INA118 can be set in the range of 1 to 10000 by means of an external resistor. The following equation models the relationship between the gain G and the value of the gain-setting resistor R_G:

$$G = 1 + \frac{50k\Omega}{R_G} \tag{3.4}$$

Table 3.1: Key characteristics of the TI INA118. [77]

Parameter	**Value**			**Unit**
	Min	**Typ**	**Max**	
Input Impedance				
Differential		10 || 1		GΩ || pF
Common-Mode		10 || 4		GΩ || pF
CMR with 1 kΩ source impedance				
G = 1	73	90		dB
G = 10	89	110		dB
Gain Error				
G = 1		±0.01	±0.1	%
G = 10		±0.02	±0.5	%
Input Bias Current		±1	±10	nA
Power Supply				
Voltage Range	±1.35	±15	±18	V
Quiescent Current		±350	±385	μA
-3 dB Bandwidth				
G = 1		800		kHz
G = 10		500		kHz

Solving for the resistor value as a function of gain:

$$R_G = \frac{50k\Omega}{G-1} \tag{3.5}$$

The gain must be chosen such that the minimum CMR is high enough to meet the ACNS guidelines while at the same time ensuring that a large DC input signal will not saturate the IA. Based on Equation 3.5, a gain of $G = 6.25$ can be achieved with a 9523 Ω resistor. Using linear extrapolation with the CMR values from Table 3.1, the minimum CMR for the chosen gain is approximately 82 dB, which exceeds the ACNS guidelines. Also, if the non-ideal output characteristics of the IA are taken into account and assuming a power supply of 3 V as well as half-supply biasing of the input signal, the selected gain allows for an input voltage range of 224 mV.

Signal Conditioning

Filtering. Immediately after the preamplifier stage, there is a first order RC HP filter whose purpose is to remove all DC noise, such as electrode half-cell potentials. The cut-off frequency was chosen to be 0.1 Hz, which ensures that frequencies above 0.5 Hz are not significantly attenuated, as required by the ACNS guidelines, while at the same time keeping the values of the filter components small. The cut-off frequency of this filter can be calculated from

$$f_c = \frac{1}{2\pi RC} \tag{3.6}$$

where f_c = filter cut-off frequency [Hz], R = resistor [Ω], and C = capacitor [F]. In order to keep the resistor size small and thus limit the amount of thermal noise, a 10 μF capacitor (C305) is employed. Therefore, according to Equation 3.6, the resistor (R301) must be equal to 160 kΩ.

A common problem of HP filters with such low cut-off frequencies is that they can take a long time to recover from saturation, an effect that is undesirable since it can prevent the monitoring of patients over a period of a few seconds. As a result, it is common to include rapid recovery circuitry that can quickly discharge the filter capacitor. Such a circuit that consisted of an analog switch, which short-circuited the filter resistor when closed, and a voltage window comparator that controlled the closure of the switch was considered for use. However, due to the large number of discrete components that were required and since each of them would have significantly added to the current consumption of the adapter, the circuit was not included in the new

design.

Gain Stage. Two circuit configurations could have been used in order to replace the digital-potentiometer-based programmable gain stage that was employed in the previous version of the adapter. The first configuration also comprises a non-inverting op-amp circuit and a digital potentiometer, but the digipot is used in a ratiometric way by connecting its wiper to the op-amp's negative input and the remaining two terminals to the reference voltage and the op-amp's output, respectively. The gain equation for this circuit is

$$G = 1 + \frac{NR_E}{(1-N)R_E} = 1 + \frac{N}{1-N} \tag{3.7}$$

where G = gain [V/V], N = ratio of the digipot setting to its maximum value (0 to 1), R_E = end-to-end resistance of the digipot [Ω] [78]. Since the R_E term cancels out, the gain of the circuit is only a function of N. However, this is also the biggest disadvantage of this circuit. By analyzing Equation 3.7, one realizes that the slope of the gain function is non-linear with respect to N. A further disadvantage is that the noise characteristics of the PGA that is built in this fashion are hard to predict at design time since they depend on the noise properties of the op amp and those of the digipot.

The second possible circuit configuration employs a PGA IC. Such a device combines the operational amplifier circuit and the resistor feedback network within a compact surface mount package with the only required external components being decoupling capacitors. This solution is advantageous since the IC is specifically intended to be used as a PGA and is thus designed to be low-noise and accurate. Furthermore, due to the lower component count, the amount of PCB space occupied by this solution would be smaller than that of the digipot-based circuit. Due to these advantages, a PGA IC (U400) is employed in the current version of the adapter.

The PGA112 manufactured by TI was chosen for this design. It features two analog inputs, binary gains (1, 2, 4, 8, 16, 32, 64, 128), and a three-pin Serial Peripheral Interface (SPI) for control. The key device properties that led to its selection are included in Table 3.2. With its 10 GΩ input impedance, it is certain that the PGA will not load down the preceding HP filter. Also, since the maximum input on-channel current is only 5 nA, an offset voltage of at most 0.8 mV will be present at the input of the PGA, which is not large enough to saturate it irrespective of the gain setting.

Table 3.3 presents the total adapter gain as a function of the PGA gain. Also

Table 3.2: Key characteristics of the TI PGA112. [79]

Parameter	**Value**			**Unit**
	Min	**Typ**	**Max**	
Input Impedance		10		GΩ
Input On-Channel Current		±1.5	±5	nA
Noise				
Input Voltage Noise Density		25		$nV/\sqrt{Hz}$
(f ≥ 10 Hz, C_L = 100 pF, V_S = 2.2 V)				
Input Voltage Noise		0.736		μV_{PP}
(f = 0,1 to 10 Hz, C_L = 100 pF, V_S = 2.2 V)				
Input Current Density		400		$fA/\sqrt{Hz}$
(f = 10 kHz and C_L = 100 pF)				
DC Gain Error				
1 ≤ G ≤ 32		0.006	0.1	%
G ≥ 50		0.006	0.3	%
Power Supply				
Voltage Range	2.2		5.5	V
Quiescent Current		1180	1650	μA

included are the maximum input signal PP amplitudes for each gain level that result in a 5 mV output signal[1].

High-Pass Filter and Patient Simulator. The output stage of the signal conditioning block, which corresponds also the output stage of the adapter, consists of a 10 μF series capacitor (C402) and a 160 kΩ shunt resistor (R401). The RC network's purpose is twofold. First, it behaves like a HP filter and removes any DC offset introduced by the PGA. Second, the resistor acts as a low impedance path between the output leads, which simulates the presence of a patient for ECG devices that measure lead impedances.

ADC Signal Conditioning

As mentioned in section 2.3.2, the purpose of this block is to further amplify the EEG signal and to limit its bandwidth so that it can be accurately digitized by the MCU's successive approximation (SAR) ADC. A diagram depicting the components that make up this block is shown in Figure 3.3.

[1]It was assumed that 5 mV is the maximum input signal amplitude of modern ECG recorders.

Table 3.3: Total adapter gain and maximum input signal amplitude that will result in a 5 mV output signal as a function of the PGA gain.

PGA Gain [V/V]	**Adapter Gain [V/V]**	**Max. Input Signal [μV_{PP}]**
1	6.25	800
2	12.50	400
4	25	200
8	50	100
16	100	50
32	200	25
64	400	12.5
128	800	6.25

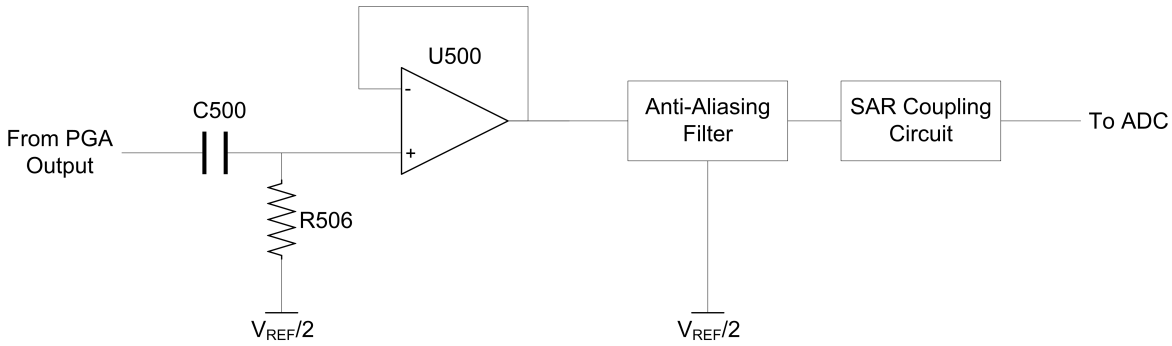

Figure 3.3: Diagram of the ADC signal conditioning block.

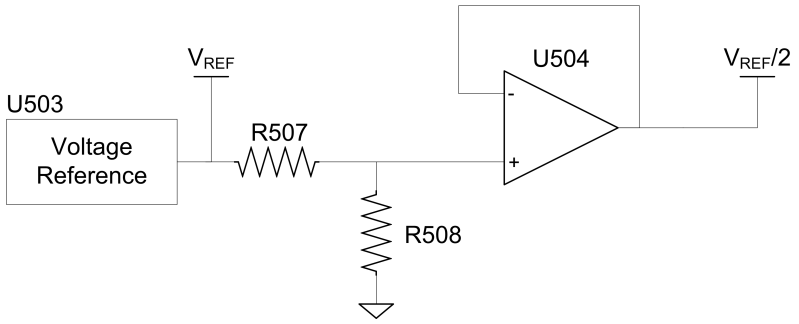

Figure 3.4: Diagram of the ADC voltage reference and its associated circuitry.

Immediately at the input of the block, the passive network consisting of capacitor C500 and resistor R506 shifts the DC level of the signal to half of the ADC's voltage reference ($V_{REF}/2$). An op-amp in the unity-gain configuration (U500) ensures that the passive network does not affect the frequency response of the subsequent filter stage. Finally, a passive circuit couples the signal to the microcontroller's ADC.

The voltage reference, the anti-aliasing (AA) filter and the SAR coupling circuit will now be discussed in more detail.

Voltage Reference. Although the ATmega1284P offers two built-in voltage references (1.1 V and 2.56 V), due to their large tolerance of approximately 9 % [80], they cannot be directly used for the accurate sampling of an EEG signal. Instead, the TI REF3112 (U503), a 1.25 V precision, low-power, low-dropout, series voltage reference, is employed. A 2:1 resistive voltage divider (R507 and R508) made up of 0.1 % resistors together with a Maxim MAX4289 op-amp (U504) connected in the unity-gain configuration generate the $V_{REF}/2$ rail. The voltage reference and its associated circuitry are shown in Figure 3.4.

Filtering and Amplification. The AA filter consists of a 4th order active LP filter. There are two main reasons why such a complex filter bank was selected instead of a simple a set of first order LP filters. First, an active filter of a given order has a sharper frequency response than a passive filter of the same order. Second, the signal can be amplified at the same time, a function that would have to be performed as a separate operation if a passive filter network were to be employed.

Due to its linear phase response, which results in a constant group delay, the LP filter features a Bessel response. However, since the passband of a Bessel filter is not completely flat, a cut-off frequency of 200 Hz was selected, which ensures that the passband gain doesn't change by more than 1 dB from 0 to 50 Hz. According to the

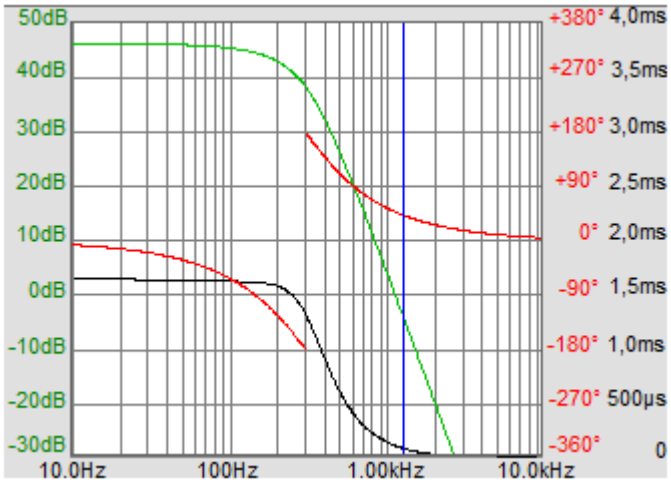

Figure 3.5: Frequency response (green), phase response (red), and group delay (black) of the 4th order active anti-aliasing filter.

ACNS guidelines, EEG should be sampled with a resolution of at least 0.5 μV. Hence, the minimum passband gain $G_{AA_{min}}$ of the LP filter is given by:

$$\frac{LSB}{G_{PRE} \times G_{PGA} \times G_{AA_{min}}} \leq 0.5\mu V \Leftrightarrow G_{AA_{min}} \geq \frac{LSB}{0.5\mu V \times G_{PRE} \times G_{PGA}} \tag{3.8}$$

where LSB = ADC's least significant bit [V], G_{PRE} = gain of the preamplifier [V/V], G_{PGA} = gain of the PGA [V/V]. Plugging in Equation 2.4, assuming that the signal will be sampled with a resolution of 8 bits, and setting the full-scale range to the same level as that of the voltage reference:

$$G_{AA_{min}} \geq \frac{1.25\,V}{0.5\mu V \times 2^8 \times G_{PRE} \times G_{PGA}} \tag{3.9}$$

While the gain of the preamplifier is fixed at 6.25 V/V, that of the PGA can take a range of values, as shown in Table 3.3. However, since the EEG typically has an amplitude less than 100 μV, the minimum gain will be determined under the assumption that the PGA will most of the time have a gain of 8 V/V or more (see Table 3.3). Hence:

$$G_{AA_{min}} \geq \frac{1.25\,V}{0.5\mu V \times 2^8 \times 6.25 \times 8} = 195.3125 \tag{3.10}$$

There is no upper bound on the AA filter's gain, since under normal circumstances, the PGA's gain will automatically be adjusted so that the EEG signal won't exceed the 5 mV threshold. The resulting filter frequency response, which satisfies the above requirements, is shown in Figure 3.5. The passband gain is 46.35 dB, i.e., 207.69 V/V.

Table 3.4: Key characteristics of the Maxim MAX4237B. [83]

Parameter	**Value**			**Unit**
	Min	**Typ**	**Max**	
Gain-Bandwidth Product		7.5		MHz
Slew Rate		1.3		V/μs
Input Offset Voltage		$\pm$5	$\pm$50	μV
Power Supply				
Voltage Range	2.4		5.5	V
Quiescent Current		350	440	μA

The transfer function was implemented by means of a multiple-feedback (MFB) filter topology. This topology is ideal since it allows for a high gain and its sensitivity[2] to component tolerances is small and constant:

$$S_R^{\omega_0} = S_C^{\omega_0} = -\frac{1}{2} \tag{3.11}$$

where ω_0 = filter cut-off frequency [rad], $S_R^{\omega_0}$ = sensitivity of ω_0 to variations of the values of the filter resistors [dimensionless], $S_C^{\omega_0}$ = sensitivity of ω_0 to variations of the values of the filter capacitors [dimensionless] [81].

A Maxim MAX4237B op-amp is at the heart of each of the two second-order sections that make up the active filter (U501 and U502). The MAX4237B is a very high precision, single-supply, rail-to-rail op-amp whose specifications (see Table 3.4) meet the requirements imposed by the active filter design. Also, due to its very low input offset voltage, the series combination of the two second-order sections will typically cause at most a 1.1 mV offset at the ADC's input, which is much less than 1 LSB.

SAR Coupling Circuit. The analog inputs of SAR ADCs do not behave as a static load but instead present a dynamic load that changes throughout the sampling process. Therefore, for optimum performance, an external interface circuit is needed in order to couple the signal to be digitized to the SAR input. [84]

The recommended coupling circuit consists of a buffer op-amp followed by a RC LP filter [85]. However, since the input signal for this stage is generated by one of the op-amps (U502) of the AA filter, the buffer op-amp can be ignored. The capacitor (C106) provides a nearly perfect input source for the ADC since it tracks the input

[2]Sensitivity is defined as the "measure of the vulnerability of a filter's performance to changes in component values". [82]

signal and charges the sampling capacitor, while the resistor (R105) isolates the op-amp's output stage from the capacitive load and the charge injection effects caused by the ADC [85].

The procedure for correctly sizing the RC components is detailed in [85]. The value of the capacitor C is related to the size of the ADC's sampling capacitor C_{SH} by means of the following relationship:

$$20 \times C_{SH} \leq C \leq 60 \times C_{SH} \tag{3.12}$$

Once a value for C is chosen, the resistor R can be selected using the following two equations:

$$R = \frac{1}{2\pi \times C \times f_Z} \tag{3.13}$$

$$R \geq \frac{R_O}{9} \tag{3.14}$$

where R_O = open-loop output resistance of the driving op-amp [Ω]. The quantity f_Z, which represents the zero that is added to the open-loop-gain curve of the op-amp, can be calculated using the equation:

$$f_Z = \frac{K}{2\pi t_{ACQ}} = \frac{\ln\left[\frac{2^{N+1}}{C/C_{SH})+1}\right]}{2\pi t_{ACQ}} \tag{3.15}$$

where N = ADC resolution, t_{ACQ} = ADC acquisition time [s].

As a result of this procedure, a 330 pF C0G/NP0 ceramic capacitor was selected for C and 5.6 kΩ resistor for R. The stability of the design was checked and found to be satisfactory according to Equations (12) and (16) in [85].

Microcontroller

The core of the device is composed of the Atmel ATmega1284P microcontroller. As it can be seen from Figure 3.6, the MCU has many onboard peripherals that simplify the design of an embedded system. The ATmega1284P was chosen to replace the ATmega32A from the previous version of the adapter since it has an additional 8-bit timer/counter, a universal asynchronous receiver/transmitter (USART) that can be used in SPI mode, and two times the amount of electronically erasable programmable read-only memory (EEPROM), which was intended to store 24 hours of aEEG.

The key hardware design considerations given by the manufacturer that were fulfilled are summarized below:

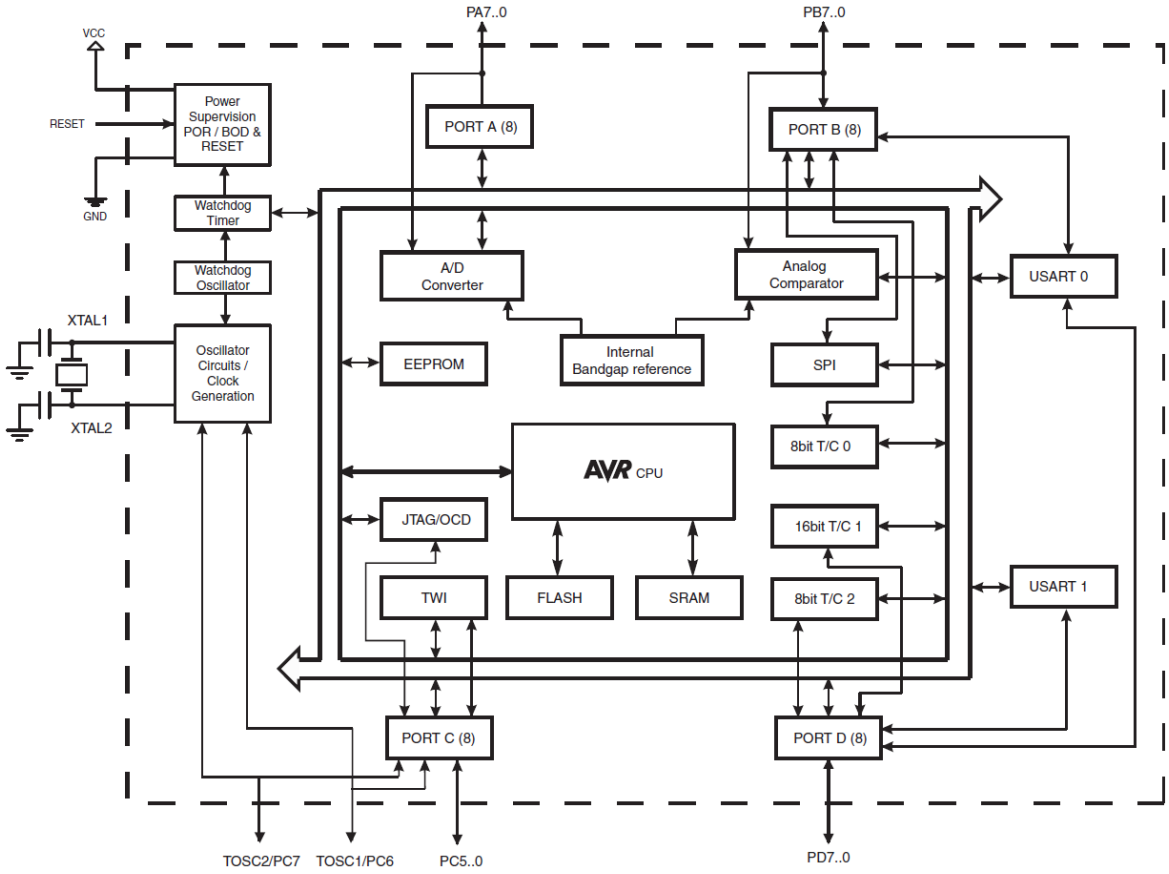

Figure 3.6: Functional block diagram of the Atmel ATmega1284P. *Reproduced from* [80].

- Every VCC pin is bypassed by means of small 100 nF ceramic capacitor (C100, C101, and C102).
- An LC network (L100 and C105) is used to connect the analog power supply (AVcc) to the AVCC pin.
- The RESET pin is pulled high and protected from noise by means of an external RC network (R100 and C103).
- The AREF pin to which the ADC's voltage reference connects is bypassed with a 100 nF ceramic capacitor (C104).

The MCU operates on an internal RC oscillator, which provides an approximate 8 MHz clock. Since the performance of the internal oscillator is voltage and temperature dependent, its frequency can be calibrated by means of an external oscillator. To this end, a 32.768 kHz tuning fork crystal with a ±20 ppm frequency tolerance is connected between pins PC6/TOSC1 and PC7/TOSC2.

Table 3.5: Mapping between USART pins in Master SPI mode and SPI control lines. *Reproduced from* [80].

USART	SPI	Comment
TxD	MOSI	Master Out only
RxD	MISO	Master In only
XCK	SCK	(Functionally identical)
(N/A)	SS	Not supported

Three of the analog input pins (PA0/ADC0, PA1/ADC1, and PA2/ADC2) are connected directly to the X, Y, and Z outputs of the accelerometer. The accelerometer lines were not interfaced to the ADC by means of SAR coupling circuits in order to save PCB space and to avoid increasing the current consumption of the adapter. Since only the average acceleration value over a pre-determined time period is important, any distortion that is introduced due to the lack of coupling circuitry will be attenuated. The EEG signal is connected to a fourth input (PA7/ADC7) by means of a SAR coupling circuit (R105 and C106).

In-circuit programmability is achieved via the on-board Joint Test Action Group (JTAG) interface. Its pins (PC2/TCK, PC3/TMS, PC4/TDO, and PC5/TDI) can be connected to an external programmer by means of a low-profile connector (P100). The same interface can also be used for the on-chip debugging of the firmware.

An Avago HSMF-C113 RGB LED unit (D100) is connected to pins PD5, PD6, and PD7. Each color can be turned on/off independently from the others. Resistors R102, R103, and R104 control the current that is driving the LEDs and thus their luminous intensity.

In order to optimize the PCB layout of the adapter, the PGA is controlled by means of the MCU's USART1 module running in Master SPI mode. The mapping between the USART pins and the SPI control lines is given in Table 3.5. Since the PGA features a 3-pin SPI interface with a single bidirectional data line (DIO), a 10 kΩ resistor (R101) is connected between the PD2/RXD1 and the PD3/TXD1 pins so as to allow the MCU to write to and read from the amplifier. When the MCU transmits data, the MOSI pin controls the DIO line since both the MISO pin and the PGA's transmission circuitry are in a high impedance state. On the other hand, when data is read from the PGA, the MCU stores either 0x00 or 0xFF in its SPI serial shift register, effectively pulling-up or pulling-down the DIO line, thus making it possible to read the data that is being transmitted by the PGA.

The functionality associated with pins PB0–PB4 and PD0 will be discussed in subsequent sections.

Capacitive Key. A capacitive key that senses touch through the adapter's enclosure has replaced the mechanical switch used in the previous adapter version. The key, which is connected between pins PB0 and PB1, starts/stops the EEG acquisition. The capacitive touch sensing is achieved by means of Atmel's QTouch library, which allows touch sensing to be performed on nearly all of Atmel's MCUs. As such, in addition to the MCU, the only other required hardware components are a sensor board that contains the touch-sensing electrode and an RC network. A schematic of the measurement system is shown in Figure 3.7. Although omitted from the figure, the resistor R is connected in series with the electrode and located as close to the MCU as possible.

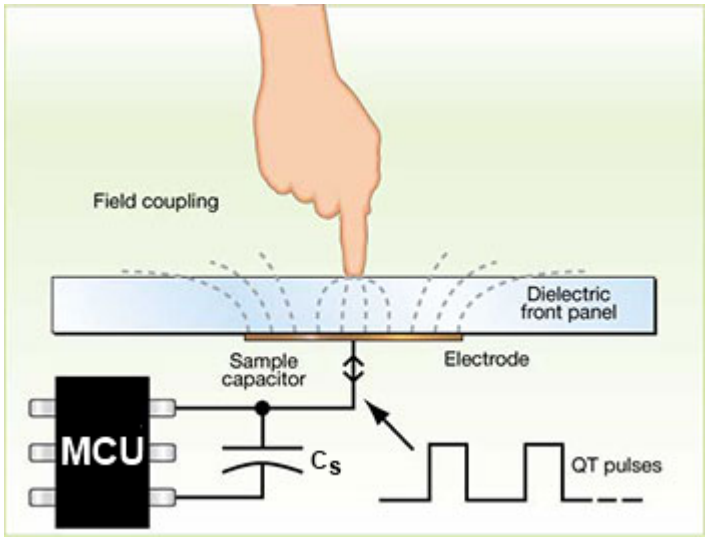

Figure 3.7: Capacitive touch sensing using the Atmel QTouch library. *Modified from* [86].

The capacitive sensing works on the principle of charge transfer. A series of voltage pulses are applied to the sampling capacitor Cs and the unknown electrode capacitance Cx until the voltage across Cs reaches a predefined level Vih. The number of pulses required to reach Vih constitutes the touch signal level. When a finger is placed on the dielectric above the electrode, additional capacitance is added. Thus, the amount of charge that is transferred with each voltage pulse is increased, which reduces the number of pulses required for Cs to reach Vih. As soon as the signal level decreases below a preset threshold, touch is reported to be detected. [86]

The sensor board consists of a 20 mm copper disc electrode on a FR4 substrate. Such an oversize electrode ensures good touch sensitivity through the 2 mm-thick walls of the adapter's ABS enclosure. The recommended values of 1 kΩ and 22 nF were used for R and Cs, respectively [86]. On the adapter PCB, the ground plane was removed

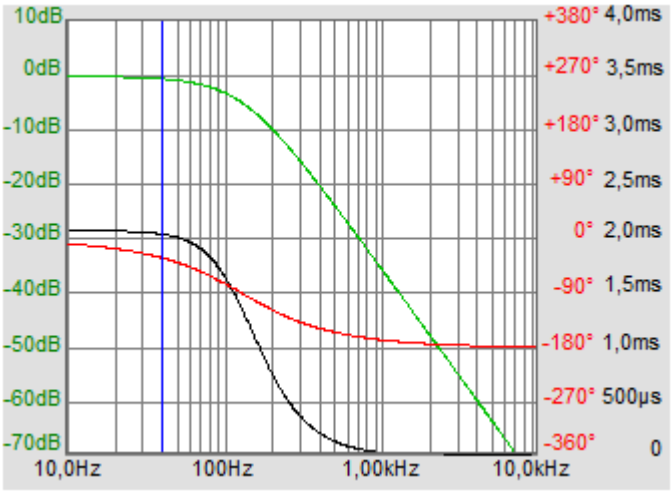

Figure 3.8: Frequency response (green), phase response (red), and group delay (black) of the 2nd order active PWM filter.

from underneath R so as to avoid the ground loading of the touch sensor [87].

PWM DAC

A DAC was included in the adapter design to generate a sinusoidal scale-indicator signal, the PP amplitude of which corresponds to that of a 100 μV input signal at the current gain level. This signal is displayed at the beginning of the recording and after each gain change. In order to avoid being attenuated by the filters present in ECG monitors, the frequency of the signal has to be in the 0.5–20 Hz range.

Seeing as though the ATmega1284P has a number of timers that can output PWM signals, the easiest as well as most cost- and space-effective way to add a DAc to the design was to filter the PWM signal with an analog LP filter. Under the right conditions, such a DAC can provide good accuracy and an excellent resolution [88].

The quality of a PWM DAC depends mainly on the LP filter. Hence, instead of filtering the signal with a passive RC network, as is common in many PWM DAC designs, a 2^{nd} order active filter is used. The filter features a Bessel frequency response (Figure 3.8) and is implemented using the Sallen-Key topolgy. This topology features a very accurate unity gain and a lower number of components than the MFB structure.

The exact signal chain is as follows. Immediately after the MCU's timer output pin (PB4/OC0B), a 2:1 voltage divider (R600 and R601) reduces the PP amplitude of the PWM signal to 1.5 V. This step is necessary in order to avoid signal distortions caused by the finite input range of real op-amps. Afterward, an op-amp in the unity-gain configuration (U600) buffers the signal prior to its filtering by the previously

Table 3.6: Key characteristics of the Maxim MAX4250. [89]

Parameter	**Value**			**Unit**
	Min	**Typ**	**Max**	
Gain-Bandwidth Product		3		MHz
Slew Rate		0.3		V/μs
Noise				
Input Voltage Noise Density (f = 10 Hz)		27		nV/$\sqrt{\text{Hz}}$
Input Voltage Noise Density (f = 1 kHz)		8.9		nV/$\sqrt{\text{Hz}}$
Input Current Density (f = 1 kHz)		0.5		fA/$\sqrt{\text{Hz}}$
Power Supply				
Voltage Range	2.4		5.5	V
Quiescent Current (Vdd = 3 V)		400		μA

described active LP filter (U601, R602, R603, C602, and C603). A 301:1 voltage divider (R604 and R605) further attenuates the amplitude of the signal to 5 mV_{PP}[3]. Finally, an analog switch (U301), which is controlled by the MCU through pin PD0, couples the output signal to the input of the C305-R301 HP filter.

U600 and U601 are both Maxim MAX4250 single-supply, low-distortion, rail-to-rail op-amps. This IC was chosen since it meets the requirements of the active LP filter and because of its excellent noise properties as well as low current consumption (Table 3.6).

The TI TS5A3159 single-pole double-throw (SPDT) switch was selected for U301 due to its small on-resistance (1.1 Ω) and minuscule current consumption (0.1 μA).

Since the scale-indicator signal must have an accurate amplitude, 0.1 % resistors were used for both of the voltage dividers.

Accelerometer

A three-axis accelerometer (U700), the MMA7341LC, is used to detect movements that may have an effect on the signal quality. The main reasons for this IC's selection were its extremely small package (3 mm×5 mm×1 mm) and low voltage operation (2.2 V–3.6 V).

[3]The choice of output voltage is explained in section 3.2.4.

In order to simplify the EEG-to-ECG adapter's PCB layout, the MMA7341LC's G-SELECT pin is grounded, which limits the accelerometer's range to 3 g, and the SELF TEST input is pulled low (R700). If desired, a test of the accelerometer can still be performed manually by removing R700 and mounting R701. The $\overline{\text{SLEEP}}$ input, which is connected to pin PB2 of the MCU, enables/disables the accelerometer's sleep mode. Each output line features a 3.3 nF capacitor (C701–C703) that reduces the clock noise induced by the switched capacitor filters present within the MMA7341LC.

Power System

Battery. The adapter is powered by a single-cell Varta PLF 263441 rechargeable lithium polymer (LiPo) battery, which has a nominal voltage of 3.7 V and a typical capacity of 380 mAh. An integrated protection circuit module (PCM) protects the cell from over-charging, over-discharging, and over-current conditions.

The battery can be recharged simply by connecting the adapter to a powered Universal Serial Bus (USB) port through the mini-AB USB socket (P201). A Maxim MAX1555 (U201) 1-Cell Li+ battery charger IC converts the +5 V input from the USB port, which is filtered by a 1 μF ceramic capacitor (C202), into a suitable power signal that can charge the LiPo battery. As long as the battery is charging, the IC's $\overline{\text{CHG}}$ status indicator pin is pulled low. Once the battery is fully charged, the pin goes into high impedance and the wire is pulled-up by resistor R200. For patient safety reasons, the level of the $\overline{\text{CHG}}$ wire is continuously monitored by the MCU through pin PB3[4].

Power Rail Generation. The Zetex ZXCL300 low-dropout voltage regulator (U200) generates the +3 V digital power rail (DVcc) rail with a maximum output current rating of 150 mA. According to the manufacturer's recommendations, a 1 μF ceramic capacitor (C200) filters the input and improves the ripple rejection while a 10 μF capacitor (C201) assures the stable operation of the regulator and decreases the output noise.

In order to keep digital nose from interfering with the sensitive analog part of the adapter, a Murata NFM21PC225B0J3D electromagnetic interference (EMI) filter (U302) separates the analog power rail (AVcc) from DVcc. The EMI filter is nothing more than a three-terminal capacitor that is specially designed to suppress noise on power rails. The half-AVcc rail is generated by means of a standard half-supply generator circuit consisting of a 2:1 voltage divider (R402 and R403), a bypass capacitor

[4]For more details, see section 3.2.4.

(C403) and a buffer op-amp (U401). Due to its excellent noise characteristics (see Table 3.6), the MAX4250 is used as the buffer op-amp. The 2:1 voltage divider is constructed with standard 0.1 % resistors in order to create an accurate voltage level.

Some additional filtering is performed in order to ensure that the power rails are as noise-free as possible. Murata BLM18A chip ferrite beads (F300 and F400) attenuate any high-frequency noise that may propagate on the half-AVcc rail from the exterior of the adapter through connectors P302 and P400. Also, bypass capacitors with a value of 100 nF located as close as possible to the supply pins of all ICs further filter the DVcc and AVcc power rails. Finally, the DVdd pin of the PGA (U400), which powers both the analog output stage of PGA and digital the SPI interface, is connected to the DVcc power rail through a NFM21PC225B0J3D filter (U402).

3.2.4 Embedded Software

The embedded software that runs on the ATmega1284P MCU and controls its operation is coded in the C language and downloaded into the MCU by means of the AVR Studio 4 integrated development environment (IDE) and the AVR Dragon programmer. All of the functions that facilitate the access to the MCU's peripherals are provided by the WinAVR open source software development kit [90].

Appendix A.2 contains the block diagram of the main routine while the complete source code can be found in Appendix C. The following sections describe the functions that are included in the block diagram.

Initialization State

Upon being powered up, or after a reset, the ATmega1284P performs a number of initialization steps:

- The MCU status register (MCUSR) is read in order to determine if a watchdog timer reset has occurred. If so, and if a region in the EEPROM indicates that the reset was brought about by the adapter being connected to a USB port, once all of the initialization steps are complete, the software will transition to the `Charging State`.
- MCUSR is cleared.
- Internal pull-up resistors on all I/O ports are disabled.
- Configure pin that controls the analog switch as an output pin and set switch in its "normally closed" position.

- Initialize accelerometer by configuring the MCU pins that are connected to its control lines as outputs. Subsequently, the IC's sleep mode is enabled so that it doesn't consume current while unused.
- Internal RC oscillator is calibrated by means of the external 32.768 kHz crystal.
- Set clock division factor to 2 in the clock prescale register (CLKPR) so that the MCU runs at 4 MHz.
- Enable watchdog in the system reset mode with a 2 sec time-out.
- Configure pins that are connected to the RGB LED as outputs.
- Initialize PGA. In order to communicate with the PGA, the MCU's USART1 is used in SPI mode 0 with a baud rate of 1 MHz. The gain is set to 8 V/V.

During the initialization process, all the three LEDs are turned off.

Standby State

After the initialization steps are completed, unless a USB connection has been detected, the system enters a standby state in order to conserve battery power. This state is also activated if the user presses the start/stop key while the system is in the `Recording State`.

During this state, the accelerometer's sleep mode is activated and the MCU enters a low-power sleep mode in which the majority of its peripherals, including the calibrated RC oscillator, are turned off. Every 1 sec, an interrupt triggered by Timer/Counter2, which is running asynchronously with the 32.768 kHz crystal, wakes the MCU so that the status of the start/stop key can be checked. If touch is detected for a minimum of 5 sec and a maximum of 5.5 sec[5], the MCU will transition to the `Recording State`. Otherwise, it will re-enter the low-power sleep mode. In order to aid the user with touching the key for the required amount of time, the blue LED starts flashing as soon as touch is detected. Once 5 sec have elapsed, the blue LED stays on continuously.

While in this state, all the three LEDs are turned off, except when touch is detected.

Recording State

The `Recording State`, which is indicated by a flashing green LED, consists of three different phases: setup, sampling, and status checking. During the setup phase, which

[5]The upper limit is needed in order to detect unintentional touch, i.e., when an object unintentionally contacts the sensor.

occurs when the recording state is entered, all of the required peripherals and software modules are initialized and configured. Afterward, the execution alternates between the sampling and status checking phases.

As implied by its name, while in the sampling phase, new EEG and accelerometer data samples are acquired, processed, and analyzed. In the case of the accelerometer signals, the data samples of each axis are grouped into 200 msec windows and the interval average acceleration[6] over each window is computed. If the average acceleration in any of the three axes exceeds a threshold, which will be determined empirically during testing, the red LED will start flashing.

The new EEG samples are analyzed by a software module that determines whether the gain of the adapter needs to be increased or decreased according to the following algorithm. The data samples are grouped into 1 sec windows and the maximum PP amplitude over each window is calculated. If the calculated value is inferior to the lower threshold associated with the current adapter gain (see Table 3.7), the gain level is increased by one step. On the other hand, in order for the gain to be decreased, the maximum PP amplitude must exceed the upper threshold for two consecutive windows.

Table 3.7: Lower and upper peak-to-peak signal amplitudes that cause increases/decreases of the adapter gain as a function of the adapter gain level.

Gain (V/V)	**Lower Threshold (μV_{PP})**	**Upper Threshold (μV_{PP})**
6.25	400	-
12.50	200	400
25.00	100	200
50.00	-	100

During the status checking phase, which starts after all of the new signal samples have been processed and analyzed, the amount of time since the start of the recording state and the status of the capacitive key are checked. If 1 min or more has elapsed since the recording state was entered, a flag indicating that the MCU should transition to the `Display Scale State` is set. However, if touch is detected for a minimum of 1 sec and a maximum of 1.5 sec, the previous flag is overridden and the MCU will instead transition to the `Standby State`.

[6]The interval average acceleration is used to detect net accelerations that last equal to or greater to the time interval over which the average is computed. [91]

Display Scale State

In this state, the PWM DAC outputs a sinusoidal scale-indicator signal with a frequency of approximately 15 Hz and an amplitude equivalent to an 100 μV input signal at the present gain step. For example, when the adapter gain is set to 25 V/V, the output signal is 2.5 $\mathrm{mV_{PP}}$ since 2.5 $\mathrm{mV_{PP}}/25 = 100\,\mu\mathrm{V}$. The PP amplitude of the scale-indicator signal associated with each gain step is indicated in Table 3.8.

Table 3.8: Amplitude of the scale-indicator signal as a function of the adapter gain.

Gain (V/V)	**Scale-Indicator Amplitude ($\mathbf{mV_{PP}}$)**
6.25	0.625
12.50	1.250
25.00	2.500
50.00	5.000

By design, if the PWM signal being outputted by the MCU has a PP amplitude of 3 V, the signal at the DAC's output will have an amplitude of 5 mV. Hence, in order to be able to generate the scale-indicator signals for the three smallest gain levels, the PP amplitude of the PWM signal generated by the MCU is reduced appropriately.

Flashing red and green LEDs serve as a visual indicator for this state. After the scale-indicator signal has been displayed for 5 sec, the MCU transitions back to the `Recording State`.

USB Connection Detection

Except for the initilization and charging states, Timer/Counter2 is used to check the status of the $\overline{\mathrm{CHG}}$ wire every 25 msec. If a logic low level is detected, a location in the EEPROM is written in order to indicate that the presence of a USB connection has been detected. Subsequently, an infinite loop will cause the watchdog to reset the MCU. Once the steps of the `Initialization State` are complete, the MCU will transition to the `Charging State`.

Charging State

Throughout this state, which is indicated by keeping the red LED continuously lit, the status of the $\overline{\mathrm{CHG}}$ wire is checked every 500 msec. As soon as a logic high level is detected, the MCU transitions to the `Standby State`.

3.3 6-channel System

3.3.1 Overview

The 6-channel system consists of three separate entities: an EEG cap into which the measurement electrodes are embedded, a wireless EEG (WEEG) system that records the signal and transmits it wirelessly to a computer, and a PC software that can be used to visualize, store and transmit the recorded data. The WEEG system itself is sub-divided into the portable measurement unit (PMU), which is located in the EEG cap, and the computer interface unit (CIU) that is permanently connected to the measurement computer. The Panasonic Toughbook CF-19, which is the most commonly used laptop in ambulances in the Helsinki district, is used as the measurement computer.

A block diagram of the system is shown in Figure 3.9, while the schematics of the PMU's analog front end and those of the CIU are included in Appendix B.1 and Appendix B.2, respectively. Each of the three blocks are discussed further in subsequent sections.

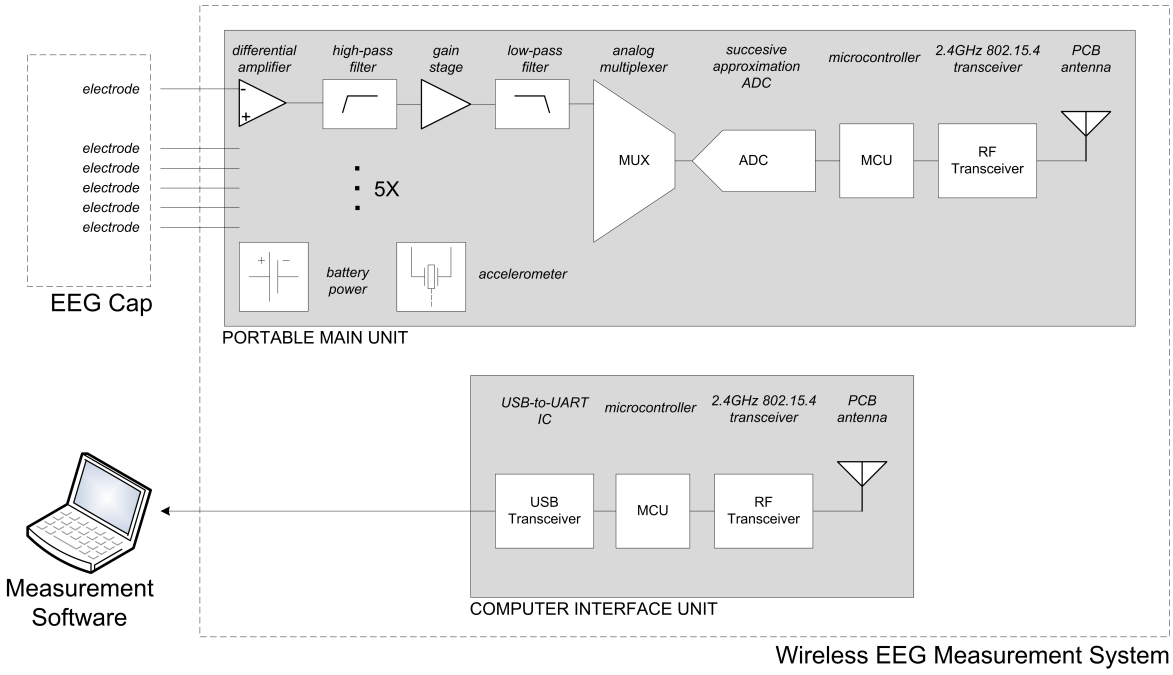

Figure 3.9: Block diagram of the 6-channel system.

3.3.2 Wireless EEG System

Past Work

Several versions of the WEEG system have been designed and constructed by a research group from the Department of Automation Science and Engineering headed by Professor Jukka Lekkala. M.Sc. Timo Salpavaara developed the signal recording electronics and B.Sc. Jarmo Verho was responsible for the wireless interface and the devices' firmware.

As it can be observed in Figure 3.9, the design of the PMU follows that of a typical EEG bioamplifier, which was described in section 2.3.2. Even though it has been omitted from Figure 3.9 for clarity purposes, the input of each channel possesses a transient protection circuit consisting of a series resistor and two clamping silicon diodes. The EEG signal is pre-amplified by means of an IA. Any DC offset that may be present at the output of the IA is removed by means of a HP filter ($f_c \approx 0.16\,\text{Hz}$), prior to the signal being further amplified. After LP filtering ($f_c \approx 116\,\text{Hz}$), the EEG signal is digitized by a SAR ADC. The signal samples are then grouped into packets by the MCU and transmitted wirelessly to the CIU, which transfers them to the measurement computer.

The previous version, i.e., version 3, of the WEEG system (WEEG3) is pictured in Figure 3.10. The system was able to measure 6 channels of EEG as well as dual-axis acceleration for the identification of movement artefacts. The recorded data was transmitted to a measurement computer by means of a wireless protocol that was built upon the IEEE 802.15.4 standard. Since the 2.4 GHz industrial, scientific and medical (ISM) radio band employed by the WEEG device is reserved internationally for industrial, scientific and medical purposes other than communications, it was possible to use the device worldwide. Both the PMU and the CIU featured an on-board inverted F microstrip antenna in order to transmit and receive the 2.4 GHz signal. The PMU was powered by a 9 V PP3 primary battery while the CIU drew power from the USB port.

Version 3 of the WEEG system suffered from a number of shortcomings. The PMU was composed of two plastic boxes, one of which contained the analog circuitry while the other enclosed the digital section and the power source. This configuration was due to the large connector that was used to connect the electronics and the electrodes together, as well as due to the desire to make the PMU comfortable for the patient by allowing it to follow the contour of the head. However, the resulting device was large and also heavy, especially given the usage of a PP3 battery as the power source.

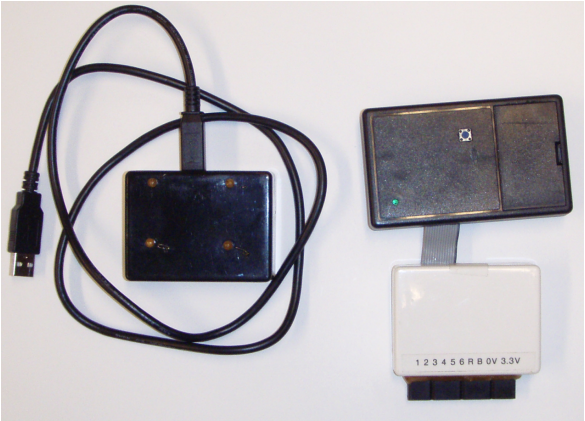

Figure 3.10: CIU (left) and PMU (right) of the WEEG3 system.

Finally, since the CIU was external to the measurement computer and was connected to it by a relatively long USB cable, the chances were high that it may be ripped out of the computer or that it may be damaged during regular use in ambulances or ERs.

Development of a New Version

As part of this thesis work, the author worked together with Prof. Lekkala's group and spearheaded the development of a new WEEG system that would overcome the aforementioned problems. The author's contributions are described in the following paragraphs.

CIU Add-in Card. Since an external CIU is not a reliable solution, the decision was made to develop it into a computer add-in card module so that it can be safely housed within the measurement laptop. The two most common interfaces in modern computers for add-in cards are PCI Express Mini (Mini PCIe) [92] and ExpressCard [93]. A comparison between the dimensions of the cards formats belonging to the two specifications is presented in Table 3.9.

Table 3.9: Card form factors belonging to the Mini PCIe and ExpressCard specifications.

	ExpressCard		**Mini PCIe**	
	34	54	Half-Mini	Full-Mini
Height (mm)	75.00	75.00	30.00	30.00
Width (mm)	34.00	54.00	31.90	58.05
Thickness (mm)	5.50	5.50	5.00	5.00

The Mini PCIe interface provide direct access to the USB 2.0 bus as well as a 3.3 V power connection, which would facilitate the conversion of the existing CIU to the new form factor. This interface holds the size advantage since both of the its card formats are smaller than either of the ExpressCard modules. However, given that Mini PCIe was originally intended for wired and wireless communication applications in mobile computers, these cards were not meant to be easily end-user-replaceable [92] and thus the Mini PCIe slot is usually located in a hard-to-reach area, deep within the computer. This location would preclude the use of a PCB antenna, since the computer's shell might induce high RF losses [94], and it would make the CIU hard to service. Furthermore, it is nearly impossible to connect such cards to a desktop computer.

The ExpressCard interface also offers an USB 2.0 connection and a power connection but it doesn't share any of Mini PCIe's disadvantages. Seeing as though the interface was developed to offer a standardized method of connecting peripheral devices to computers, the ExpressCard slot of a laptop is always located on one of the sides where it is easily accessible. In the case of desktop computers, inexpensive PCI-Express adaptors are available commercially that add an ExpressCard 34/54 slot to the computer. Furthermore, since the back of a card can extend outside of the computer, a PCB antenna could still be employed to communicate with the PMU.

In conclusion, due to the advantages of the ExpressCard format, the new version of the CIU is an ExpressCard module.

CIU Antenna. As mentioned previously, ideally, the CIU would be completely housed within the measurement computer; however, the presence of the microstrip antenna made this goal impossible. Therefore, an alternative solution was sought out.

Almost all of today's laptops come with a built-in wireless local area network (WLAN) card based on the IEEE 802.11 standard. The three most common 802.11 protocols nowadays are 802.11b, 802.11g and 802.11n, all of which operate in the 2.4 GHz frequency band. Therefore, most of today's laptops have a built-in 2.4 GHz antenna. In order to improve the signal strength, some laptops have two antennas, while laptops with 802.11n WLAN cards have as many as three. Since these antennas are designed to operate in the same frequency band as the CIU-PMU wireless link, it is logical to assume that the CIU could make use of one of the on-board WLAN antennas.

In RF systems, one must ensure that the characteristics of the antenna match those of the transceiver. In particular, the output impedance of the transceiver must be equal

to that of the antenna so that maximum power is delivered to/from the antenna [95]. Therefore, if the CIU is to use the WLAN antenna, its impedance must match that of the inverted F antenna, which is 50 Ω [96]. Fortunately, all three 802.11 protocols that operate in the 2.4 GHz bandwidth specify an impedance of 50 Ω for the transmit and receive antenna port(s) [97], [98]. Hence, as long as the cable that establishes the connection to the built-in antenna and any intermediary connectors have an impedance equal to 50 Ω, in theory, the CIU could use one of the WLAN antennas to communicate with the PMU. Since this approach has never been attempted before, the microstrip antenna was kept on the CIU's PCB as a backup measure.

PMU form factor. In order to make the PMU lighter and more compact, the two separate enclosures had to be combined into one. This necessitated the placement of the analog and digital parts on one compact PCB, the replacement of the PP3 battery, and finding a new, smaller connector. This last task proved to be a challenge.

In order to be considered defibrillator-proof, the new connector must obey the minimum clearance and creepage distance[7] required by the IEC 60601-1 standard. According to the 2005 revision of the standard, a minimum clearance and creepage distance of 4 mm must be maintained [73]. Also, the insulation must be able to withstand a 5 kV defibrillator pulse. However, a connector with these properties could not be found in the inventory of the university's electronics suppliers. Even if such a connector would have been found, it most likely would have been prohibitively large, seeing as though a typical connector with 8 loaded circuits, a voltage rating of 300 V, a minimum clearance distance of 2.5 mm and a minimum creepage distance of 4.0 mm has a width of 40.64 mm [99]. In addition, since the literature does not contain any information about the effects of a defibrillator pulse on scalp electrodes, it is not clear if such stringent requirements are indeed required for the PMU connector.

The connector that was finally chosen is the Molex SPOX™. It features clearance and creepage distances of 2 mm and a voltage rating of 250 V. Furthermore, the header is fully shrouded and locks to its mating part, which ensures a strong mechanical connection. Additional relevant properties of the connector are presented in Table 3.10.

[7] Clearance distance is defined as the "separation of two conductive parts by air alone". Creepage distance is defined as the "separation of conductive parts on a nonconductive plane, e.g., tracks on a printed circuit board". [76]

Table 3.10: Relevant properties of the Molex 2.50 mm pitch SPOX header.

Property	Value
Durability (max. mating cycles)	30
Lock to mating part	Yes
Plating	Tin
Number of rows	1
Orientation	Right angle
Polarized to mating part	Yes
Shrouded	Fully
Operating temperature range (°C)	-40 to +150
Termination interface	Through hole
Maximum current (A)	3
Maximum voltage (V)	250

3.3.3 PC Software

The development of the PC software that processes, displays and stores the data recorded using the WEEG device was started by Mika Pänkälä [71] as part of his M.Sc. work. Initially the WEEG system was meant to be controlled with a User Datagram Protocol (UDP) socket interface, an architecture that would have allowed the WEEG software to be written in any programming language and to run on any operating system, as long as both of these supported UDP sockets. However, this architecture proved too challenging to implement on the WEEG microcontroller and therefore the idea was abandoned. Instead, it was decided to employ a USB interface and implement the measurement software using the C programming language on the Microsoft Windows platform.

The software developed by Pänkälä was very rudimentary. It featured a simple user interface that consisted only of a menu bar, a status bar and the signal area. From the menu bar, one was able to start/stop the measurement, and configure the system parameters, e.g., sampling frequency, transceiver power, and register patient information. While a recording was in progress, the status bar displayed the sampling frequency, the number of data packets received from the CIU as well as the status of the PMU's battery. The signal area was divided into three distinct sections. The top 70% was allocated for the display of the EEG signals in the referential montage while the remaining 30% was divided into two side-by-side panels, one of which displayed the data received from the accelerometers while the second was used to show the possible annotations that can be added to the recorded data and also to select the EEG vertical sensitivity. The raw recorded data was stored together with the annotations and the

patient information in an EDF+ file.

The software also lacked some more advanced features such as digital filtering, a way to control the length of data displayed data, a means to save technical information about the recording as well as a means to easily transfer the data away from the measurement computer. Also, it was computer-resource-intensive since the whole screen window was redrawn every time there was a new data point, which also led to flickering. Furthermore, the software's robustness, usability and fault-tolerance, which are all important elements in medical software, were not optimal. Clearly, if the WEEG system was to be used in the field, a more advanced software was required.

The new features of the software as well as any improvements of existing functionality are described in the next sections.

Graphical Elements

Signal Display. One of the most important of the new features is the way the EEG signal is displayed on the screen. A new more flexible and lean drawing routine was coded, which draws the signals in the in the same manner as the signals on ECG monitors are drawn, i.e., from left to right with only small portions of the old signal erased at any one time. Thus, the drawing function only redraws the area of the screen where a new data sample is to be placed. In addition to being less resource intensive than the previous algorithm, the new function eliminates the flickering problem. Also, the program window can now be resized freely since the its size is checked every time the function is executed.

In accordance with the ACNS recommendations, a user-selectable horizontal scaling control has been added, which allows the technician to select the signal length in seconds that is displayed at any time during the recording. This option is a digital version of the traditional paper-speed control that is found on paper recorders.

Digital FIR LP filters were added to the software in order to remove high-frequency artefacts present in the EEG data so as to aid the caregiver in the interpretation of the data. The design and testing of the DSP filters are described in [100]. Similar to the horizontal scaling control, the DSP filter can be changed at any time during the recording. Although initially it was planned to also include HP filters and a 50/60 Hz notch filter, since the sharp frequency response required of the HP filter would have induced a significant delay, while the notch filter with its non-linear phase would have induced signal distortions in the gamma band of the EEG signal, these filters are not included in the final software version.

Graphical User Interface. The graphical user interface (GUI) is arguably one of the most important aspects of a computer software since the user's impression of a program is shaped by his interactions with the GUI. Therefore, a significant amount of effort was dedicated to creating a GUI that is as intuitive and as easy-to-use as possible while at the same time making it possible for the software to be controlled only with a touch screen.

Two toolbars have been added to the top of the main window in order to easily give the user access to all of the program's features without having to go through the menus. The first toolbar features buttons with colorful and easy-to-recognize icons that give access to all of the program's auxiliary windows. The buttons are large enough so that they can be pressed with one's index finger when a touch screen is employed. The vertical and horizontal scaling, as well as the LP filter are selectable from drop down lists located on the second toolbar, which is situated immediately under the first. Some items, which should be accessed during the recording process, e.g., the system parameters, are disabled prior to the start of the recording. Similarly, those options which are not useful when a recording is not in progress, e.g., patient information, are disabled at software startup and once a recording is complete.

A "Full-Screen" mode similar to that found in many web browsers has been implemented. The purpose of this feature is to maximize the amount of screen space available for displaying recorded signals while offering a very simplistic GUI. To this end, when entering the full-screen mode, the two toolbars and the menu bar are hidden and the signal display area is extended until the window's title bar. In this mode, the only graphical way to control the software is through the system menu, which is accessed by left-clicking the program icon, and which contains commands for entering/exiting the full-screen mode and for starting/stopping the recording.

The functionality of the status bar has been improved. In the present version, it is divided into four panels. The fist panel displays throughout the recording an estimate of the length of signal (in units of hours:minutes:seconds) that can still be recorded based on the selected sampling frequency and the space available on the storage device. The second panel displays the last annotation that has been made, as well as the time-offset (in seconds) from the beginning of the recording at which it was made. The final two panels are used to indicate the status of the PMU's battery, with the first panel depicting the status graphically while second displays a status text.

Finally, a number of usability improvements have been made to facilitate the control of the software. A keyboard shortcut was assigned to every user-interface element, e.g., `Ctrl + S` starts/stops the recording, `Ctrl + Q` quits the program. Since some

functions are only available during the recording, an effort was made to reuse the shortcuts in order to reduce their number, e.g., `Ctrl + P` is used to open the *Parameters* window when not recording while it opens the *Patient Information* window during a recording. The method for adding annotations to the recording has also been upgraded. Now, in addition to keyboard shortcuts, it is possible to enter an annotation by left-clicking or by touching the screen anywhere in the signal display area and selecting an annotation from the menu that appears. This feature is useful for computers that lack keyboards, e.g., tablet PCs, or when the user does not remember the necessary keyboard shortcut and wants to enter an annotation quickly.

Auxiliary Windows. The software's auxiliary windows allow the user to change operating parameters, perform data entry and obtain information about the software itself. Two new windows were added while two others were updated with new features.

In the past version, the annotations a section of the main signal display area was reserved for the display of the annotations. In the current version, the annotations are displayed in a separate floating window that appears only if the user presses on the appropriate toolbar button. In order to minimize that screen area taken up, the window is adaptive in that it resizes horizontally to match the length of the longest annotation and vertically so that annotations that do not have a text associated with them are not displayed.

A *Recording Information* window has also been added. Since the EDF+ specification made provision for a recording information field in the header of the file, it was fairly straightforward to implement this feature since only the UI had to be created. Accessible only while a recording is in progress, this window allows the technician to store information about the recording, e.g., recording number, recording device identification, in the same file as the recorded data. Free-form comments can also be typed-in. Since the field has a fixed size, only a limited amount of characters can be stored. Thus, the user is continually informed of the amount of remaining space by means of two textboxes.

The *Patient Information* and *Parameters* windows were updated in order to make data entry easier and to reflect the new features of the software. In the case of the *Patient Information* window, the `Tab` key can be used to move the cursor sequentially through the various data fields, while the `Enter` and `Esc` key can be used to save or cancel, respectively, the changes that have been made in the window and then close it. Also, a textbox at the bottom of the window informs the user of the amount of characters that can still be typed in.

The *Parameters* window is now separated into four tabs. Except for the transmitter power option, which has been removed, the *Settings* tab contains all of the configuration options that were present in the past version of the *Parameters* window. Whenever a new destination folder is selected, the program checks if the user has the appropriate write permissions for the location. If the folder is valid and the permissions are correct, the maximum possible recording length in hours and minutes is calculated based on the amount of free space on the disk where the folder is located. This information is displayed to the user in a textbox immediately underneath the destination folder. A second tab entitled *Viewable Screen Size* allows the user to adjust the markings of a vertical ruler displayed on the screen with the cm markings of a real ruler. This type of calibration is also found in commercial EEG software such as Nicolet One and is necessary in order to have an accurate vertical sensitivity setting, which has units of μV/cm, since the number of pixels per cm in the vertical direction varies between different monitors. The *SSH Configuration* tab allows one to configure the settings related to the upload of the measurement data, as described in the following section. The *Annotations* tab, from where the annotations texts can be edited, constitutes the fourth and final tab.

Operating Modes

In addition to the standard recording mode in which the EEG signals are displayed, two new operating modes have been added: aEEG and simulation.

aEEG Mode. The aEEG mode can be entered at any time simply by pressing on the identically-named button on the first toolbar. As is implied by its name, in this mode, the aEEG signals that are computed in real-time from the raw EEG of each channel are displayed[8]. While the aEEG signals are displayed in a similar fashion to the raw EEG signals, some differences exist. First, since the aEEG signal is already appropriately processed and scaled, the vertical scaling, the horizontal scaling, and the LP filter drop down lists are disabled. Second, two horizontal amplitude markers are used to indicate the 10 and 60 μV levels for each channel. Finally, a number of vertical lines are used to indicate one hour intervals. In order to prevent these time indicators from changing position every time the aEEG signal reaches the right edge of the program window, the number of one-hour intervals that can fit in one window is calculated whenever the window is resized; only as much aEEG data as can fit in those intervals is displayed before the rendering of the signal recommences at the left

edge of the window.

The aEEG signals are not stored since they can be easily recomputed by means of commercial EEG analysis software once the recording is complete.

Simulation Mode. For testing the functionality of the software, such as the digital signal processing (DSP) routines, or the signal display, it is useful to have a means to playback a deterministic test signal and compare the results to that which was expected. To this end, a method to use previously recorded EDF+ files as the software's signal source was implemented. This feature was coded in such a way that only the signal source changes in the simulation mode and nothing else, i.e., the software's other functions remain intact.

This feature would not be needed while the system is in use in the field and therefore it is only available after the software is compiled with the `SIMULATION` preprocessor macro definition. If this macro is defined, a new menu item titled *Load EDF+ File* appears in the *File* menu. Once an appropriate file has been loaded, the playback can be started in the same way as a recording would normally be started.

Software Architecture and Design

Automatic Upload of Measurement Data. In past versions of the software, no automatic means existed for the transfer of the recorded data away from the measurement computer. If the system were to have been used in an ambulance, upon the patient's arrival at a medical center the recorded data would have had to be transferred manually. Hence, the current version supports the automatic uploading of the measurement data at the end of the recording.

The Secure Shell (SSH) protocol was chosen for the upload of the data. Its selection was based on three factors. First, since it is a secure protocol intended to provide security and data integrity over an unsecure network, all of the traffic is encrypted and both the server and the user are authenticated prior to the start of the communication [101]. Second, SSH implementations exist for all major server operating systems, i.e., Windows, Linux, and Unix [102]. Third, the existence of open-source SSH client library libcurl made it straightforward to add SSH functionality to the software [103].

The upload feature is enabled from the *SSH Configuration* tab in the *Parameters* window. From the same tab, the user can set the address of the server, its port and the path where the data should be stored. If desired, login credentials can be securely

[8]The exact implementation of the aEEG algorithm is discussed in section 3.5.

stored in order to make the upload completely automatic. Otherwise, prior to the uploading of the data, the software will prompt for a user name and password.

WEEG Hardware System Check. It is a commonly-accepted truth that even the best designed hardware will fail at some point whether due to discharged batteries, loose connectors, firmware crashes, or other reasons. In order to detect possible hardware failures, a function was added that allows the software to check the status of the WEEG system.

The function is able to detect the following error conditions:

- unavailable CIU, whether due to disconnection or firmware error
- access to the CIU serial port is denied
- undetectable or unresponsive PMU
- excessive checksum errors.

Possible remedies are suggested to the user in a pop-up window according to the error condition which was detected. In addition to its diagnostic features, the routine can also automatically detect the serial port number of the CIU. If more than one possible port is found, the user is asked to select the correct one from the *Parameters* window.

The function is called more than once during program execution. It is executed during the start-up process of the software and also whenever the operating system detects a change in the serial port configuration of the computer. The user can also call the function manually by clicking the appropriate button on the toolbar. No matter how the routine is called, after the status of the WEEG system is checked, the toolbar button's icon is updated in order to reflect the status of the system, with a blue checkmark indicating that the system is operational while a red 'x' indicates that an error condition has been detected.

Asynchronous Input/Output. Arguably one the most common input/output[9] (I/O) model used in applications is synchronous I/O [104]. In this model, once an I/O request is made, the application waits until it is completed [105]. In the case of writing data to the hard disk drive (HDD), the application waits until the write request completes. This I/O model was also being used in past versions of software. Once the sampling thread obtained data from the CIU, it would execute a write command and wait for its completion. Under normal operating conditions, this model would not cause any problems. However, some modern laptops, especially those that

are ruggedized, features a HDD protection system that parks the disk's read/write heads automatically, effectively causing all HDD activity to cease, if excessive motion is detected. Since the writing was done synchronously from the `Sampling` thread, the thread would be blocked for an arbitrary amount of time, which led to lost data samples.

In order to overcome this shortcoming, the new version of the software employs asynchronous I/O. In this model, an I/O request is initiated in a similar manner to the synchronous I/O by calling a write function. However, in this case, the function returns almost instantly with information about whether or not the operating system (OS) has accepted the request. If the request has been accepted, the calling thread can continue executing until the OS signals that the I/O operation is complete. The thread must then interrupt its current job and process the completion information from the I/O operation. Since this additional task would complicate the design of the sample thread, an additional thread was created specifically for I/O, as described in the next paragraph. [105]

Multithreading. In a multithreaded program, multiple streams of instructions are executed concurrently with each stream usually handling a different task [107]. This programming paradigm affords two main advantages. Naturally independent control flows, such as the rendering of GUI and communication with a peripheral, can be separated into independent threads. On top of facilitating the design of the software, this separation also improves performance, since a relatively slow task does not affect other parts of the program, e.g., accessing a peripheral does not slow down the GUI [108].

Past versions of the software already made use of this paradigm by employing two threads. A `Sampling` thread received data from the CIU and stored it on the HDD while the `Main` thread handled the GUI and all other program functions. As mentioned previously, asynchronous I/O requires the calling thread to perform some additional processing once the I/O request completes. Therefore, a `Storage` thread was created that handles all I/O-related operations. The thread operates as a finite-state machine (FSM); its state diagram is displayed in Figure 3.11.

In order to keep logically separate tasks independent from each other, the automatic uploading of measurement data is carried out by the new `Upload` thread, which is started at the end of a measurement and exits once the data transfer has finished.

[9] I/O is a term that is "used to describe any program, operation or device that transfers data to or from a computer and to or from a peripheral device. Every transfer is an output from one device and an input into another." [106]

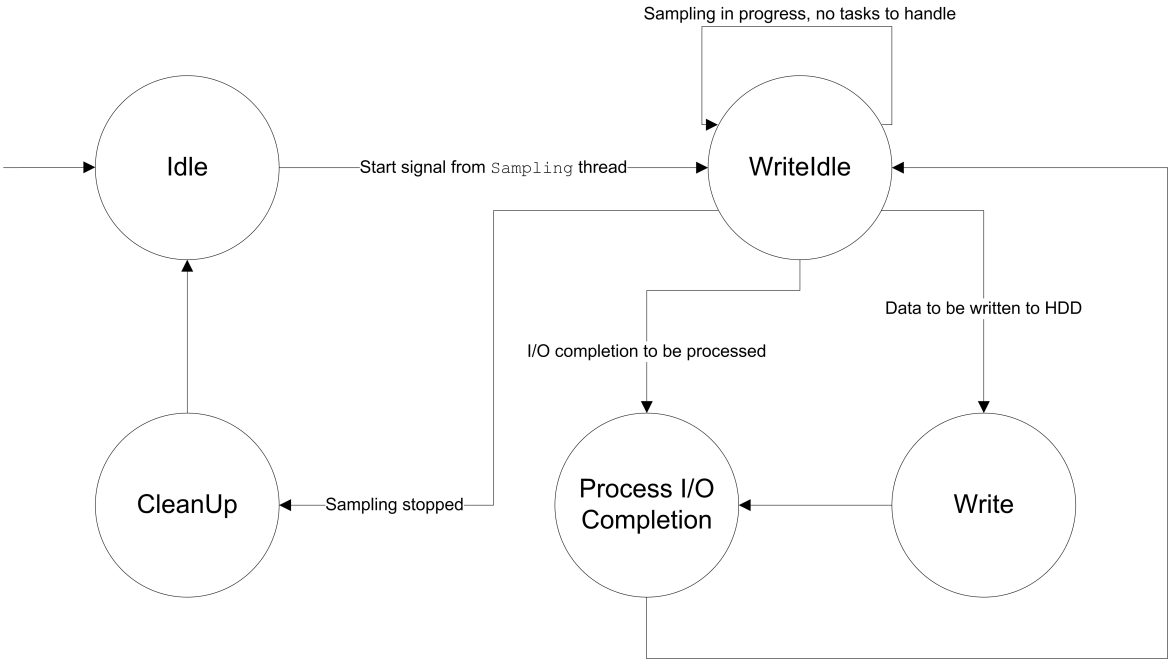

Figure 3.11: State diagram of the PC recording software's storage thread.

This separation also allows the GUI to display the status of the upload in real-time.

Application Logging. An effective logging strategy is central to the tackling of software bugs, especially in the later stages of the development cycle when the bugs are more intricate and difficult to discover [109]. Although logging can also be used for performance and security tuning, in the present case only a debugging log was required and thus the resulting logging strategy is quite straightforward.

At software startup, a new log file is created and the version of the software as well as the versions of the external libraries are logged. Subsequently, all handled software exceptions from all of the program's threads and all hardware errors conditions detected by the WEEG system check are logged. Whenever a message needs to be logged, it is first categorized as a software error, a hardware error or version information. Then, the thread as well as the exact function where the message originated are recorded. Finally, the message is stored together with any relevant error number generated by the OS or by the software library.

The logs are saved in Extensible Markup Language (XML) files by means of the libxml2 XML C parser library [110].

Reliability Fine-Tuning. In order to improve the reliability of the software, a number of important modifications were made. First, the Windows screen saver is

now automatically disabled for as long as the software is running, and the system is prevented from entering sleep mode or turning off the display.

Second, the priority of the process has been set to "high" while the priority of the `Sampling` thread was set to the highest possible value, i.e., time critical [111]. The combination of these two factors maximizes the amount of CPU time assigned by the operating system to the `Sampling` thread, thus allowing for a nearly real-time operation of the system thus reducing the risk of a bottleneck between the CIU and the software. In addition, even though all other threads have normal priority, the elevated priority level of the process ensures that the software is highly responsive overall.

Utilities

EDF File Editor (EFE). The purpose of the EFE is to allow the technician to easily correct errors or omissions in the patient or recording information after the measurement has been stopped. The EFE application is accessible from the *Utilities* menu.

Software Installation Utility. The installation utility is tasked with the installation of all necessary external components that will allow the PC software to run correctly on any machine that has a Windows operating system newer than XP SP1. During the installation process, the utility installs the USB drivers required to interface with the WEEG's CIU, checks and installs if necessary the .NET framework 2.0, places the executable of the software and of the EFE in a common location, and creates shortcuts both on the user's desktop and in the *All Programs* menu.

3.3.4 Quick-Application Cap

Past Work

A quick-application EEG electrode cap that can be used by doctors, nurses and EMTs both in a hospital environment as well as for prehospital care must meet a number of requirements. It must be as easy and as fast to apply as possible, so that it won't unnecessarily delay the care-giver. Hence, little to no preparation time is required. The cap must also not interfere with other emergency care procedures. Once it has been affixed to the patient, it must remain immobile under all circumstance until its use is no longer required. Last but not least, the cap must provide support for the WEEG device and reduce the chance for damage.

An initial version of such a quick application electrode cap that can be used by non-EEG specialists was designed by M.Sc. Aino Salmi [70]. The cap was constructed with polyester-based materials that could be easily sterilized, either by washing or by wiping with detergent. In order to allow for different head shapes and sizes, the cap consisted of four separate parts that were interconnected by adjustable Velcro straps. Also, the majority of the materials were elastic so that the cap would still feel comfortable even if it was placed tightly on a person's head. This version of the cap could be applied in under two minutes. Based on the location of the cap's bands, the best electrode locations were determined with finite element modeling (FEM) by Dr. Katrina Wendel [112]. The chosen locations are highlighted in red in Figure 3.12.

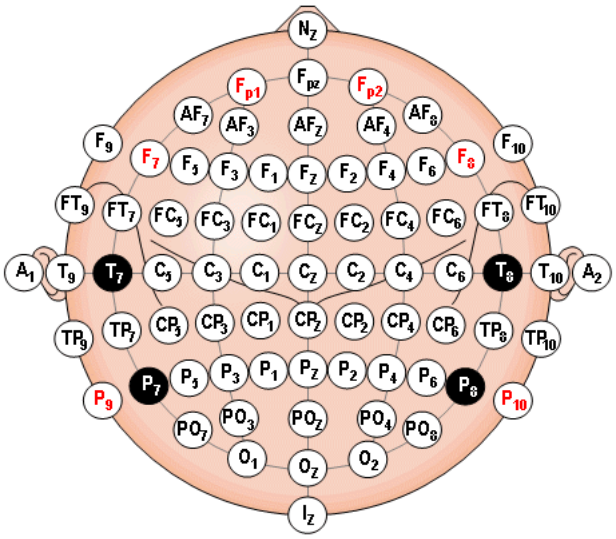

Figure 3.12: Electrode locations (red) from the 10/10 system used in the 6-channel system. *Modified from* [10].

Salmi's cap satisfied most of the above-mentioned requirements, except for the first two. With its intricate construction made up of 9 separate straps and 7 possible adjustment points, it was not easy to apply and adjust. Also, the ends of electrode leads were not attached to the cap in any way, which allowed them to hang loosely thus making the band's application more difficult. Finally, the cap had the potential to interfere with standard paramedic work. In cases where the exact mechanism of a head injury is unknown and the potential for a cervical spinal injury exists, EMTs typically immobilize the patient's neck and spine using a rigid cervical collar with supportive blocks and a backboard with straps [113]. Throughout the procedure, one EMT applies the equipment while another manually immobilizes the patient's head using his hands [114, 115]. Since the cap covered the majority of the dorsal and lateral parts of the head, it would have interfered with the manual immobilization

procedure. Even worse, if the patient would have been in the supine position, the cap could not have been applied since the patient's head cannot be moved until it has been completely immobilized.

Present Work

Prior to designing the new version of the cap, a number of EMT training videos depicting how a patient's neck is immobilized by means of a cervical collar were analyzed. It was concluded that irrespective of whether the patient is in the supine position or seated, prior to the application of the collar, the posterior region from the inion to the base of the neck is free from any obstructions and thus is a potential spot for an attachment band. The same is true also of the region from inferior part of the chin to the neck. Furthermore, the forehead as well as the superior part of the head are also unobstructed and therefore can continue to be used for the electrode band and as a location for the WEEG electronics, respectively.

The schematic of the new cap is depicted in Figure 3.13. As it can be seen from the figure, the new cap consists of three structural bands and two attachments straps. The 'over-the-head' (OTH) band runs from the left to the right ear and is needed in order to maintain the cap on the patient's head. Also, it serves as an anchor point for the electronics band, which runs sagittally on the patient's head and is affixed to the forehead band. The cap is secured to the patient's head by means of a chin strap and a 'behind-the-head' (BTH) strap. Hence, in comparison with Salmi's band, the new design has only 2 points of adjustment.

From the measurement electronics standpoint, this design is nearly identical to the previous version. The PMU is housed within the electronics band on top of the patient's head and the electrode locations have remained the same. However, two important enhancements were made. First, instead of having to completely remove the electronics band in order to insert the WEEG device, an opening on the side of the band has been created for this purpose. The opening is sealed with hook-and-loop fasteners. Second, in order to keep the leads from moving around freely, small-diameter holes were drilled in their endpoints. This modification allowed the leads to be easily sown to the forehead band, thus completely immobilizing them.

The sowing and assembly of the new cap was carried out by Christina Mjema.

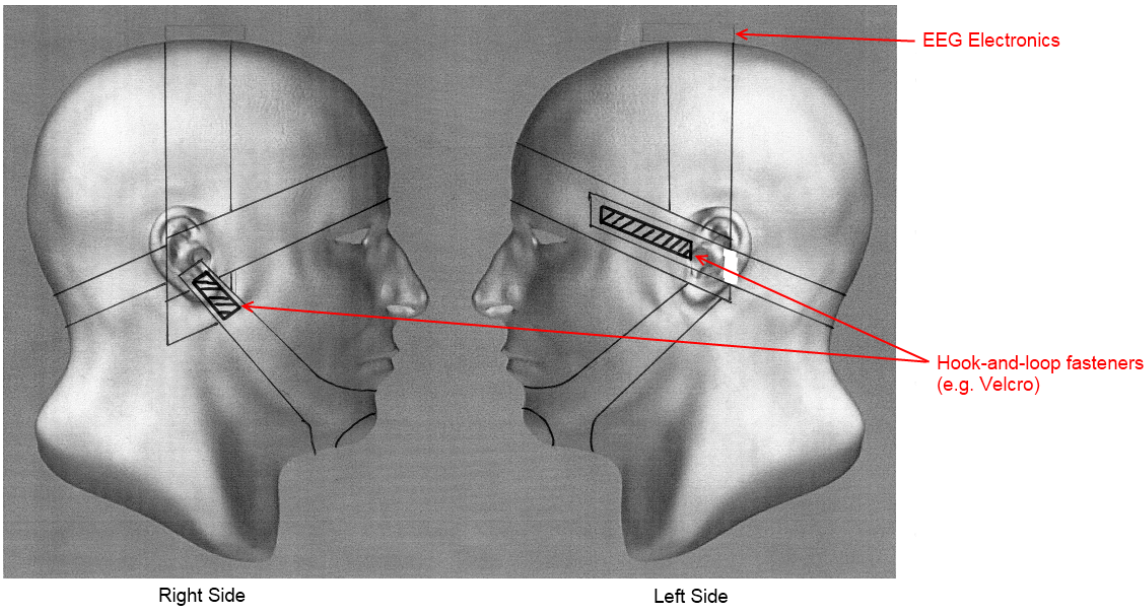

Figure 3.13: Sketches of the new quick-application cap.

3.4 Electrodes

Bioelectrodes act as transducers that convert the ionic currents inside the patient's body to electronic currents that can be measured with electronic amplifiers. The "charge-transfer" occurs at the electrode-skin interface, a model of which was shown in Figure 2.2. A more detailed explanation of the phenomena that occur at the electrode-skin interface is beyond the scope of this work and the interested reader is referred to McAdams' article for an excellent treatment of the subject [116].

One of the most common types of electrodes used for EEG scalp measurements is the cup electrode. As shown in Figure 3.14, it consists of a conically formed metal disk with a hole at its apex, which allows the introduction of electrolyte gel and also enables the abrasion of the skin by means of a hypodermic needle. The electrode can be immobilized with elastic bandages, a wire mesh, or a strong adhesive. Traditionally, cup electrodes have been manufactured from gold due to this material's high conductivity and inertness. Recently, Ag/AgCl has also become common. Although the quality of the signal normally obtained with cup electrodes is excellent, the preparation is relatively long since it is a three-step process, which must be repeated for each individual electrode: skin abrasion, introduction of the electrolyte gel, and immobilization. Hence, this electrode type is unsuitable for use in emergencies.

In this work it was decided to use disposable, self-prepping Zipprep electrodes, which are manufactured by Aspect Medical Systems (Norwood, USA). Zipprep elec-

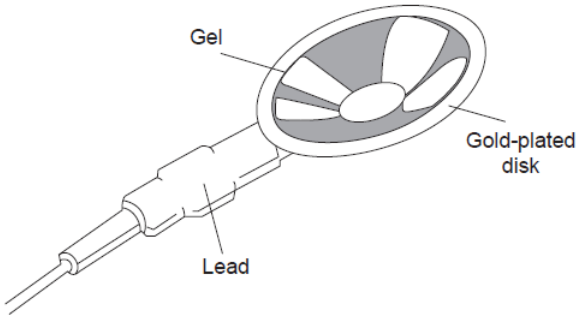

Figure 3.14: Conical metal disk EEG electrode. *Reproduced from* [116].

trodes consist of an Ag/AgCl sensor that is mounted on a rectangular piece of medical grade foam with a porous sponge that contains electrolyte gel placed on top of the sensor. The sponge also doubles as a skin preparation pad since it abrades the skin underneath it when pressure is applied on top of the electrode. The remaining unoccupied area of the foam backing is covered with a strong adhesive to ensure that the electrode will remain immobile once applied. Since the electrolyte gel and the adhesive do not have to be added manually, Zipprep electrodes can be applied very quickly, simply by peeling the plastic cover off and applying pressure. Even with no preparation, the impedance of these electrodes was found to be less than 15.7 kΩ at all of the measurement locations shown in Figure 3.12; after a short preparation that consisted of 2 seconds of rubbing and pressing, the impedance decreased to 3.6 kΩ [70]. The three major short-comings of these electrodes are that they can be used only for short-term recordings (max. 24 hours), they cannot be applied on hair, and they command a high price. Additionally, irritation might occur if the skin has been excessively abraded by the porous sponge.

3.5 Implementation of the aEEG Algorithm

Initially, it was planned that the aEEG algorithm would be implemented in both systems. In the 6-channel system, it would aid the medical professional in ascertaining the condition of the patient in real-time, while in the 1-channel system it would serve as a compressed report for the physician. However, upon consulting Dr. Ville Jäntti, a clinical neurophysiologist from the Seinäjoki central hospital, it was agreed that relying only on the aEEG data without having access to the original EEG would not be clinically useful. Hence, the aEEG algorithm was only programmed in the PC software of the 6-channel system.

A major difficulty in programming the aEEG algorithm was that a detailed digital

implementation of it has never been described in literature. Due to this reason, the current implementation was created by combining information from the original article by Maynard et al. [54] with data obtained from Osselton's overview of aEEG [57] and the general description of the algorithm as implemented in Guger Technoologies' g.CFMtoolbox [117]. The four steps of the resulting algorithm are described in the following paragraphs.

Asymmetric bandpass filtering. In this step, the spectrum of the EEG data is first flattened and then narrowed by means of two separate filters. The coefficients of the flattening filter correspond to the parameters of an autoregressive (AR) all-pole model of the spectrum of the *sc4102e0* EEG dataset obtained from the Sleep-EDF EEG database [118]. This dataset was chosen since it does not contain any significant alpha or beta activity. The AR parameters were estimated using the Burg method and the order of the model was determined empirically using MATLAB 7.11 by finding the smallest order that resulted in a AR model which followed closely the spectral envelope of the EEG data.

The narrowing of the spectrum is accomplished by means of a FIR bandpass (BP) filter. The lower and upper cut-off frequencies are 1.46 and 21.77 Hz, respectively, so as to ensure that the region from 2-20 Hz is not attenuated. Although the Parks-McClellan (optimal) algorithm is the most common method of designing linear-phase FIR filters, due to the large overshoot it introduces at the start of the upper transition region, the BP filter was instead designed using the Fourier method with a Kaiser window. The minimum stopband attenuation of the resulting filter is 40 dB.

Rectification and amplitude compression. After removing the sign of all negative samples, the signal's amplitude is semi-logarithmically compressed. Samples whose amplitude lies between 1 μV and 10 μV are not changed while samples larger than 10 μV are replaced with the value of their base-10 logarithm. As is customary in CFM monitors, the original EEG signal is clipped at 100 μV in order to prevent the need for gain adjustments during a recording.

Time compression. As described in section 2.5, the original CFM device, which worked in the analog domain, employed a PP detector and a slow paper speed in order to compress the signal in the time domain. In the digital domain, this function is accomplished simply by splitting the signal into fixed-size data windows and selecting the largest sample from each window. Seeing as though in the frequency domain this procedure is similar to LP filtering, the bigger the window is, the more

the high-frequency components of the signal, which are an indication of the character of the cerebral activity, will be attenuated. Hence, a trade-off must be made between the amount of compression and the information content of the resulting signal. An arbitrary windows size of 200 samples was selected.

In order to avoid the LP filtering effect that occurs when multiple samples are drawn on the same physical pixel on the computer screen, the drawing algorithm ensures that only one sample is drawn per physical pixel.

3.6 Testing

In order to verify the functionality and the performance of both systems, the following tests were carried out.

3.6.1 Quick-Application Cap

Since the new cap is fundamentally different from the previous version, at first, a test version of it was built, which consisted only of the bands that immobilize it on the patient's head, i.e., forehead band, OTH band, BTH strap, and chin strap. While the bands were constructed from a material that is not particularly stretchable, the straps were elastic so as to allow the cap to fit a multitude of individuals. In order to simulate the presence of the WEEG4, an identical enclosure was affixed in the middle of the OTH band and filled with three AAA batteries. Subsequently, the comfort and immobility of the cap were evaluated with seven volunteers, three of which were female and had long hair. Based on the results of this evaluation, a final prototype was constructed.

3.6.2 Electrical

Several electrical tests were performed using the equipment from the department's electronics lab. The main tools that were employed are the Tenma 72-7720 multimeter, the Tektronix TPS2014 portable oscilloscope, the TTi TG230 signal generator, and the Oxford XC-90III medical calibrator. Whenever the peak-to-peak amplitude or the RMS value of a signal had to be determined from an oscilloscope measurement, the measurement data was imported into MathWorks MATLAB version 7.11 directly from the oscilloscope by means of the Instrument Control Toolbox (ICT) and analyzed there.

Current consumption and operating time

Both devices' current consumption was measured during all of their respective operating stages by connecting a 10 Ω, 1 % resistor in series with the battery. One oscilloscope probe was connected on each side of the resistor and the measured voltages were imported into MATLAB. Once the RMS voltage drop was calculated, the RMS current flow was determined simply by Ohm's law.

Since both systems are assumed to consume the most current while recording, the theoretical operating time was estimated by dividing the battery capacity by the current that is consumed during the recording mode. The actual operating time was determined by starting a recording with fully charged batteries and letting both system record until the batteries ran out.

In the case of the 1-channel system, the amount of time that the system can remain unused in the standby mode before the battery is emptied, also known as the shelf-time, is an interesting parameter to determine. Since the adapter is never powered off completely, the shelf-time depends on the battery capacity and the amount of current that is consumed while in the `Standby State`. Hence, this parameter will be calculated by multiplying the operating time with the ratio of the RMS current consumed in the `Recording State` to that consumed in the `Standby State`.

CMR

6-channel System. The A_{CM} of each channel was determined by inputting a known sinusoidal signal (amplitude of 936 mV_{PP}, DC offset of 1.69 V, and frequency of 50 Hz) to all six input channels as well as to the reference channel and then measuring the voltage at the output of the IA stage. A channel's A_D was obtained by measuring the IA's output when a 1 mV_{PP}, 5 Hz sinusoid generated by the calibrator was inputted. For both measurements, the average PP amplitude of the output signal was calculated in MATLAB by averaging the PP amplitudes of 10 signal periods.

Once A_{CM} and A_D were determined, the channels' CMR was calculated by means of Equation 2.2.

1-channel System. This system's A_D was measured by inputting a 115.81 mV_{PP}, 50.51 Hz sinusoid from the signal generator and measuring the IA's output. On the other hand, A_{CM} proved to be impossible to measure due to the IA's extremely high CMR, which is typically in the 90–110 dB range for a gain of 6.25 [77] and which attenuated the common-mode signal so much so that it was not possible to measure it with the oscilloscope. However, since the minimum CMR of the IA for this gain level

exceeds the ACNS guidelines, as mentioned in section 3.2.3, it was assumed that the system's CMR is adequate for measuring EEG.

Frequency response

6-channel System. The frequency response of a system is typically measured by using a sinusoidal input signal whose frequency is swept over the range of interest. In particular, the gain of the system as a function of frequency is determined from the amplitudes of the input and output signals, which are simultaneously measured at discrete frequency points (e.g., every 10 Hz).

Due to the large gain of this system, it was not possible to connect the signal generator directly to its inputs since a signal with a small-enough amplitude, which would not saturate the amplifiers, and a DC offset which equalled half of the supply voltage couldn't be generated. Therefore, the required input signal was generated by passing a 100 mV_{P-P}, sinusoid through an attenuator PCB that reduced the sinusoid's amplitude to 1 mV and biased it appropriately.

The frequency range was from 0.05 to 100 Hz[10]. For each frequency point, the EDF+ file containing the recorded signals was imported into MATLAB, where the gain of each channel was calculated from the average PP amplitude of the recorded signal.

1-channel System. Since the gain of this device is much less than that of the 6-channel system, the signal generator was connected directly to its inputs. The same process as before was repeated, with the only differences being that the measurement data was collected by means of the oscilloscope and the frequency range was extended to 500 Hz.

Noise

6-channel System. The noise level was measured by tying together the 6 input channels, the *Reference* channel and the *Bias* output. In this way, whatever output signal ariose would be due to the noise generated by the WEEG4 electronics. A 1-minute recording was performed and the RMS amplitude of the signal recorded by each channel was calculated using MATLAB.

[10]The upper limit is due the sampling frequency of the WEEG4, which is set to 200 Hz. Thus, in order to satisfy the Shanon-Nyquist theorem, the highest frequency that can be recorded is 100 Hz.

1-channel System. The measurement of this system's noise is more involved because there is no built-in way of recording the output signal. Also, since the noise is expected to be in the sub-mV level, it cannot be measured with the TPS2014 oscilloscope. Therefore, instead of determining the RMS noise level, the noise spectrum of the device would have to be measured by means of a spectrum analyzer. The adapter's inputs would be tied together in the same manner as those of the 6-channel system and its output attached to the spectrum analyzer. Unfortunately, it was impossible to measure the noise spectrum of the device due to lack of access to a spectrum analyzer.

Signal-to-noise ratio

In order to ascertain the quality of the signals acquired by both systems, their respective signal-to-noise ratios (SNRs) were compared to the SNR of a commercial Neuroscan system. Mathematically, if the noise being measured is considered to be random, the SNR is defined as

$$\mathrm{SNR(dB)} = 20\log_{10}(\frac{A_{signal}}{A_{noise}}) \tag{3.16}$$

where A_{signal} = RMS amplitude of the desired signal and A_{noise} = RMS amplitude of the noise.

Five-minute recordings were performed with each system while a $100\,\mu$V, 5 Hz sinusoidal waveform generated by the calibrator was being inputted. The 5 Hz input signal was defined as the desired signal while the remaining signal after the desired signal's removal from the recording with a narrow BP filter was considered as the noise signal. It was assumed that the amount of noise added by the systems, which overlaps with the desired signal's bandwidth, is insignificant compared to the desired signal's power and thus can be ignored.

Since the two systems have different bandwidths and since the measurement setup was not the same, their SNR was computed with slightly different methods. The exact methodology is described next.

6-channel System. The 6-channel-system data was acquired by simultaneously connecting the calibrator's output between the inputs of the 6 channels and the *Reference* input, which was shorted to the *Bias* terminal. In the case of the Neuroscan, the data was recorded in the following manner:

1. Calibrator output connected between *Channel 1* and the *Reference* input. To improve the rejection of common-mode noise, the *Gnd* input terminal was shorted

with the *Reference*.

2. The 5 min recording was carried out with the signal sampled at 500 Hz, a gain of 1000 and a bandwidth ranging from 0.05 to 100 Hz.

In order for the resulting SNR values to be comparable, the same steps were used to process the data from both systems:

1. Since the signal power is distributed in a narrow bandwidth around 5 Hz, a FIR BP filter centered at 5 Hz with a -3 dB bandwidth of 1.4 Hz was used to extract the desired signal.

2. The noise signal was obtained by filtering the recording with a FIR bandreject (BR) filter centered at 5 Hz with a bandwidth of 1.6 Hz.

3. DC offset of the noise signal was removed by means of a HP FIR filter with a 0.25 Hz cut-off frequency.

4. Seeing as though the theoretical upper cut-off frequency of the WEEG4 PMU is larger than that of the Neuroscan, a LP FIR filter with a cut-off frequency of 100 Hz was applied to the noise signals.

5. Finally, the RMS levels of the signals were computed and the results plugged into Equation 3.16 to calculate the SNR.

1-channel System. The system's output signal with the 5 Hz input waveform and the PGA gain set to 1 was recorded by the Neuroscan. The SNR of the Neuroscan was calculated from dataset that was recorded for the 6-channel system.

The processing steps were identical to those described previously, with the following exceptions:

- Step 3: cut-off frequency of the HP filter was changed to 0.184 Hz.
- Step 4 was omitted since the Neuroscan set the upper cut-off frequencies for both datasets.
- Step 5: since the noise signal from the 1-channel system's dataset was made up of components from the Neuroscan and from the adapter, the following supplementary steps were performed only for this dataset:
  - RMS signal levels were converted from $\mathrm{mV_{RMS}}$ to $\mu\mathrm{V_{RMS}}$ by dividing them by A_D.

– The adapter's RMS noise level was obtained by subtracting the Neuroscan RMS noise level from the scaled RMS noise level calculated in the previous step.

3.6.3 Software

6-channel System. The testing of the PC software was carried out in three stages. In the first stage, Microsoft's Application Verifier 4.0 was used to test the quality of the software. The Application Verifier is a runtime verification tool that helps to detect subtle programming errors, e.g., misuse of locks in multithreaded applications, heap corruption, incorrect handles. Three categories of tests were run on the software: basics, compatibility, and miscellaneous.

The second stage consisted of inputting a $100\,\mu$V, 5 Hz sinusoid signal from the calibrator on all six channels of the WEEG4 device. This test signal made it especially easy to test the sensitivity, timebase and filter options, as well as the aEEG mode. Furthermore, data was entered in all of the fields of the *Patient Information* and the *Recording Information* windows, and all of the annotations were tried out.

Finally, in order to test its reliability, the software was left to record until the batteries of the WEEG4 ran out.

1-channel System. For testing purposes, the adapter was connected to the Agilent M3046A patient monitor and its output was observed, at first while inputting a $25\,\mu$V sinusoid, and then with 50 and $100\,\mu$V input signals. In this way, it was possible to test the state transitions as well as to see the effects of the gain adaptation both on the test signal and on the scale-indicator signal. Once these tests were completed, the adapter was plugged into an USB port in order to check the charging mechanism and to ascertain that the firmware stops the recording and transitions to the `Charging State` as soon as the connection is detected.

Chapter 4

Results

4.1 Introduction

In this chapter, the results of the work accomplished during this thesis are presented and briefly commented. Section 4.2 describes the hardware and software problems encountered during the construction of the 1-channel system and the modifications they engendered. The components of the 6-channel system are the subject of section 4.3. Section 4.4 contains the results of the electrical tests while those of the software tests are included in section 4.5.

4.2 1-channel System Implementation

The design and assembly of the new EEG-to-ECG adapter was the most time-consuming part of this thesis. Due to the challenges that were encountered with the previous version of the adapter, the first stage of the design consisted of analyzing the requirements of each section of the planned circuit. At this stage, two circuit parts were designed that weren't included in the final prototype due to current consumption and circuit footprint constraints: a radiofrequency filter that would have filtered high-frequency signal components at the input of the IA and a rapid recovery circuit, which was described in section 3.2.3. Once the full circuit was finalized, low noise components with small footprints were selected and every major section of the circuit was assembled and tested separately to ensure that it functions as intended. After this testing stage, the PCB layout of the new adapter was designed. Since the PCB contains both analog and digital sections, careful attention was paid to respect good layout practices, especially the principle of segregation. For protection against the ingress of fluids, the adapter's electronics were housed in an IP54 ABS enclosure.

Although the design stage took more time than expected, the resulting hardware worked on the first try and only minor tweaks were required, as described in the next section. Figure 4.1 includes different pictures of the new adapter prototype.

(a) External view with Zipprep electrode.

(b) The adapter compared to a standard 9 V battery.

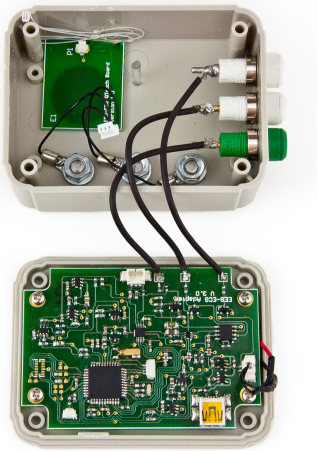

(c) Circuit board.

Figure 4.1: Final prototype of the EEG-to-ECG adapter.

In Figure 4.1(a), the input (left side) and output connectors (top) of the 1-channel system as well as the RGB LED's light guide and the area where the capacitive key is located are clearly visible. The green input connector is for the bias electrode, which is typically located in the Fpz location, while the two white connectors represent the input channel. They are connected to two electrodes also located on the forehead, usually in the Fp1 and Fp2 locations. The three limb leads cables of an ECG monitor connect to the output connectors on top of the adapter's enclosure. Since the EEG signal is outputted by the rightmost connector and is referenced to the remaining two, only one limb lead has to be displayed on the monitor in order to be able to visualize the patient's EEG.

Figure 4.1(b) is included in order to show how the adapter's size compares to that of a standard 9 V battery. The adapter measures $80 \times 60 \times 30$ mm and weighs only 87 g, including the battery.

Figure 4.1(c) shows the interior of the adapter. As it can be observed from the picture, the battery, the capacitive sensor, and the adapter's outputs interface with the PCB by means of connectors. On the other hand, the three input connectors have connecting wires that are directly soldered to the PCB in order to respect the IEC 60601-1 creepage requirements. In order to save space and keep the interior of the enclosure tidy, the battery is located underneath the PCB. A final observation that can be made is that no hole has been drilled in the enclosure for the mini-USB socket. Due to the wide distance between the socket and the wall of the enclosure, the hole would have to have been excessively large in order to be able to plug in a mini-USB cable. In future versions of the adapter, the mini-USB socket will be placed closer to the enclosure's wall.

4.2.1 Hardware

The following sections describe the differences between the original design and the actual prototype, as well as any problems encountered during the construction.

Transient Protection

Due to their substantial size and large cost, the three RNX075 resistors are not included in this version of the adapter prototype. Instead, their presence is simulated with 39 kΩ, 1 % resistors placed in series with each input channel (R302, R303, and R304).

Preamplifier

In the design stage, a $R_G = 9523\,\Omega$ resistor was proposed in order to obtain a gain $G = 6.25$. The closest standard 0.1 % resistor value available is 9.53 kΩ, which results in a theoretical gain of 6.247. A resistor with a 0.1 % tolerance and a temperature coefficient of ±15 ppm/°C is used as so as to ensure an accurate, stable gain over a wide temperature range.

ADC Signal Conditioning

In order to minimize the changes of the AA filter's characteristics due to component tolerances, the filter capacitors (C502, C503, C505, C506) are of the C0G/NP0 ceramic type, which are the most precise type of ceramic capacitor since they hold their nominal

value over a wide temperature and voltage range [81, 82]. Due to their low cost and the small difference in filter characteristics resulting from their usage, the filter resistors are of the standard 1 % variety.

PWM DAC

The initial design called for the various scale-indicator signals to be generated by decreasing the amplitude of the PWM signal outputted by the MCU's timer. However, when this approach was tested, it was discovered that the more the PWM signal's amplitude was reduced, the more noise was present in the sinusoidal signal. This result led to the realization that reducing the amplitude of the PWM signal is equivalent to a reduction of the DAC's resolution.

In the corrected design, R604 is equal to 180 kΩ and R605 is equal to 75 Ω, which sets the attenuation ratio of the output voltage divider to 2401:1. The peak-to-peak amplitude of the output signal generated in this way has an amplitude of approximately 0.625 mV. By changing the gain of the PGA, the amplitude of the output sinusoid can be adjusted to the value needed to indicate a 100 μV input signal for all of the possible adapter gains.

Power System

During testing, it was observed that the 2:1 PWM voltage divider (R600 and R601) was increasing the noise level of the half AVcc rail. Hence, a NFM21PC225B0J3D EMI filter (U602) is placed in series with R601 so as to attenuate the noise signal.

4.2.2 Embedded Software

The first version of the embedded software contained various minor errors, which were easily fixed, and a number of important bugs that led to major code changes. These bugs and the fixes that they required are discussed in the paragraphs below. The size of the final code is given in Table 4.1.

Table 4.1: Amount MCU memory taken up by the embedded software broken down by memory type.

Memory Type	Amount Consumed (bytes)
Flash	8010
SRAM	536
EEPROM	1

Recording State

Two problems were observed while the adapter was operating in this state. First, buffer overflows were occurring due to the amount of processing that was being carried out in between ADC samples. Although the signals were being sampled at 2.5 kHz, the samples were being processed at a rate of 1.7 kHz. Even when the frequency of the MCU's oscillator was increased to 8 MHz the processing speed did not match the sampling speed. Since the accurate measurement of the EEG signal's amplitude takes precedence, it was decided to forgo the measurement of the adapter's acceleration. Once all of the accelerometer-related code was removed, no more buffer overflows occurred.

The second problem which was observed was that the DC level of the EEG signal at the input of the ADC fluctuated continuously. The cause of these fluctuations was determined to be the current spikes created by the flashing green LED. Hence, in order to prevent the corruption of the EEG signal, this state is now indicated by keeping the green LED lit continuously.

Display Scale State

Due to the change in the way the scale-indicator signal is generated, which was detailed in the previous section, the PGA gain is now adjusted at the beginning of this state so that the resulting output signal has the correct amplitude. The PGA gain as a function of the required scale-indicator amplitude is given in Table 4.2.

Table 4.2: PGA gain required in order to generate an appropriately-sized scale-indicator signal as a function of the adapter gain.

Gain (V/V)	Scale-Indicator Amplitude (mV_{PP})	PGA Gain (V/V)
6.25	0.625	1
12.50	1.250	2
25.00	2.500	4
50.00	5.000	8

Capacitive Key

During the initial testing of the software, it was realized that 500 msec is too short of a time interval for the user to remove their hand from the capacitive key. Hence, the maximum touch length was increased by 500 msec in both the `Standby` and the `Recording` states.

4.3 6-channel System Implementation

4.3.1 WEEG4 Device

All of the changes detailed in section 3.3.2 were successfully implemented by Professor Lekkala's group. Switching to the ExpressCard interface proved to be more challenging than initially expected since at the time, the ExpressCard specification was only available to the members of the PCMCIA Association. However, an Internet search yielded two useful results: a PowerPoint presentation in which the electrical characteristics of the interface were described, and a circuit schematic that included the pinout of the ExpressCard connector. Together with the brief summary of the standard given on the PCMCIA Association's website, these results made it possible to successfully construct the CIU prototype.

Connecting the CIU to the CF-19's WLAN antenna was a two-step process. First, a Hirose U.FL-R-SMT antenna interface connector was added on the CIU's PCB. Since the microstrip antenna is still present, the position of the coupling capacitor can be changed so that the RF signal is transmitted either via the U.FL connector or the on-board antenna. The second step consisted of making the physical connection between the CIU and the antenna. With the help of a CF-19 service manual, the laptop was disassembled and a 150 mm-long U.FL coaxial cable was added between the ExpressCard slot and the antenna PCB. Subsequent testing showed that the WEEG system can indeed function with the WLAN antenna. Furthermore, although quantitative measurements were not carried out, qualitatively, the operating range of the system seems to be extended. Though unexpected, this result is logical due to the WLAN antenna's physically larger size and its superior location on the side of the laptop's screen.

The size of the PMU was reduced by fitting the previously segregated analog and digital sections within a PacTec PP enclosure (external dimensions: $94.5 \times 63.2 \times 27.9$ mm). Although this made it necessary to create a new PCB, the circuitry has remained identical to the previous version of the device. In order to enable the transition to the new enclosure, the PP3 battery was replaced with three AAA batteries.

The complete WEEG version 4 (WEEG4) system is displayed in Figure 4.2. As it can be observed from the figure, the size of the system has greatly decreased compared to version 3. Although in the figure the CIU's microstrip antenna can be seen extending outside of the laptop, this section of the PCB will be removed so that the CIU can be completely housed within the laptop.

Figure 4.2: Final prototype of the WEEG4 device. Measurement laptop (top), WEEG4 CIU (bottom-left) and PMU (bottom-right).

4.3.2 PC Software

Overview

Most of the functionality of the software was coded in C/C++, with the EFE being the only exception since C# was used for it. In order to make the software integrate closely with the Microsoft Windows operating systems and to optimize its performance, instead of using functions from the C/C++ standard libraries, wherever it was possible, the functions provided by the Windows Software Development Kit (SDK) version 6.1 were called. As a result, the recording software can run on any 32-bit version of Windows after XP SP1, i.e., XP SP2/SP3, Vista, and 7. Also, on a laptop that features an 1.60 GHz AMD Turion 64 X2, 2 gigabytes of random access memory (RAM) and

Windows Vista SP2, the software consumes at most 1 % of the central processing unit (CPU).

The only major challenge encountered during the development of the software was the upgrade of the serial interface from the version implemented in the WEEG3 to the one in WEEG4. Since the two interfaces were radically different, the `Sampling` thread and its associated functions had to be completely rewritten. On the other hand, this allowed the optimization of the operation of this thread and of the amount of computer resources that it required.

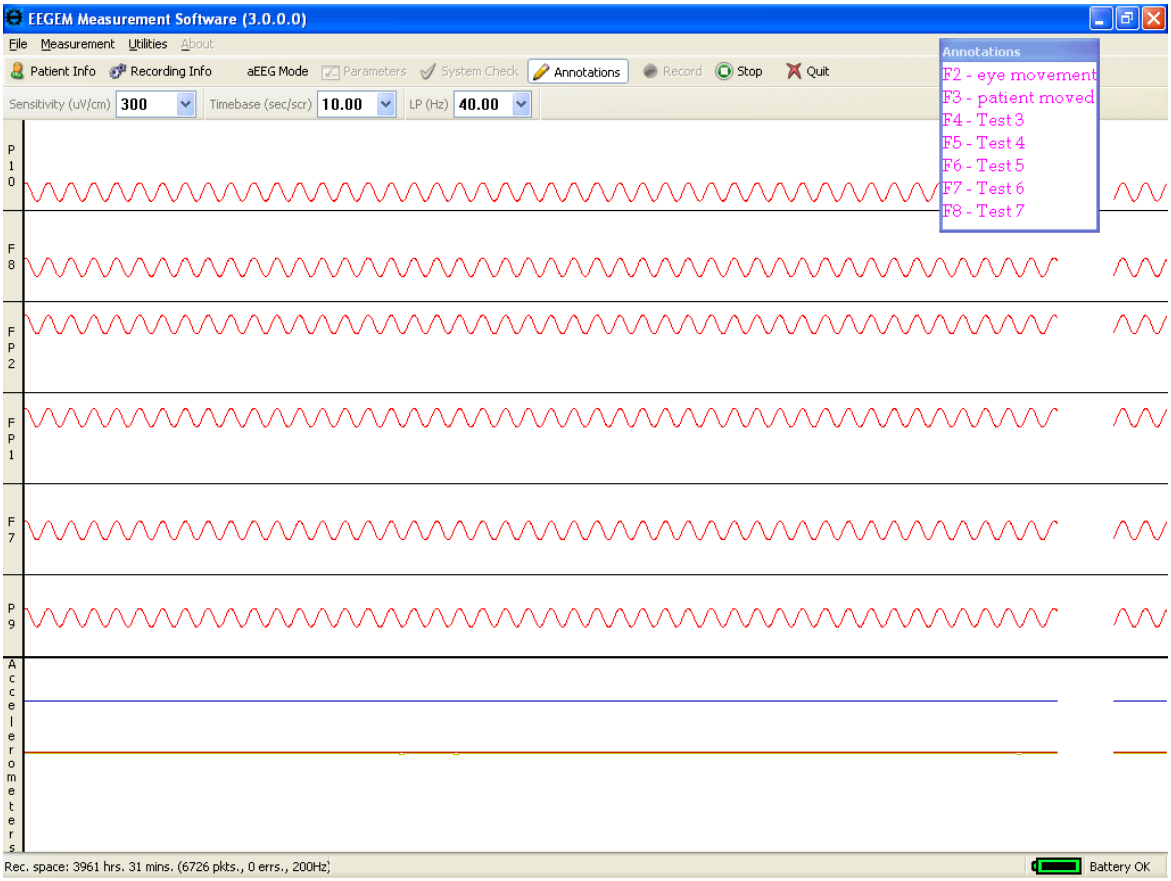

Figure 4.3: Main program window of the 6-channel system's PC recording software. The *Annotations* auxiliary window is displayed in the upper left corner.

A screenshot of the main program window is shown in Figure 4.3. The main part of the window is divided into two sections, with the larger top section being used to display the EEG signals while the smaller bottom section is reserved for the three accelerometer signals[1]. Each EEG channel is clearly labeled so as there is no confusion as to the origin of the signal that is displayed. The two toolbars used to control the software's operation are located underneath the menu bar, at the top of the window. The status bar, which displays an estimate of the remaining recording time based on

the available hard disk space, the last annotation that has been made, and the status of the WEEG4's battery, is located at the bottom of the window.

Screenshots of all the auxiliary windows are included in Figure 4.4. Their functionality has already been described in section 3.3.3 and will not be repeated here.

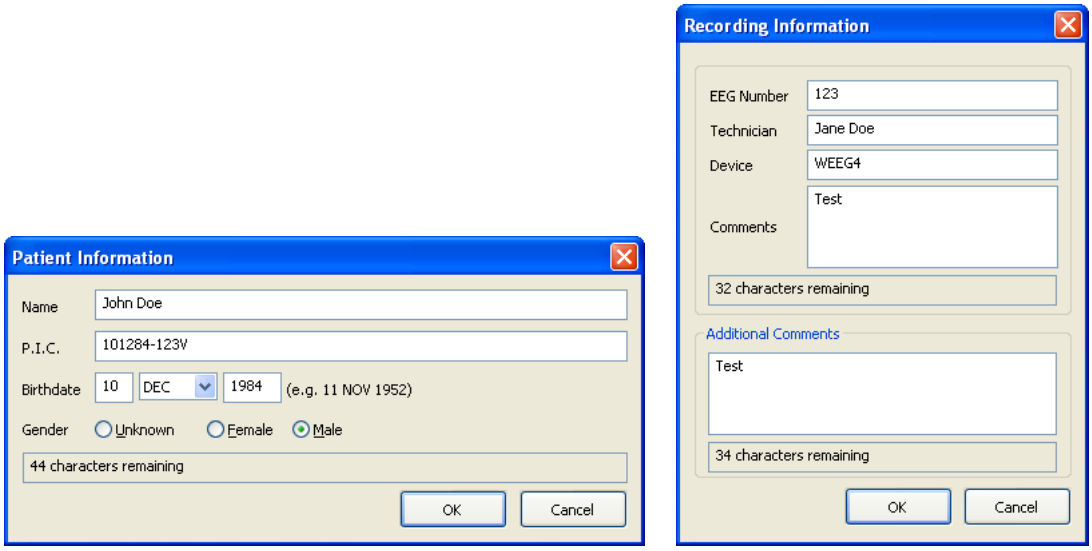

(a) Patient Information. (b) Recording Information.

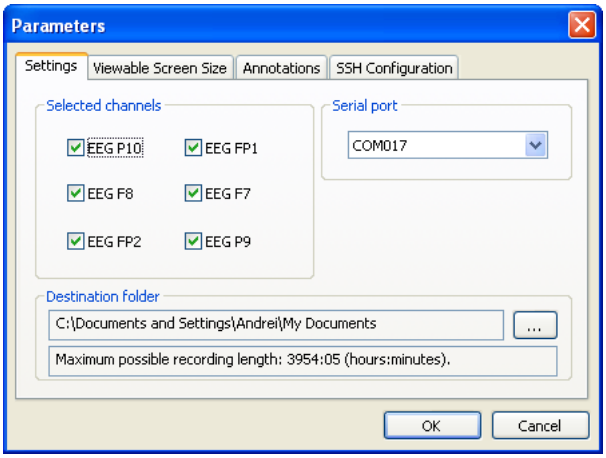

(c) Parameters.

Figure 4.4: Auxiliary windows of the of the 6-channel system's PC recording software.

[1]The display of the accelerometer signals can be toggled on/off by adding/omitting a "-g" on the command line when starting the software. If the accelerometer signals are not displayed, the whole window is occupied by the EEG signals.

EDF File Editor

The program window of the EFE is depicted in Figure 4.5. The exact same fields that are available in the *Patient Information* and *Recording Information* windows are also available here. At first, all of the user interface elements are disabled until a file is opened by pressing on the *Browse* button. Once the desired changes have been made, the new information is saved to the EDF file by pressing on the *Save* button.

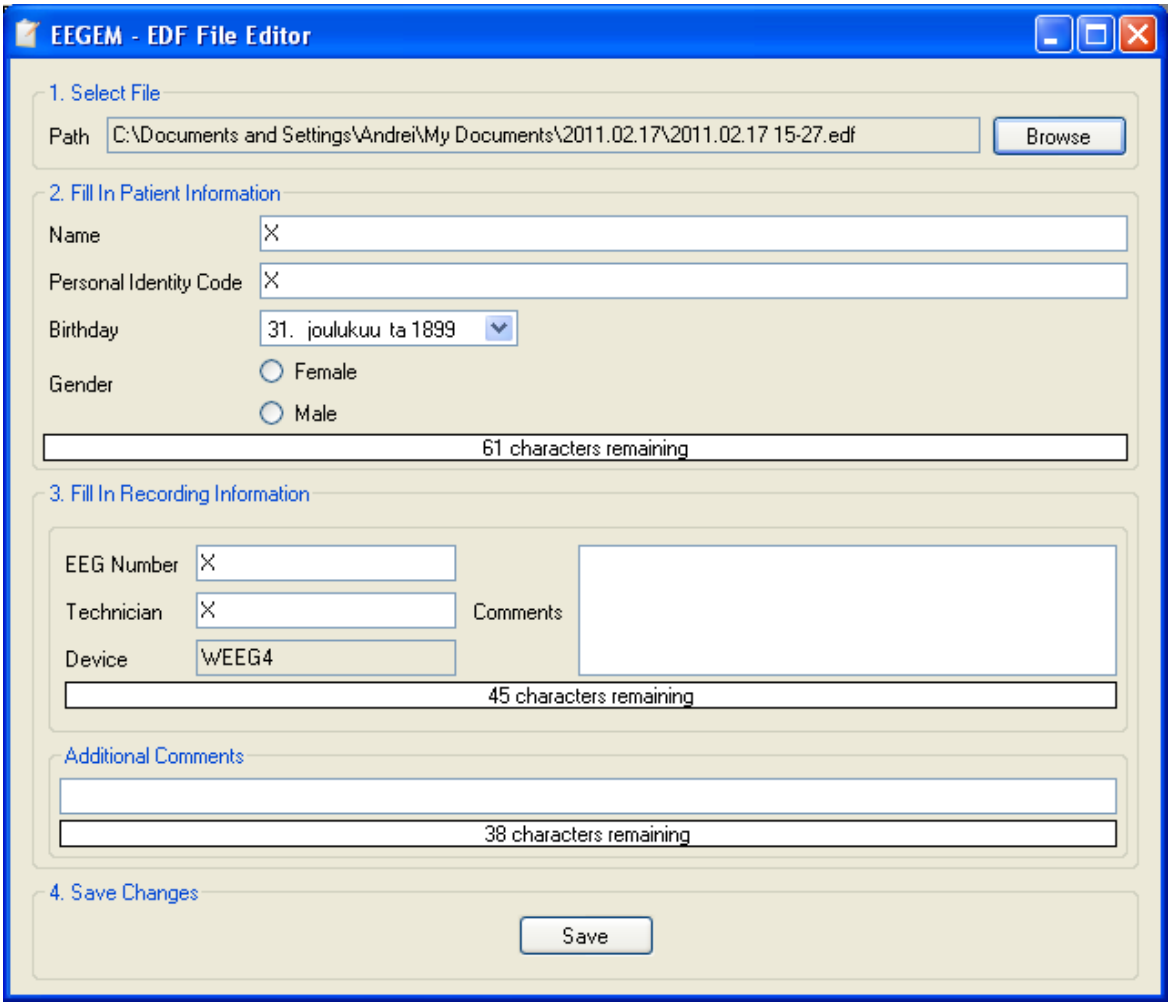

Figure 4.5: Main program window of the EDF File Editor.

4.3.3 Quick-Application Cap

Overall, the test version of the cap performed very well. It fit the heads of all the test subjects and remained nearly immobile even if the head was moved. However, it was observed that for some of the test subjects the OTH band had a tendency to slide down towards the forehead band whenever the subject moved their head. In

order to prevent this from occurring, plastic U-shaped supports were sewn into the cap material in the region where the OTH and the forehead bands intersect on both sides of the head (Figure 4.6). Some test subjects also indicated a certain amount of discomfort with the chin strap due to its sharp edges and its narrow width.

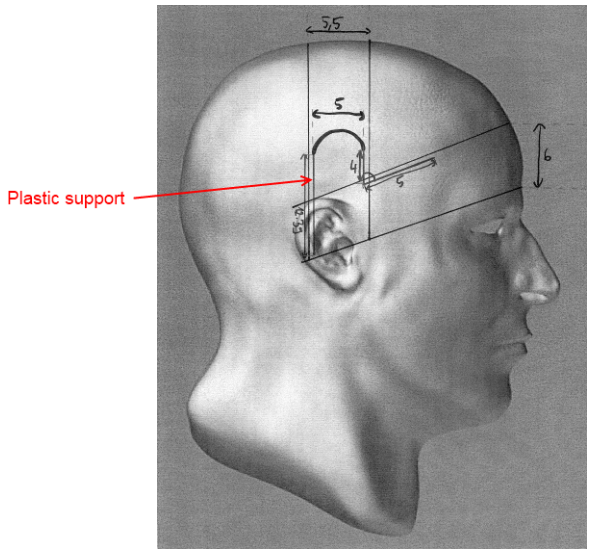

Figure 4.6: Plastic U-shaped support used to reinforce the OTH band of the quick-application cap.

The final cap design is shown in Figure 4.7. The major changes compared to the test version include a longer, thicker chin strap with a smooth material covering its edges in order to increase comfort. Also, as it can be seen in the figure, the chin strap is now attached to the rest of the cap by means of a metal ring located adjacent to the left temple. Furthermore, all of the long sections of hook-and-loop fabric located on the attachment straps were replaced by series of 1-cm long pieces in order to maintain the straps' elasticity.

Sewing the electrode leads to the forehead band has proven to be an excellent solution. The leads remain completely immobile while the cap is being applied on the head, thus significantly facilitating the attachment of the electrodes.

Qualitative testing has shown that depending on the patient's head size and hair length, the cap can be applied in 2 to 3 minutes, with the slowest part being the peeling of the plastic electrode covers.

(a) Front view. (b) Left side view.

Figure 4.7: Final version of the quick-application cap. Ambu Blue Sensor P electrodes were used here instead of the Zipprep electrodes.

4.4 Electrical Tests

Once both systems were fully operational, the tests described in section 3.6.2 were carried out. The results that were obtained are included hereafter.

4.4.1 6-channel System

Current consumption and operating time

The WEEG4 has three operating states, each of which is indicated by a different color and illumination pattern of the on-board LED. When the device is first turned on, the device enters the `Initialization` state, which is signaled by a solid red light. The `Recording` state is indicated by a flashing green light while the `Standby` state, which occurs in-between `Recording` states, is indicated with a flashing red light. The average current consumption in each of these states is given in Table 4.3.

Table 4.3: Current consumption of the WEEG4 in its three operating states.

State	Current consumed (mA_{RMS})
Initialization	43.23
Standby	35.37
Recording	36.97

Using ordinary alkaline AAA batteries (≈925 mAh), it was possible to record continuously for approximately 22.97 hours without stopping the system.

CMR

As it can be observed from Table 4.4, the CMR of all channels exceeds the 80 dB threshold recommended by the ACNS guidelines.

Table 4.4: CMR of the WEEG4's six channels.

Channel	CMR (dB)
P10	82.80
F8	82.29
Fp2	83.67
Fp1	81.62
F7	82.38
P9	81.81

In theory, the measurement procedure was not entirely proper, since the sinusoids that were used to measure the common- and differential-mode gains had different frequencies. However, since the gain of the IA doesn't start decreasing until the tens of kilohertz range, it can be safely assumed that the differential gain at 50 Hz is identical to the one at 5 Hz.

Frequency response

The frequency responses of the WEEG4's six channels are depicted in Figure 4.8. According to the plot, the system's upper and lower -3 dB points are 0.22 and 45 Hz, respectively. Although the lower -3 dB point is very close to the theoretical value of 0.16 Hz, there is a a 71 Hz difference between the theoretical and the actual upper -3 dB point. Since all six channels have a nearly identical behavior, the most likely explanation for this discrepancy is that during the assembly of the PMU, one or more of the components that make up the low-pass filters were replaced by mistake with erroneous components.

Noise

The RMS noise level of each channel (Table 4.5) at the input of the ADC was calculated from the recorded signals after the DC offset was removed by means of a FIR HP filter with a cut-off frequency of 0.42 Hz. The noise at the input of the adapter was estimated by dividing the noise at the ADC input by the theoretical gain of the WEEG4.

All channels exhibit excellent noise properties over the 0.22–45 Hz frequency range. If the actual bandwidth of the system would be approximately equal to the theoretical

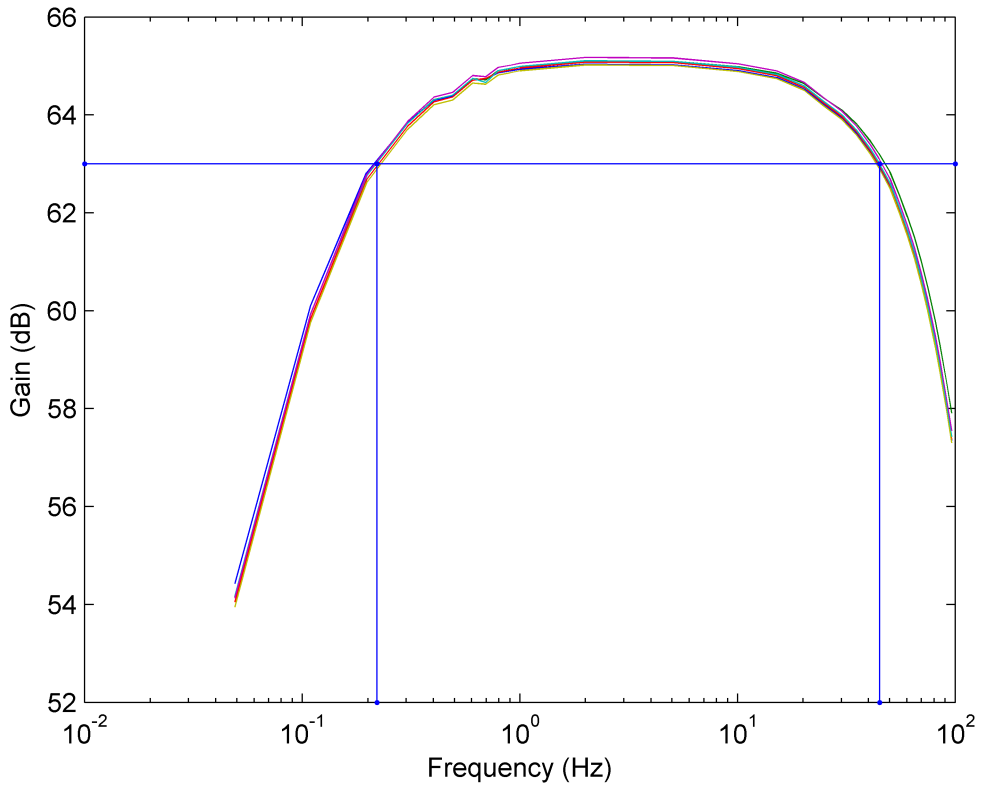

Figure 4.8: Frequency responses of the WEEG4's six channels. The horizontal blue line indicates the -3 dB level and its intersections with the two vertical lines point to the lower and upper cut-off frequencies of 0.22 and 45 Hz, respectively.

Table 4.5: RMS noise level of the WEEG4's six channels over the 0.22–45 Hz frequency range.

Channel	ADC Input Noise (mV_{RMS})	Channel Input Noise (μV_{RMS})
P10	0.729	0.384
F8	0.754	0.397
Fp2	0.740	0.390
Fp1	0.750	0.395
F7	0.749	0.394
P9	0.717	0.377

one, the noise levels would be higher, but assuredly still acceptable.

Signal-to-noise ratio

Table 4.6 contains the SNR of the Neuroscan while the SNR values of the WEEG4 PMU's six channels are included in Table 4.7. Due to the PMU's reduced bandwidth,

in order for the Neuroscan and the WEEG4 SNR values to be comparable, the cut-off frequency of the LP filter used in step 4 of the SNR calculation procedure was changed to 44 Hz.

Table 4.6: SNR of the Neuroscan over the 0.25–44 Hz frequency range.

Signal (μV_{RMS})	**Noise (μV_{RMS})**	**SNR (dB)**
34.06616	0.36293	39.45

Table 4.7: SNR of the WEEG4's six channels over the 0.25–44 Hz frequency range.

Channel	**Signal (mV_{RMS})**	**Noise (mV_{RMS})**	**SNR (dB)**
P10	65.58336	0.76401	38.67
F8	66.08018	0.77651	38.60
Fp2	65.84909	0.77749	38.56
Fp1	66.06427	0.77862	38.57
F7	66.48686	0.77722	38.64
P9	65.39020	0.75657	38.73
Average	65.90899	0.77174	38.63

As it can be appreciated by comparing the two tables, the SNR of the two systems is very similar, with only a 0.82 dB difference between the SNR of the Neuroscan and the average SNR of the WEEG4 channels. This results indicate that under laboratory conditions, the WEEG4's signal quality is comparable to that of a commercial EEG system.

Table 4.8 summarizes the electrical characteristics of the 6-channel system.

4.4.2 1-channel System

Current consumption, operating time, and shelf-time

The average current consumption for each of the adapter's four main states is given in Table 4.9. If the green LED would be blinking instead of remaining lit continuously, the amount of current consumed in the `Recording State` would decrease by 5.16 mA_{RMS}.

With the battery fully charged, the operating time with the adapter in the `Recording` state was found to be approximately 19.1 hours. Based on this value, the adapter's shelf-time was estimated to be 26.9 hours.

[2]Once the previously-described electronics assembly error is corrected, the actual upper cut-off frequency of the system will be approximately 116 Hz.

Table 4.8: Summary of the 6-channel system's characteristics.

Parameter	**Value**
No. EEG channels	6
Sampling frequency (Hz)	200–1000
Storage frequency (Hz)	equal to sampling frequency
Resolution (bits)	16
Bandwidth (Hz)	0.22–45[2] (-3 dB)
CMR (dB)	82
Input impedance (MΩ)	≈1000
Noise (μVrms)	0.389 (over -3 dB bandwidth)
Power source	3× AAA batteries
Max . operating time (hours)	23
Weight (g)	PMU - 108
	CIU - 10
Dimensions (mm)	PMU - 60 × 93 × 25
	CIU - 70 × 34 × 5
Comments	- Measures triaxial acceleration
	- Data stored in EDF+ format

Differential gain

The differential gain was measured to be 6.18 V/V. The 1.12 % difference between the measured gain and the theoretical one is mainly a consequence of measurement noise, since the sum of the gain-setting resistor's tolerance and the IA's typical gain error is only 0.12 %.

Table 4.9: Current consumption of the 1-channel system in four of its operating states.

State	**Current consumed (mA_{RMS})**
Initialization	22.31
Standby	17.20
Recording	24.20
Display Scale	22.41

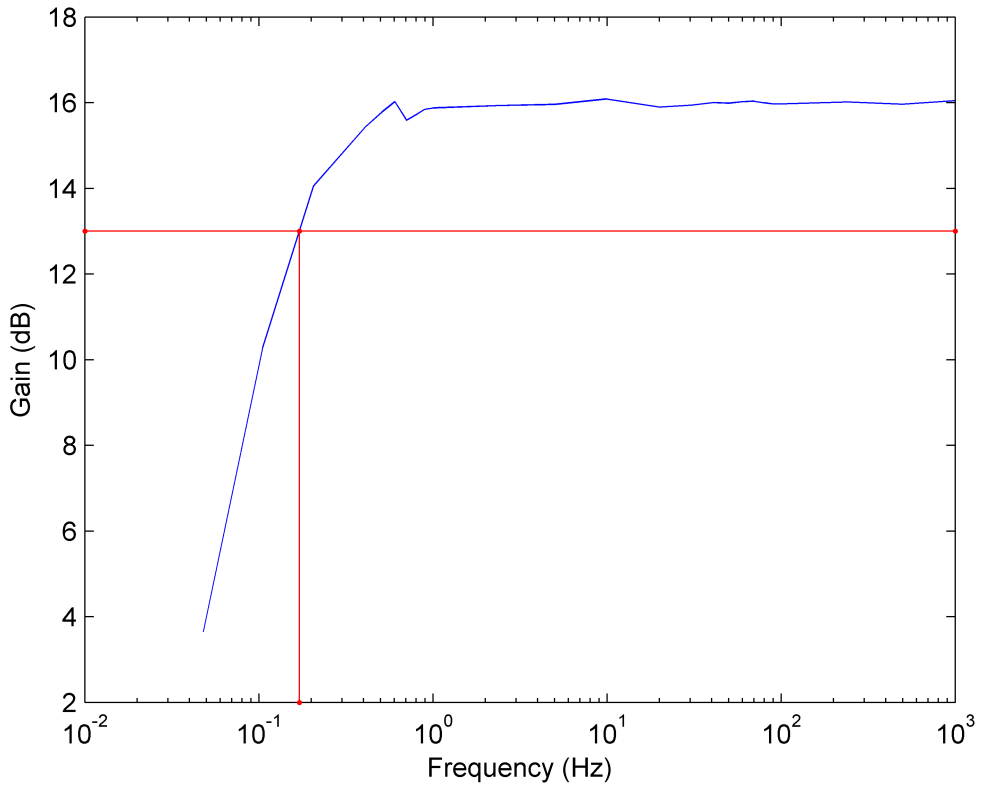

Figure 4.9: Frequency response of the 1-channel system. The horizontal red line indicates the -3 dB level and its intersection with the vertical line points to the lower cut-off frequency of 0.171 Hz.

Frequency response

The frequency response of the adapter is shown in Figure 4.9. Based on this plot, the lower -3 dB frequency of the system is 0.171 Hz.

The dip at 0.7 Hz is not a property of the system but is instead caused by a change in the way the measurement data was processed. Up until this frequency, it was impossible to filter the noise from the measured signals since the oscilloscope's sampling frequency was too low. However, as of this frequency, FIR LP filters were employed in order to attenuate the noise and thus improve the accuracy of the results.

Signal-to-noise ratio

The SNR of the adapter and that of the Neuroscan are presented in Table 4.10. Based on these results, the SNR of the adapter is higher than that of the Neuroscan by approximately 3.94 dB.

Table 4.10: SNR of the Neuroscan and of the 1-channel system over the 0.184–100 Hz frequency range.

	Signal (μV_{RMS})	**Noise (μV_{RMS})**	**SNR (dB)**
Neuroscan	34.06616	0.46172	37.36
Adapter	34.38543	0.29597	41.30

4.5 Software Tests

4.5.1 6-channel System

The PC software passed the selected Application Verifier tests with no errors or warnings being reported. Therefore, it is certain that the software is free from major programming errors. Furthermore, all of the software's functions worked properly when it was tested with the 100 μV signal and thus no further modifications were necessary. Finally, even after 22.97 hours of continuous operation, the software continued to be responsive and the amount of physical memory it was allocated by the Windows operating system had not increased.

4.5.2 1-channel System

A picture of the adapter's output when connected to the Agilent M3046A patient monitor is depicted in Figure 4.10. On the third signal-display row, to right of the red "Auto" text, the signal amplitude was changed from 50 to 100 μV. Once the new amplitude was detected by the adapter, the gain was decreased by half (i.e., from 50 to 25 V/V), and the firmware transitioned to the `Display Scale State`, as it can be observed at the beginning of the second signal-display row. After outputting the scale-indicator signal for 5 sec, the firmware transitioned back to the `Recording State`. Since the amplitude of the scale-indicator signal is identical to that of the new output signal, the correctness of the PWM DAC source code is verified. Also, the gain change is confirmed by the fact that the amplitude of the output signal is now the same as it was for the 50 μV signal when the gain was twice as large (see third signal-display row).

The DC level of the adapter's output signal fluctuates whenever the firmware transitions to and from the `Display Scale State`. This is due to the large time constant of the C305-R301 HP filter.

The USB charging detection mechanism works as designed. Unless the battery is completely charged, two seconds after the adapter is connected to an USB port,

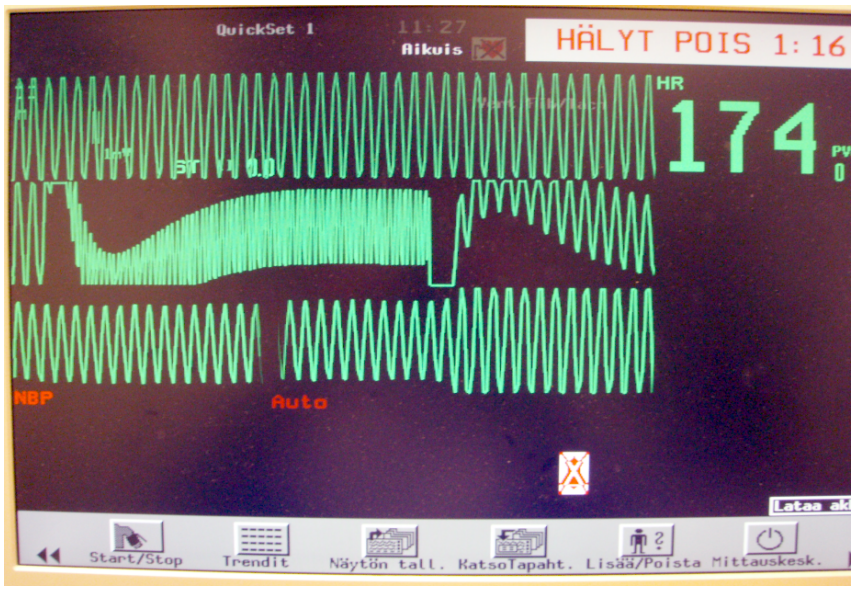

Figure 4.10: Block diagram of the 6-channel system.

the firmware transitions to the `Charging State` and remains there for as long as the battery is charging.

Chapter 5

Discussion

5.1 Introduction

Prior work has demonstrated that the information contained in the EEG is valuable in several emergent conditions, e.g., seizures and status epilepticus [18, 15], encephalopathies [16], identifying the etiology of altered mental states and comas [1]. In addition to aiding in establishing a diagnosis, the EEG can also be used to ascertain survival rates [16]. However, due to the shortcomings of conventional recorders (i.e., large dimensions, technical complexity, long preparation time), the EEG has remained underused in EM [18, 1]. In this study, two portable EEG systems have been developed especially for use in emergency situations. Both systems are small, portable, and can be applied quickly, while being comparable to commercial recorders in terms of the quality of the measured signals. To the knowledge of the author, these systems are a first of their kind.

Based on the results detailed in the previous chapter, it can be said that from an engineering perspective, the main objective of finalizing the development of the two systems has been reached. Nevertheless, now that both systems are operational, it is imperative that their shortcomings are analyzed in order to understand how the designs can be improved in the future.

Section 5.2 includes an analysis of the implementation of the 1-channel system while section 5.3 analyzes the 6-channel system. A comparison between the characteristics of the 6-channel system and the commercial offerings reviewed in chapter 2 is carried out in section 5.4. Finally, section 5.5 discusses the significance of the results that have been achieved in this thesis while section 5.6 explores future avenues of research.

5.2 1-channel System

5.2.1 Construction and Appearance

Compared to the previous adapter prototype, the new version has a cleaner appearance and is more rugged due to its thick ABS enclosure, which also protects the electronics from the ingress of fluids. Also, since all of the components have been fastened down within the enclosure and there are no other moving parts, the reliability of the system is increased. Furthermore, both the input and output connectors are constructed from heavy-duty materials, which make them suitable for an extended use.

The only weakness of the assembly is the hole that has to be made through the enclosure in order to be able to connect to the adapter's mini-USB socket. Although the space between the socket and the enclosure can be filled with a sealant, e.g., silicone, fluids could still damage the socket itself and potentially reach the adapter's PCB. Hence, in future versions of the adapter, alternative charging methods should be explored. One approach could involve inductive charging, where an electromagnetic field would be used to transfer energy from the charger to the adapter.

5.2.2 Analog Hardware

The quality of the measured signals is excellent, as illustrated numerically by the supernal CMR and SNR values. Also, since a high-precision PGA is employed, the adapter's gain accuracy is approximately 99 %, which is an excellent result, especially when considering the 25 % tolerance of the previous version.

An issue that needs to be resolved is the presence of noise on the half AVcc rail. Since the adapter's output signal is referenced to this rail, it is not affected by the noise. However, the signal sampled by the ADC is referenced to the circuit ground and hence is somewhat corrupted by the noise. Although this poses only a minor problem for the detection of the PP amplitude of the EEG signal, in future versions, the EEG signal will be stored on-board for later playback and thus it must be as noise-free as possible.

A second issue that needs resolving is the location of the transient protection resistors. Ideally, they should be placed within the adapter enclosure so that they can benefit from the protection it affords. However, the resistors' large size makes this option unpractical. Another solution is to build the resistors into the input electrode leads. While this would save space within the enclosure, it would also make heat dissipation more straightforward.

5.2.3 Digital Hardware

Due to the careful prototyping of the major circuit parts that preceded the construction of the final PCB, no major problems were discovered during the testing phase. Although it was time-consuming to get it operational due to a bug in the QTouch library, the capacitive start/stop key has proven to be a great replacement for the mechanical on/off switch.

A number of enhancements are suggested for future versions. First, the operating time should be increased to 24 hours. The easiest way to achieve this goal is by replacing the battery with a higher capacity one. For example, the Varta PLF 323450 has a typical capacity of 590 mAh while being only 0.6 mm thicker than the current battery. However, the current consumption of the adapter's circuitry must also be decreased. One way of doing so is by replacing the MCU with a less power-hungry one from the same family. For example, the ATmega164PA has the same peripherals as the ATmega1284P and its memory is large enough to accommodate the embedded software while at the same time consuming approximately 1.3 mA less current in the active state. Additionally, the power consumed by the green LED can be decreased if a filter is added to its power rail, thus making it possible to have the LED blink without disturbing other parts of the circuit.

The second enhancement is related to the safety of the device. Although the recording of the EEG is stopped when the adapter is connected to a powered USB port, a galvanic connection still exists between the patient and earth ground through the adapter, a condition that renders the patient more susceptible to macroshock. Although this situation can be avoided by ensuring that no patient is connected to the adapter while it is charging, a safer alternative would be to employ an isolation amplifier in the preamplifier stage.

Thirdly, due to the data processing challenges described in section 4.2.2, the MMA7341L accelerometer must be replaced with a unit that has a a digital interface and on-board signal processing functions to automatically detect shocks. A possible replacement is the MMA8453QT, a new IC manufactured by Freescale Semiconductor. This IC measures acceleration in 3 dimensions, possesses an Inter-Integrated Circuit (I^2C) interface, and automatically performs freefall and shake detection. Moreover, compared to the MMA7341L, the MMA8453QT is cheaper and consumes roughly 1/3 of the power.

5.2.4 Embedded Software

Once the modifications detailed in section 4.2.2 were implemented, the embedded software worked very well. Even though the code that processed the accelerometer data had to be removed, given that inexpensive accelerometer ICs exist that have built-in shock detection routines, this is not considered a setback.

Since the source code only consumes 6 % of the flash memory and only 3 % of the SRAM (or approximately 50 % of both memory types if the MCU is replaced by an ATmega164PA), more functions can be added in the future. However, in order to ensure that the additional functionality won't slow down the processing of the EEG signal, multirate signal processing techniques should be implemented. More precisely, since the EEG signal is sampled at 2.52 kHz but the signal's bandwidth only extends to 100 Hz, the digitized signal can be downsampled by a factor of 25. Since LP filtering of the data is a part of the downsampling procedure, an added benefit of this approach is a reduction of the amount of noise in the digitized EEG signal.

Additional functionality that could be added to the adapter include the checking of the battery status and the measurement of the electrode impedance.

5.3 6-channel System

5.3.1 Hardware

Except for the reduced bandwidth, the WEEG4 PMU performs exceptionally well. With its high CMR, high SNR, and low noise values, the PMU is able to record quality signals. Furthermore, its long operating time, which could be extended even further if needed with higher capacity AAA batteries, ensures that the EEG can continue to be recorded while the patient is being transported and until their condition is stabilized in the ER. Finally, the SPOX connector has proven to be reliable and mechanically solid. Nevertheless, its ability to withstand defibrillation pulses still needs to be ascertained.

Changing the form factor of the CIU to the ExpressCard format has proven to be an excellent choice. If the measurement laptop's 2.4 GHz WLAN antenna is easily accessible, as is the case with the Toughbook CF-19, the CIU can be completely housed within the laptop and protected from damage by the laptop's hard exterior shell. Furthermore, qualitative testing has shown that the WLAN antenna extends the operating range of the system to tens of meters. However, if needed, a PCB antenna can still be employed by having a part of the CIU extend outside of the ExpressCard slot.

Seeing as though all 21 electrodes of the 10-20 system are required in order for an EEG recording to be considered comprehensive according to the ACNS guidelines, future versions of the WEEG system may have the capability to measure more than six EEG channels. Several challenges would have to be solved in order to build such a system. The IEEE 802.15.4 standard, upon which the wireless link of the WEEG system is based, was intended for low-rate communication. Hence, a higher-bandwidth wireless link might be required if the number of channels is increased. The circuit design would also have to be reconsidered since the number of electronic components would increase significantly with additional channels. A possible solution to this problem could be to replace the general-purpose discrete analog ICs that are used currently with an integrated solution, such as Imec's ultra low-power 8-channel EEG acquisition IC, which consumes only 2.3 μA of current and includes an 11-bit ADC [119].

5.3.2 PC Software and aEEG Algorithm

From a purely engineering point of view, the software meets the user-friendliness criterion. The EEG signals are displayed in a manner that should be easily understandable by medical professionals: in a referential montage, with the vertical sensitivity in units of μV/cm, and left-to-right, identical to the way that the ECG is drawn in patient monitors. The user interface has been kept tidy, with all elements featuring clear labels and easy-to-recognize icons. Furthermore, all of the software's functions are easily accessible since they are only one click, one touch, or one keystroke away.

Two refinements are possible in order to further enhance the quality of the software. In the present version, EEG signals from different channels are not allowed to overlap on the screen. Instead, if the current vertical sensitivity causes the signal to exceed the bounds of the horizontal rectangle that it is assigned, the signal is clipped at the top and/or at the bottom of the rectangle's edges. Another factor that can cause signal clipping is the slight difference between the DC level of a channel and the half-supply level, which causes the EEG signal to shift either to the top or to the bottom of the rectangle (see Figure 4.3). Seeing as though in many commercial EEG applications the signals are allowed to overlap, a similar system could be implemented in this software in order to handle both issues.

A second refinement could be the inclusion of an EEG streaming protocol. Such a protocol would allow the real-time transmission of the recorded data to the medical unit where the patient is being transported to and/or to a specialist in a remote location for consultation. The protocol would have to encrypt the data for security purposes and work reliably over whichever connection is used to access the Internet,

e.g., 3G/4G cellular connection, WLAN. Finally, it should have a low overhead so that the data streaming can take place even when the network is congested.

aEEG Algorithm

The aEEG algorithm is a potentially useful addition to the recording software, especially since it could provide the medical professional with a quick overview of the neurological state of the patient. However, its value in emergency situations still needs to be established by means of detailed clinical measurements. One potentially challenging aspect is the handling of artefacts in the EEG data, which can erroneously increase the amplitude of the aEEG signal. EOG signals are particularly problematic since their frequency can overlap that of the aEEG's asymmetric bandpass filter and thus cause large deviations in the output signal.

Although the current implementation of the algorithm works well, the drawing of the aEEG signals could be improved in the following way. Instead of drawing one sample per pixel, the drawing speed could be fixed at the start of the recording. In this way, the resulting signal could be more easily compared to examples from literature, which are typically drawn at 6 cm/hour. However, this method will lead to more than one sample being drawn to the same pixel column, with a line connecting the high and low values. Since all information about the local signal density is lost as a result, a pixel color coding scheme should be used. For example, if more than one sample maps to the same pixel, the pixel's color would reflect the amount of times that it has been "written", e.g., blue = only one sample has been written on the pixel, red = more than 5 samples have been written on the pixel.

5.3.3 Quick-Application Cap

The new version of the quick-application cap possesses many advantages when compared with the previous version, and especially when compared with traditional EEG caps. Since the electrode leads are short, braided together, and sewn within the cap's fabric, the possibility of cable motion and power line artifacts is reduced. Also, the absence of long leads, such as those present in wired EEG recorders, facilitates the movement of caregivers around the patient. Furthermore, because it doesn't completely cover the head, additional sensors, e.g., an intracranial pressure monitor, can be used in conjunction with the cap. Finally, if the patient does not perform any abrupt head movements, the cap can be immobilized solely by means of the BTH strap. This characteristic is especially useful if the patient's dorsal mental region is

occupied, for example due to endotracheal intubation.

Compared with traditional EEG caps, the quick-application cap can be placed on the head extremely quickly. The Zipprep electrodes, which don't require any preparation, contribute significantly to the reduction of the application time. However, they are also the limiting factor, since the speed at which the electrode covers can be peeled off is the slowest part of the application procedure. Nevertheless, with training and experience, the covers can be peeled off much quicker. A further disadvantage of this electrode type is that the EEG can only be measured from sub-hairline locations. Active pin electrodes and other novel electrode designs could be used in future versions of the cap in order to overcome this shortcoming.

One potential inconvenience of the quick-application cap is its behavior when subjected to the standard cap cleaning procedure. EEG caps are normally cleaned in a two-step process, first by immersing them in alcohol and then in a soap solution. Since, traditional caps are manufactured from a continuous piece of rubber, they dry relatively quickly. On the other hand, the quick-application cap is made up of woven textiles, which can absorb liquids. Thus, the cap takes longer to dry. One way to get around this problem is to have more than one cap exemplar on hand. In this way, while one cap is drying, another one can be used.

5.4 Comparison with Commercial Systems

Seeing as though no complete EEG system exists that is especially intended for emergency use, the electronics of the 6-channel system and the quick-application cap are compared separately to the products that were reviewed in sections 2.6.1 and 2.6.2, respectively. The 1-channel system has been excluded from this discussion since it has no commercial equivalent.

5.4.1 Electronics

As it can be observed from Table 4.8, the 6-channel system is smaller, lighter, and possesses a higher input impedance than all of the products presented in section 2.6.1. Furthermore, its theoretical bandwidth, measured CMR, actual operating time, and resolution are comparable to the commercial offerings. However, it also measures a smaller number of channels at a lower sampling frequency. Also, the storage frequency is not independent of the sampling frequency.

Before one can draw any conclusions based on this comparison, it is important to remember that the commercial products that were reviewed are intended for long-

term ambulatory measurements. Hence, although its characteristics are similar, the 6-channel system cannot be considered a direct competitor to these products. Instead, these similarities should be considered as an endorsement of the quality of the WEEG4's electronics.

5.4.2 Quick-Application Cap

The following comparison will focus on three aspects: the number of times a cap can be used, the electrode types and their location, and the amount of time needed to attach the cap.

Number of Uses. Both the BraiNet and the StatNet products are one-time use only. However, the Fast'nEasy cap with its integrated electrodes and leads is reusable, just like the cap that was designed in this thesis. On one hand, having a disposable cap is advantageous because no time is spent sterilizing it after use. On the other hand, since the quick-application cap must also protect the WEEG electronics in addition to providing a stable support for the electrodes and their leads, it would be challenging to manufacture a disposable version of it since the material should at the same time be very strong and very cheap.

Electrodes. With its 6 measurement channels, the quick-application cap has the least number of electrodes. Also, all of the measurement locations are below the hairline, as opposed to the three commercial caps, which have electrodes spread out all over the head. The reason for choosing only sub-hairline locations was to allow self-prepping Zipprep electrodes to be employed. Clinical testing is needed in order to determine whether the locations that have been chosen are sufficient in order to quickly determine a patient's neurological condition, and also whether more measurement locations are needed for this purpose.

Application Time. Compared to the three commercial models, the quick-application cap is much faster to apply. Although in the company's brochures the advertised application time for the BraiNet is 1 minute, this cannot include the time it takes to affix the electrodes, even if they are of the self-prepping variety. Hence, the 10–15 minute estimates found in some of the official marketing presentations are likely closer to reality. In the case of the StatNet, since for most patients the hair must be first be moved away from the electrode locations, the application most likely takes between 5 and 10 minutes. Finally, though nothing is mentioned in its datasheet on the subject

of application time, the Fast'nEasy cap undoubtedly takes a long time to apply due to its large number of electrodes. Furthermore, the cap isn't suitable for use in the field since it covers the whole head, which would make it challenging to apply it quickly and accurately in an emergency.

5.5 Significance of the Work

As shown in the previous section, the characteristics of the 6-channel system are comparable to those of commercial systems. In addition, the system is small, light, portable, and features a short preparation time due to the quick-application cap. The same is true also of the 1-channel system. Even though it couldn't be directly compared to any product currently on the market, the quality of the EEG measured with it rivals that of the Neuroscan.

Nevertheless, the true value of this work doesn't lie in the quality of the individual components, or in the way that the software and hardware were designed, but in the fact that now there are two fully-working systems that can be used to record a patient's EEG wherever an emergency may occur and a neurological disorder is suspected. Since no specialized medical personnel is needed in order to operate either of the two systems, the recording method envisaged is much simpler than traditional EEG recordings, but also less expensive. Furthermore, the clinical data that will be gathered by means of these two systems in ambulances, ERs, and ICUs could help in establishing guidelines for the application of EEG in emergency situations. Finally, the knowledge that has been gained through the design of both systems can be employed for the future commercialization of an EM EEG recorder.

5.6 Future Development

The natural continuation of this thesis is the validation of both systems in a hospital environment. To this end, a study involving the 6-channel system will commence at the Seinäjoki Central Hospital in April 2011. The study has already been approved by the Ethical Committee of the Pirkanmaa Hospital District. In the first stage, the system will be used to measure the EEG of healthy patients. Once its reliability in a clinical environment has been established, the system will be employed in PSG studies. Afterward, measurements will be carried out in the ICU, an electrically hostile environment for EEG recordings due to the many electrical machines connected to the patient (e.g., respirator, ECG monitor, electrical infusion pump). If the ICU

measurements are successful, the system will be tried out in the ER. Beyond thoroughly testing the 6-channel system, this study will also help establish the utility of a portable, wireless EEG system in other clinical specialties outside of EM.

It is highly probable that the testing of the 1-channel system will take place in the Helsinki University Central Hospital since a study involving the previous version of the adapter had already been approved by the Ethical Committee of the Hospital District of Helsinki and Uusimaa in 2009. One novel aspect that could be investigated as part of a future study is the minimum number of channels that is required in order to get a quick overview of a patient's neurological state. The results of such a study would determine the amount of channels that should be implemented in a future version of the adapter.

Once both systems have been thoroughly validated in a hospital environment and any issues addressed, the systems' performance should be tested in an ambulance. Due to the small number of caregivers, the large number of tasks that they must accomplish, and the small amount of physical space available, in order for the systems to be successful in this environment, they must prove to be low-maintenance and unobtrusive. In other words, once the systems have been connected to the patient and the recording started, no further user interaction should be required under normal circumstances. Furthermore, the quality of the recorded signals should not be significantly reduced by the constant movement of the ambulance or the challenging recording environment. It is very likely that some fine-tuning of the systems will be required as a result of the experience gained at this stage.

In parallel with the real-life measurements, both systems could be developed further. One of the most important items that must be studied is the effect of defibrillator pulses on scalp electrodes. Besides aiding in the selection of appropriate transient protection resistors for both systems, since no prior information exists on the subject, such a study would elicit strong interest within the medical community. From an electronics point of view, the usability of the systems would be improved by the addition of an automated means to check the electrode impedance at the start and end of each recording. Also, in order to enhance the 6-channel system's portability by allowing the PMU to operate independently of the measurement computer, the recorded EEG data could first be stored onboard and only transmitted when in range of the CIU. The system's recording software can be enhanced by implementing real-time streaming of the EEG data, as discussed in section 5.3.2.

In addition to the enhancements detailed in the previous chapter, two additional changes can be made to the 1-channel system. First, the EEG that is measured could

be stored onboard in solid-state memory. Seeing as though many patient monitors, especially those that are located in ambulances, do not possess a means to easily output the recorded data, this would allow a physician to easily assess how the patient's condition evolved over time. Also, the optimal approach for expanding the adapter's electronics in order to accommodate more measurement channels should be determined. Assuming that a method for displaying more than three signals on a standard patient monitor can be devised, the next challenge lies in keeping the electronics as small and as simple as possible. If the adapter were to be commercialized, the most likely solution would be to replace the discrete analog components with an ASIC.

Chapter 6

Conclusion

This thesis focused on the continuation of the development of two portable EEG systems that are intended for use in ambulances and ERs. Due to the nature of the environment in which they will be used, the resulting systems should make it easy to obtain and analyze the EEG.

The development of the devices started with a review of background information about the EEG, with a particular emphasis on its diagnostic potential and its current use in EM. This was followed by an analysis of methodologies and guidelines for its recording, an examination of the aEEG algorithm, and a brief summary of portable EEG recorders as well as quick-application caps available on the market.

Following this review, the shortcomings of the existing prototypes of the 6-channel and the 1-channel system were analyzed. As a result, the 6-channel system's electronics were miniaturized, the quick-application cap was redesigned in order to make it easier to apply, and the recording software's feature set was expanded to include an improved drawing algorithm, digital filtering, the ability to control the vertical sensitivity as well as the time scale, automatic uploading of the recorded file, and an implementation of the aEEG algorithm. The 1-channel system was completely redesigned in order to improve its adaptative gain accuracy, reduce the circuit noise, and enhance its resistance to the ingress of fluids. Also, a capacitive key used to start/stop the recording and the ability to output a sinusoidal signal with an amplitude equivalent to 100 μV at the system's current gain level were added. For both systems, every design choice has been meticulously analyzed and documented.

The electronics and the software of both systems were thoroughly tested to ensure the recording of high-quality signals as well as reliable operation. Also, the 6-channel system's characteristics were compared to those of commercial devices, with the results of the comparison commented in the last part of the thesis. Based on the results of

the testing, a number of changes and enhancements were suggested.

As a result of the work accomplished during this thesis, two EEG systems suitable for recording in emergency situations have been developed, and their quality demonstrated. The clinical readiness of the two systems will be proven by means of real-life tests in ambulances and hospitals, which are scheduled to begin in April 2011.

References

[1] R. E. D. Bautista, S. Godwin, and D. Caro, "Incorporating abbreviated EEGs in the initial workup of patients who present to the emergency room with mental status changes of unknown etiology," *Journal of Clinical Neurophysiology: Official Publication of the American Electroencephalographic Society*, vol. 24, no. 1, pp. 16–21, Feb. 2007, PMID: 17277572. [Online]. Available: http://www.ncbi.nlm.nih.gov/pubmed/17277572

[2] H. Hooshmand and M. Maloney, "The role of EEG in the emergency room," *Clinical EEG (electroencephalography)*, vol. 11, no. 4, pp. 163–168, Oct. 1980, PMID: 7449160. [Online]. Available: http://www.ncbi.nlm.nih.gov/pubmed/7449160

[3] W. Tatum, "Long-term EEG monitoring: a clinical approach to electrophysiology," *Journal of Clinical Neurophysiology: Official Publication of the American Electroencephalographic Society*, vol. 18, no. 5, pp. 442–455, Sep. 2001, PMID: 11709650. [Online]. Available: http://www.ncbi.nlm.nih.gov/pubmed/11709650

[4] J. Praline, B. de Toffol, K. Mondon, C. Hommet, C. Prunier, P. Corcia, B. Lucas, and A. Autret, "EEG d'urgence : indications réelles et résultats," *Neurophysiologie Clinique/Clinical Neurophysiology*, vol. 34, no. 3-4, pp. 175–181, Oct. 2004. [Online]. Available: http://www.sciencedirect.com/science/article/B6VMP-4CDG0VC-1/2/837c473e82774a16697de000c859c5fd

[5] ——, "[Emergency EEG: actual indications and results]," *Neurophysiologie Clinique = Clinical Neurophysiology*, vol. 34, no. 3-4, pp. 175–181, Oct. 2004, PMID: 15501688. [Online]. Available: http://www.ncbi.nlm.nih.gov/pubmed/15501688

[6] S. V. Kothare, I. Valencia, and A. Legido, "Emergent EEG is helpful in neurology critical care practice," *Clinical Neurophysiology*, vol. 117, no. 3,

pp. 698–699, Mar. 2006. [Online]. Available: http://www.sciencedirect.com/science/article/B6VNP-4J8KNRS-2/2/74a2fd788f84bc27db06dd9951e5800e

[7] F. K. Alehan, L. D. Morton, and J. M. Pellock, "Utility of electroencephalography in the pediatric emergency department," *J Child Neurol*, vol. 16, no. 7, pp. 484–487, Jul. 2001. [Online]. Available: http://jcn.sagepub.com/cgi/content/abstract/16/7/484

[8] S. R. Benbadis, "Use and abuse of stat EEG," *Expert Review of Neurotherapeutics*, vol. 8, no. 6, pp. 865–868, Jun. 2008, PMID: 18505350. [Online]. Available: http://www.ncbi.nlm.nih.gov/pubmed/18505350

[9] P. Thomas, "[Status epilepticus: indications for emergency EEG]," *Neurophysiologie Clinique = Clinical Neurophysiology*, vol. 27, no. 5, pp. 398–405, Nov. 1997, PMID: 9480406. [Online]. Available: http://www.ncbi.nlm.nih.gov/pubmed/9480406

[10] J. Malmivuo and R. Plonsey, "Electroencephalography," in *Bioelectromagnetism - Principles and Applications of Bioelectric and Biomagnetic Fields*. New York, U.S.A.: Oxford University Press, 1995, pp. 257–264. [Online]. Available: http://www.bem.fi/book/

[11] F. L. da Silva, A. V. Rotterdam, E. Niedermeyer, and F. L. da Silva, "Biophysical aspects of EEG and magnetoencephalogram generation," in *Electroencephalography - Basic Principles, Clinical Applications, and Related Fields*, 3rd ed. Baltimore, U.S.A.: Williams & Wilkins, 1993, pp. 78–91.

[12] J. D. Bronzino, "Principles of electroencephalography," in *The Biomedical Engineering Handbook*, 2nd ed. Boca Raton, U.S.A.: CRC Press LLC, 2000.

[13] E. Niedermeyer, E. Niedermeyer, and F. L. da Silva, "The normal EEG of the waking adult," in *Electroencephalography - Basic Principles, Clinical Applications, and Related Fields*, 3rd ed. Baltimore, U.S.A.: Williams & Wilkins, 1993, pp. 131–152.

[14] D. Sherman and D. Waltherspracher, "Electroencephalography," in *Encyclopedia of Medical Devices and Instrumentation*, 2nd ed., J. G. Webster, Ed. Hoboken, U.S.A.: John Wiley & Sons, 2006, vol. 3, pp. 62–83.

[15] J. Praline, J. Grujic, P. Corcia, B. Lucas, C. Hommet, A. Autret, and B. de Toffol, "Emergent EEG in clinical practice," *Clinical Neurophysiology*, vol. 118,

no. 10, pp. 2149–2155, Oct. 2007. [Online]. Available: http://www.sciencedirect.com/science/article/B6VNP-4PG2S37-8/2/587095d52e7b4510c848c03fd4df64f7

[16] M. A. Borges, H. J. Botós, R. F. Bastos, M. F. Godoy, and N. S. A. ao de Marchi, "Emergency EEG: study of survival," *Arquivos De Neuro-Psiquiatria*, vol. 68, no. 2, pp. 174–178, Apr. 2010, PMID: 20464280. [Online]. Available: http://www.ncbi.nlm.nih.gov/pubmed/20464280

[17] O. N. Markand, "Pearls, perils, and pitfalls in the use of the electroencephalogram," *Seminars in Neurology*, vol. 23, no. 1, pp. 7–46, Mar. 2003, PMID: 12870104. [Online]. Available: http://www.ncbi.nlm.nih.gov/pubmed/12870104

[18] R. P. Brenner, "How useful is EEG and EEG monitoring in the acutely ill and how to interpret it?" *Epilepsia*, vol. 50 Suppl 12, pp. 34–37, Dec. 2009, PMID: 19941520. [Online]. Available: http://www.ncbi.nlm.nih.gov/pubmed/19941520

[19] J. Glass, "Understanding seizures and epilepsy," http://www.webmd.com/epilepsy/guide/understanding-seizures-and-epilepsy, 2009. [Online]. Available: http://www.webmd.com/epilepsy/guide/understanding-seizures-and-epilepsy

[20] G. Farnarier, "Indications urgentes de l'EEG dans la situation d'un traumatisme crânien, chez l'enfant et chez l'adulte," *Neurophysiologie Clinique/Clinical Neurophysiology*, vol. 28, no. 2, pp. 121–133, May 1998. [Online]. Available: http://www.sciencedirect.com/science/article/B6VMP-3V7P94C-3/2/4ca39886168065b65591e4c028eca5fa

[21] S. V. Kothare, D. S. Khurana, I. Valencia, J. J. Melvin, and A. Legido, "Use and value of ordering emergency electroencephalograms and videoelectroencephalographic monitoring after business hours in a children's hospital: 1-Year experience," *Journal of Child Neurology*, vol. 20, no. 5, pp. 416 –419, May 2005. [Online]. Available: http://jcn.sagepub.com/content/20/5/416.abstract

[22] K. G. Jordan, "ICU cEEG: new reality, new challenges," UCLA, 2008. [Online]. Available: http://www.jordaneuro.com/sitebuildercontent/sitebuilderfiles/UCLA2008.pdf

[23] K. G. Jordan and A. L. Schneider, "Emergency ("stat") EEG in the era of nonconvulsive status epilepticus," *American Journal of Electroneurodiagnostic Technology*, vol. 49, no. 1, pp. 94–104, Mar. 2009, PMID: 19388551. [Online]. Available: http://www.ncbi.nlm.nih.gov/pubmed/19388551

[24] J. Scozzafava, M. S. Hussain, P. G. Brindley, M. J. Jacka, and D. W. Gross, "The role of the standard 20 minute EEG recording in the comatose patient," *Journal of Clinical Neuroscience: Official Journal of the Neurosurgical Society of Australasia*, vol. 17, no. 1, pp. 64–68, Jan. 2010, PMID: 19683448. [Online]. Available: http://www.ncbi.nlm.nih.gov/pubmed/19683448

[25] B. Legros, P. Fournier, P. Chiaroni, C. Mercier, E. Degiovanni, B. Lucas, B. de Toffol, and B. Aesch, "EEG en urgence et traumatisme crânien," *Neurophysiologie Clinique/Clinical Neurophysiology*, vol. 28, no. 2, pp. 111–120, May 1998. [Online]. Available: http://www.sciencedirect.com/science/article/B6VMP-3V7P94C-2/2/84bbef8b4a91544339ae79b85d7c4101

[26] K. G. Jordan, "Continuous EEG monitoring in the neuroscience intensive care unit and emergency department," *Journal of Clinical Neurophysiology: Official Publication of the American Electroencephalographic Society*, vol. 16, no. 1, pp. 14–39, Jan. 1999, PMID: 10082089. [Online]. Available: http://www.ncbi.nlm.nih.gov/pubmed/10082089

[27] D. Prutchi and M. Norris, "Biopotential amplifiers," in *Design and Development of Medical Electronic Instrumentation*. Hoboken, U.S.A.: John Wiley & Sons, 2005, pp. 1–40.

[28] M. R. Neuman, "Biopotential amplifiers," in *Medical Instrumentation - Application and Design*, 4th ed., J. G. Webster, Ed. Hoboken, U.S.A.: John Wiley & Sons, 2010, pp. 241–292.

[29] J. H. Nagel, "Biopotential amplifiers," in *The Biomedical Engineering Handbook*, 2nd ed., J. D. Bronzino, Ed. Boca Raton, U.S.A.: CRC Press LLC, 2000.

[30] A. C. M. van Rijn, A. Peper, and C. A. Grimbergen, "High-quality recording of bioelectric events. part 1. interference reduction, theory and practice," *Medical & Biological Engineering & Computing*, vol. 28, no. 5, pp. 389–397, Sep. 1990, PMID: 2277538. [Online]. Available: http://www.ncbi.nlm.nih.gov/pubmed/2277538

[31] H. Hinrichs and F. Kreith, "Electroencephalography," in *Biomedical Technology and Devices Handbook*, J. Moore and G. Zouridakis, Eds. Boca Raton, U.S.A.: CRC Press LLC, 2004.

[32] A. Kamp, F. L. da Silva, E. Niedermeyer, and F. L. da Silva, "Technological basis of EEG recording," in *Electroencephalography - Basic Principles, Clinical Applications, and Related Fields*, 3rd ed. Baltimore, U.S.A.: Williams & Wilkins, 1993, pp. 92–103.

[33] W. Putnam and R. B. Knapp, "Biopotential sensors," http://soundlab.cs.princeton.edu/learning/tutorials/sensors/sensors.html, 1996. [Online]. Available: http://soundlab.cs.princeton.edu/learning/tutorials/sensors/sensors.html

[34] A. C. M. van Rijn, A. Peper, and C. A. Grimbergen, "High-quality recording of bioelectric events. part 2. low-noise, low-power multichannel amplifier design," *Medical & Biological Engineering & Computing*, vol. 29, no. 4, pp. 433–440, Jul. 1991, PMID: 1787761. [Online]. Available: http://www.ncbi.nlm.nih.gov/pubmed/1787761

[35] S. Franco, "Instrumentation amplifiers," in *Design with Operational Amplifiers and Analog Integrated Circuits*, 3rd ed. New York, U.S.A.: McGraw Hill Higher Education, Jul. 2003, pp. 79–91.

[36] S. M. Kuo and W. Gan, "Introduction to digital signal processing systems," in *Digital signal processors: architectures, implementations, and applications*. Upper Saddle River, U.S.A.: Pearson Prentice Hall, 2005, pp. 1–40.

[37] S. M. Kuo and B. H. Lee, "Introduction to Real-Time digital signal processing," in *Real-time digital signal processing: implementations, applications, and experiments with the TMS320C55x*. Chichester, England: Wiley, 2001, pp. 1–34.

[38] B. Kemp, "European data format," http://www.edfplus.info/, Jan. 2010. [Online]. Available: http://www.edfplus.info/

[39] "BioSemi data format (BDF)," http://www.biosemi.com/faq/file_format.htm, Apr. 2006. [Online]. Available: http://www.biosemi.com/faq/file_format.htm

[40] A. Schlögl, "GDF v2 project site," http://www.dpmi.tu-graz.ac.at/~schloegl/biosig/GDF2.0/, Jul. 2008. [Online]. Available: http://www.dpmi.tu-graz.ac.at/~schloegl/biosig/GDF2.0/

[41] R. M. Rangayyan, "Adaptive filters for removal of interference," in *Biomedical Signal Analysis*. New York, USA: Wiley-Interscience, 2002, pp. 146–158.

[42] S. R. Benbadis and D. Rielo, "EEG artifacts," *eMedicine Neurology*, Mar. 2010. [Online]. Available: http://emedicine.medscape.com/article/1140247-overview

[43] M. V. Gils, "Dealing with artefacts and noise," Tampere University of Technology, Feb. 2008.

[44] S. Franco, "Noise," in *Design with Operational Amplifiers and Analog Integrated Circuits*, 3rd ed. New York, U.S.A.: McGraw-Hill, 2002, pp. 311–346.

[45] M. Pecht, P. Lall, and R. C. Dorf, "Passive components," in *The Electrical Engineering Handbook*. Boca Raton, U.S.A.: CRC Press LLC, 2000.

[46] I. F. of Clinical Neurophysiology, G. Deuschl, and A. Eisen, *Recommendations for the practice of clinical neurophysiology: guidelines of the International Federation of Clinical Neurophysiology*. Elsevier Health Sciences, 1999.

[47] "Guidelines," http://www.acns.org/, Nov. 2009. [Online]. Available: http://www.acns.org/

[48] "Guideline 1: Minimum technical requirements for performing clinical electroencephalography," *Journal of Clinical Neurophysiology: Official Publication of the American Electroencephalographic Society*, vol. 23, no. 2, pp. 86–91, Apr. 2006, PMID: 16612222. [Online]. Available: http://www.ncbi.nlm.nih.gov/pubmed/16612222

[49] "Guideline 8: Guidelines for recording clinical EEG on digital media," *Journal of Clinical Neurophysiology: Official Publication of the American Electroencephalographic Society*, vol. 23, no. 2, pp. 122–124, Apr. 2006, PMID: 16612229. [Online]. Available: http://www.ncbi.nlm.nih.gov/pubmed/16612229

[50] American and F. R. on the Treasury of the French Language Project, "Webster's revised unabridged dictionary (1913 + 1828)," http://machaut.uchicago.edu/websters. [Online]. Available: http://machaut.uchicago.edu/websters

[51] J. C. Sigl and N. G. Chamoun, "An introduction to bispectral analysis for the electroencephalogram," *Journal of Clinical Monitoring*, vol. 10, no. 6, pp. 392–404, 1994. [Online]. Available: http://www.springerlink.com/content/l156022437116322/

[52] H. Viertiö-Oja, V. Maja, M. Särkelä, P. Talja, N. Tenkanen, H. Tolvanen-Laakso, M. Paloheimo, A. Vakkuri, A. Yli-Hankala, and P. Meriläinen, "Description of the entropy algorithm as applied in the Datex-Ohmeda s/5 entropy module," *Acta Anaesthesiologica Scandinavica*, vol. 48, no. 2, pp. 154–161, Feb. 2004, PMID: 14995936. [Online]. Available: http://www.ncbi.nlm.nih.gov/pubmed/14995936

[53] D. A. Kaiser, "Basic principles of quantitative EEG," *Journal of Adult Development*, vol. 12, no. 2-3, pp. 99–104, Aug. 2005. [Online]. Available: http://www.springerlink.com/content/y835007782032664/

[54] D. Maynard, P. F. Prior, and D. F. Scott, "Device for continuous monitoring of cerebral activity in resuscitated patients." *British Medical Journal*, vol. 4, no. 5682, p. 545–546, Nov. 1969, PMC1630343.

[55] P. F. Prior, D. E. Maynard, P. C. Sheaff, B. R. Simpson, L. Strunin, E. J. M. Weaver, and D. F. Scott, "Monitoring cerebral function: Clinical experience with new device for continuous recording of electrical activity of brain," *British Medical Journal*, vol. 2, no. 5764, pp. 736–738, Jun. 1971, PMID: 43262864326286 PMCID: 1796304.

[56] V. Jäntti, P. Prior, and D. Maynard, "Neljä päivää EEG-valvontaa sydämenpysähdyksen jälkeen," *Duodecim*, vol. 8, no. 110, pp. 785–790, 1994.

[57] J. W. Osselton, "Electroencephalographic monitoring in epilepsy," *Clinical Physics and Physiological Measurement*, vol. 12, no. 3, pp. 203–217, 1991. [Online]. Available: http://www.iop.org/EJ/abstract/0143-0815/12/3/001

[58] C. Theda, "Use of amplitude integrated electroencephalography (aEEG) in patients with inborn errors of metabolism - a new tool for the metabolic geneticist," *Molecular Genetics and Metabolism*, vol. 100 Suppl 1, pp. S42–48, 2010, PMID: 20303809. [Online]. Available: http://www.ncbi.nlm.nih.gov/pubmed/20303809

[59] C. B. Yucha, P. Tsai, K. S. Calderon, and F. Kreith, "Ambulatory applications for monitoring physiological parameters," in *Biomedical Technology and Devices Handbook*, J. Moore and G. Zouridakis, Eds. Boca Raton, U.S.A.: CRC Press LLC, 2004.

[60] G. Technologies, "Clinical systems - TREA ambulatory EEG," http://www.grasstechnologies.com/products/clinsystems/trea1.html, Aug. 2010. [Online]. Available: http://www.grasstechnologies.com/products/clinsystems/trea1.html

[61] C. Laboratories, "Easy ambulatory 2," Jul. 2006. [Online]. Available: http://www.cadwell.com/products/eeg/easyambulatoryeeg/ambulatorybrochure.pdf

[62] Lifelines, "Trackit ambulatory EEG recorders," Nov. 2005. [Online]. Available: http://www.llines.com/pdfs/Trackit_Brochure_1005.pdf

[63] W. Graphtek, "Ambulatory EEG recorder," http://www.walter-graphtek.com/ambulatoryrecording_enu.html, Jan. 2010. [Online]. Available: http://www.walter-graphtek.com/ambulatoryrecording_enu.html

[64] CareFusion, "NicoletOne ambulatory EEG," Jul. 2006. [Online]. Available: http://www.viasyshealthcare.com/prod_serv/downloads/321_NicoletOne_Ambulatory_EEG.pdf

[65] BrainScope, "ZOOM-100DC 510(k) premarket notification," Aug. 2009. [Online]. Available: http://www.accessdata.fda.gov/cdrh_docs/pdf8/K082886.pdf

[66] "Jordan NeuroScience," http://www.jordaneuro.com/, Mar. 2010. [Online]. Available: http://www.jordaneuro.com/

[67] A. Schneider, "BraiNet - benefits and overview," Aug. 2007. [Online]. Available: http://www.jordaneuro.com/sitebuildercontent/sitebuilderfiles/BraiNetBenefitsandOverview.ppt

[68] H. Inc., "StatNet," http://www.hydrodot.net/Products/statnet.html, 2010. [Online]. Available: http://www.hydrodot.net/Products/statnet.html

[69] B. P. GmbH, "Selecting a suitable EEG recording cap," Nov. 2009. [Online]. Available: http://www.brainproducts.com/filedownload.php?path=downloads/Tutorial/Selecting_a_cap_Tutorial-001.pdf

[70] A. Salmi, "Attachment band for EEG monitoring in emergency medicine," M.Sc. Thesis, Tampere University of Technology, Tampere, Finland, May 2006.

[71] M. Pänkälä, "Development of EEG measurement software for emergency medicine," M.Sc. Thesis, Tampere University of Technology, Tampere, Finland, Mar. 2007.

[72] A. Tuomi, "EEG interface for portable ECG recorders," M.Sc. Thesis, Tampere University of Technology, Tampere, Finland, Mar. 2009.

[73] "Defibrillator proof applied parts," http://www.medteq.info/med/node/58. [Online]. Available: http://www.medteq.info/med/node/58

[74] G. Healthcare, "Entropy module, E-ENTROPY," Mar. 2006. [Online]. Available: http://www.gehealthcare.com/euen/patient_monitoring/docs/M1034923.pdf

[75] E. Anderson and E. Schlaepfer, "Overvoltage protection for sensitive amplifier applications - part 1," http://www.eetimes.com/design/automotive-design/4009908/Overvoltage-protection-for-sensitive-amplifier-applications-Part-1, Dec. 2006. [Online]. Available: http://www.eetimes.com/design/automotive-design/4009908/Overvoltage-protection-for-sensitive-amplifier-applications-Part-1

[76] D. Prutchi and M. Norris, "Design of safe medical device prototypes," in *Design and Development of Medical Electronic Instrumentation*. Hoboken, U.S.A.: John Wiley & Sons, 2005, pp. 97–146.

[77] T. Instruments, "INA118 precision, low power instrumentation amplifier," Sep. 2000. [Online]. Available: http://www.ti.com/lit/gpn/ina118

[78] M. I. Products, "AN864 - EPOT applications: Gain adjustment in Op-Amp circuits," Nov. 2001. [Online]. Available: http://pdfserv.maxim-ic.com/en/an/AN864.pdf

[79] T. Instruments, "PGA112 Zero-Drift, programmable gain amplifier with mux," Sep. 2008. [Online]. Available: http://www.ti.com/lit/gpn/pga112

[80] Atmel, "ATmega1284P 8-bit microcontroller with 16/32/64/128K bytes In-System programmable flash," Jan. 2010. [Online]. Available: http://www.atmel.com/dyn/resources/prod_documents/doc8272.pdf

[81] S. Franco, "Active filters: Part 1," in *Design with Operational Amplifiers and Analog Integrated Circuits*, 3rd ed. New York, U.S.A.: McGraw-Hill, 2002.

[82] T. Kugelstadt, "Active filter design techniques," Jan. 2008. [Online]. Available: http://focus.ti.com/lit/ml/sloa088/sloa088.pdf

[83] Maxim, "MAX4237 SOT23, very high precision, 3V/5V Rail-to-Rail op amps," Aug. 2001. [Online]. Available: http://datasheets.maxim-ic.com/en/ds/MAX4236-MAX4237.pdf

[84] R. Downs and M. Oljaca, "Designing SAR ADC drive circuitry - part 1: A detailed look at SAR ADC operation," Feb. 2005. [Online]. Available: http://www.en-genius.net/includes/files/acqt_022106.pdf

[85] M. Oljaca and B. C. Baker, "Start with the right op amp when driving SAR ADCs," Oct. 2008. [Online]. Available: http://e2e.ti.com/cfs-filesystemfile.ashx/__key/CommunityServer.Components.PostAttachments/00.00.00.15.30/EDN-oct-16-2008-op-amp-and-rc-load-oljaca-and-baker.pdf

[86] A. Corporation, "Atmel QTouch library user guide," Jul. 2010. [Online]. Available: http://www.atmel.com/dyn/resources/prod_documents/doc8207.pdf

[87] P. Russell, "Atmel QTouch layout quick reference," Jan. 2010. [Online]. Available: http://www.avrfreaks.net/index.php?module=Freaks%20Files&func=viewFile&id=4024

[88] R. Stein and J. Day, "AN655 - D/A conversion using PWM and R-2R ladders to generate sine and DTMF waveforms," Jan. 2003. [Online]. Available: http://ww1.microchip.com/downloads/en/AppNotes/00655a.pdf

[89] Maxim, "MAX4250 Single-Supply, Low-Noise, Low-Distortion, Rail-to-Rail op amp," Sep. 2005. [Online]. Available: http://datasheets.maxim-ic.com/en/ds/MAX4249-MAX4257.pdf

[90] "WinAVR: AVR-GCC for windows," http://winavr.sourceforge.net, Oct. 2006. [Online]. Available: http://winavr.sourceforge.net

[91] M. J. B. Rogers, K. Hrovat, K. McPherson, M. E. Moskowitz, and T. Reckart, "Accelerometer data analysis and presentation techniques," Sep. 1997. [Online]. Available: http://ntrs.nasa.gov/archive/nasa/casi.ntrs.nasa.gov/19970034695_1997067108.pdf

[92] PCI-SIG, "PCIe mini card electromechanical specification revision 1.2," Oct. 2007. [Online]. Available: http://www.pcisig.com/members/downloads/specifications/pciexpress/PCI_Express_Mini_CEM_12_26Oct07_ncb.pdf

[93] P. Association, "ExpressCard 2.0 standard," Feb. 2009. [Online]. Available: http://www.usb.org/developers/expresscard/EC_specifications/ExpressCard_2_0_FINAL.pdf

[94] F. Semiconductor, "Compact integrated antennas," Jul. 2006. [Online]. Available: http://www.freescale.com/files/rf_if/doc/app_note/AN2731.pdf

[95] R. Struzak, "Basic antenna theory," The Abdus Salam International Centre for Theoretical Physics ICTP, Trieste, Italy, Feb. 2007. [Online]. Available: http://wireless.ictp.trieste.it/school_2007/lectures/Struzak/5Anten_theor_basics.pdf

[96] A. Andersen, "2.4 GHz inverted f antenna," Apr. 2008. [Online]. Available: http://focus.ti.com/lit/an/swru120b/swru120b.pdf

[97] "IEEE std 802.11-2007, IEEE standard for information technology - telecommunications and information exchange between systems - local and metropolitan area networks-Specific requirements - part 11: Wireless LAN medium access control (MAC) and physical layer (PHY) specifications," Jun. 2007. [Online]. Available: http://standards.ieee.org/getieee802/download/802.11-2007.pdf

[98] "IEEE std 802.11n-2009, IEEE standard for information technology - telecommunications and information exchange between systems - local and metropolitan area networks-Specific requirements - part 11: Wireless LAN medium access control (MAC) and physical layer (PHY) specifications - amendment 5: Enhancements for higher throughput," Oct. 2009. [Online]. Available: http://standards.ieee.org/getieee802/download/802.11n-2009.pdf

[99] Weidmüller, "SL 5.08/8/90 side entry header, 8 way - datasheet," Jan. 2007. [Online]. Available: http://www.farnell.com/datasheets/57081.pdf

[100] A. D. Jakab and W. El-Kary, "EEG noise filtering," Dec. 2007.

[101] T. Ylönen, "RFC 4251, the secure shell (SSH) protocol architecture," Jan. 2006. [Online]. Available: http://tools.ietf.org/html/rfc4251

[102] O. Project, "OpenSSH portable release for Linux/Solaris/etc," http://www.openssh.com/portable.html, Sep. 2010. [Online]. Available: http://www.openssh.com/portable.html

[103] D. Stenberg, "libcurl - the multiprotocol file transfer library," http://curl.haxx.se/libcurl/, Oct. 2010. [Online]. Available: http://curl.haxx.se/libcurl/

[104] T. Jones, "Boost application performance using asynchronous I/O," http://www.ibm.com/developerworks/linux/library/l-async/, Aug. 2006. [Online]. Available: http://www.ibm.com/developerworks/linux/library/l-async/

[105] M. Corporation, "Synchronous and asynchronous I/O," http://msdn.microsoft.com/en-us/library/aa365683%28VS.85%29.aspx, Oct. 2010. [Online]. Available: http://msdn.microsoft.com/en-us/library/aa365683%28VS.85%29.aspx

[106] "Webopedia - I/O," http://www.webopedia.com/TERM/I/I_O.html, 2010. [Online]. Available: http://www.webopedia.com/TERM/I/I_O.html

[107] P. M. Encyclopedia, "Multithreading definition," http://www.pcmag.com/encyclopedia_term/0,2542,t=multithreading&i=47522,00.asp, 2010. [Online]. Available: http://www.pcmag.com/encyclopedia_term/0,2542,t=multithreading&i=47522,00.asp

[108] S. Herb, "A fundamental turn toward concurrency in software," *Dr. Dobb's Journal*, vol. 30, no. 3, Mar. 2005. [Online]. Available: http://www.drdobbs.com/architecture-and-design/184405990

[109] C. Chan, "Effective logging practices ease enterprise development," http://www.ibm.com/developerworks/java/library/j-logging/, Aug. 2005. [Online]. Available: http://www.ibm.com/developerworks/java/library/j-logging/

[110] D. Veillard, "libxml2 - the XML c parser and toolkit of gnome," http://xmlsoft.org/, 2010. [Online]. Available: http://xmlsoft.org/

[111] M. Corporation, "Scheduling priorities," http://msdn.microsoft.com/en-us/library/ms685100%28v=VS.85%29.aspx, Sep. 2010. [Online]. Available: http://msdn.microsoft.com/en-us/library/ms685100%28v=VS.85%29.aspx

[112] K. E. Wendel, "The effects of cerebrospinal fluid on electrode placement for emergency EEG recordings," M.Sc. Thesis, Tampere University of Technology, Tampere, Finland, Apr. 2006.

[113] "Pre-Hospital cervical spinal immobilization following trauma," Sep. 2001. [Online]. Available: http://static.spineuniverse.com/pdf/traumaguide/1.pdf

[114] L. Medical, "Spinal immobilization," http://www.laerdal.com/nav/7160016/Spinal-Immobilization.html, 2010. [Online]. Available: http://www.laerdal.com/nav/7160016/Spinal-Immobilization.html

[115] C. Hurt, "Paramedic skills," Nov. 2008. [Online]. Available: http://www.moteclife.co.uk/docs/Education/Paramedic%20Skills.pdf

[116] E. McAdams, "Bioelectrodes," in *Encyclopedia of Medical Devices and Instrumentation*, 2nd ed., J. G. Webster, Ed. Hoboken, U.S.A.: John Wiley & Sons, 2006, vol. 1, pp. 120–166.

[117] G. T. OEG, "g.CFMtoolbox - cerebral function analysis," http://www.gtec.at/products/g.BSanalyse/g.CFMtoolbox/gCFMtoolbox.htm, 2008. [Online]. Available: http://www.gtec.at/products/g.BSanalyse/g.CFMtoolbox/gCFMtoolbox.htm

[118] A. L. Goldberger, L. A. N. Amaral, L. Glass, J. M. Hausdorff, P. C. Ivanov, R. G. Mark, J. E. Mietus, G. B. Moody, C. Peng, and H. E. Stanley, "PhysioBank, PhysioToolkit, and PhysioNet : Components of a new research resource for complex physiologic signals," *Circulation*, vol. 101, no. 23, pp. e215–220, Jun. 2000. [Online]. Available: http://circ.ahajournals.org/cgi/content/abstract/101/23/e215

[119] IMEC, "Smart implant ultra-low-power design," http://www.imec.be/ScientificReport/SR2008/HTML/1225134.html, Apr. 2009. [Online]. Available: http://www.imec.be/ScientificReport/SR2008/HTML/1225134.html

Appendix A

1-channel System

A.1 Schematics

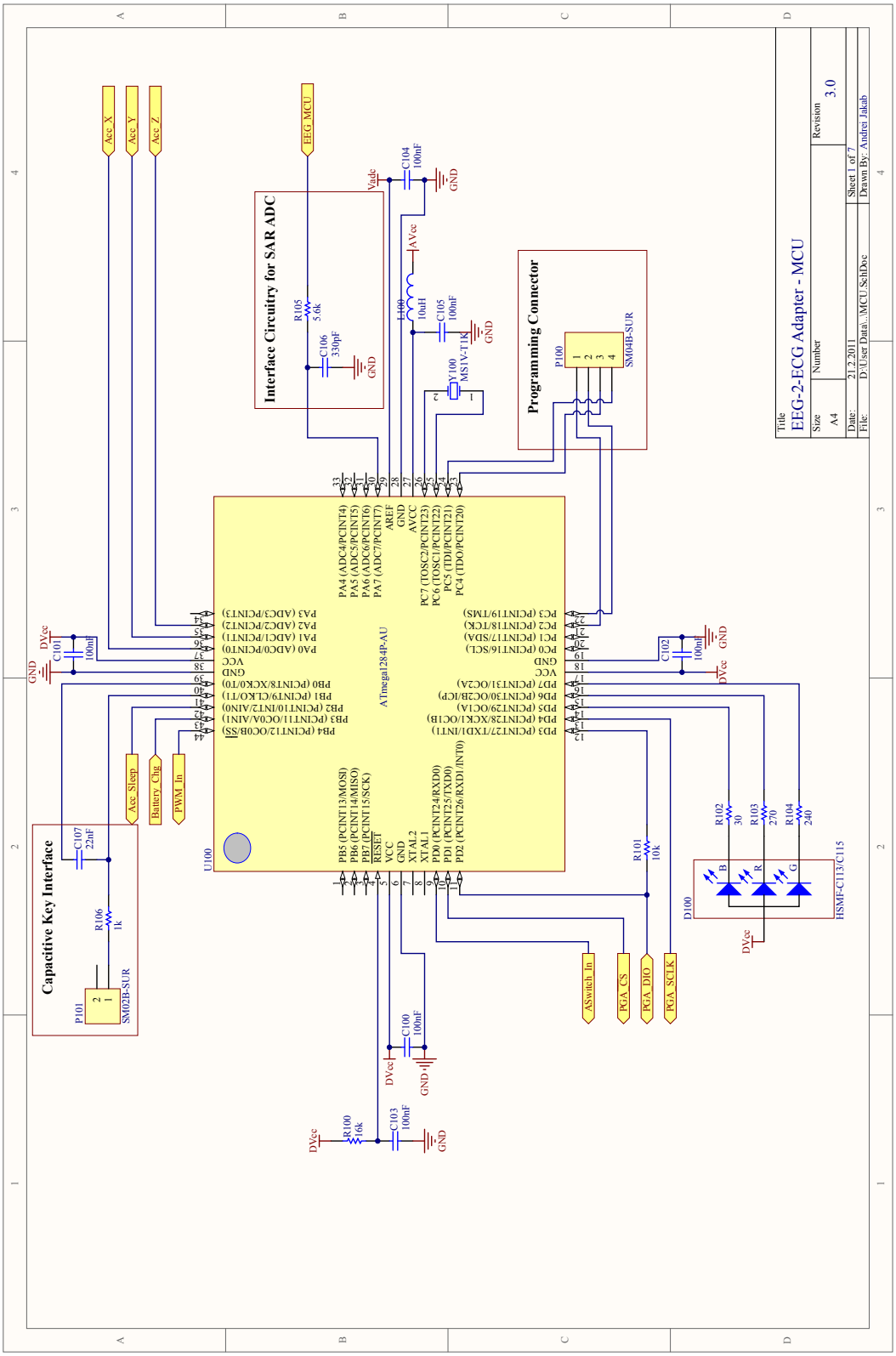

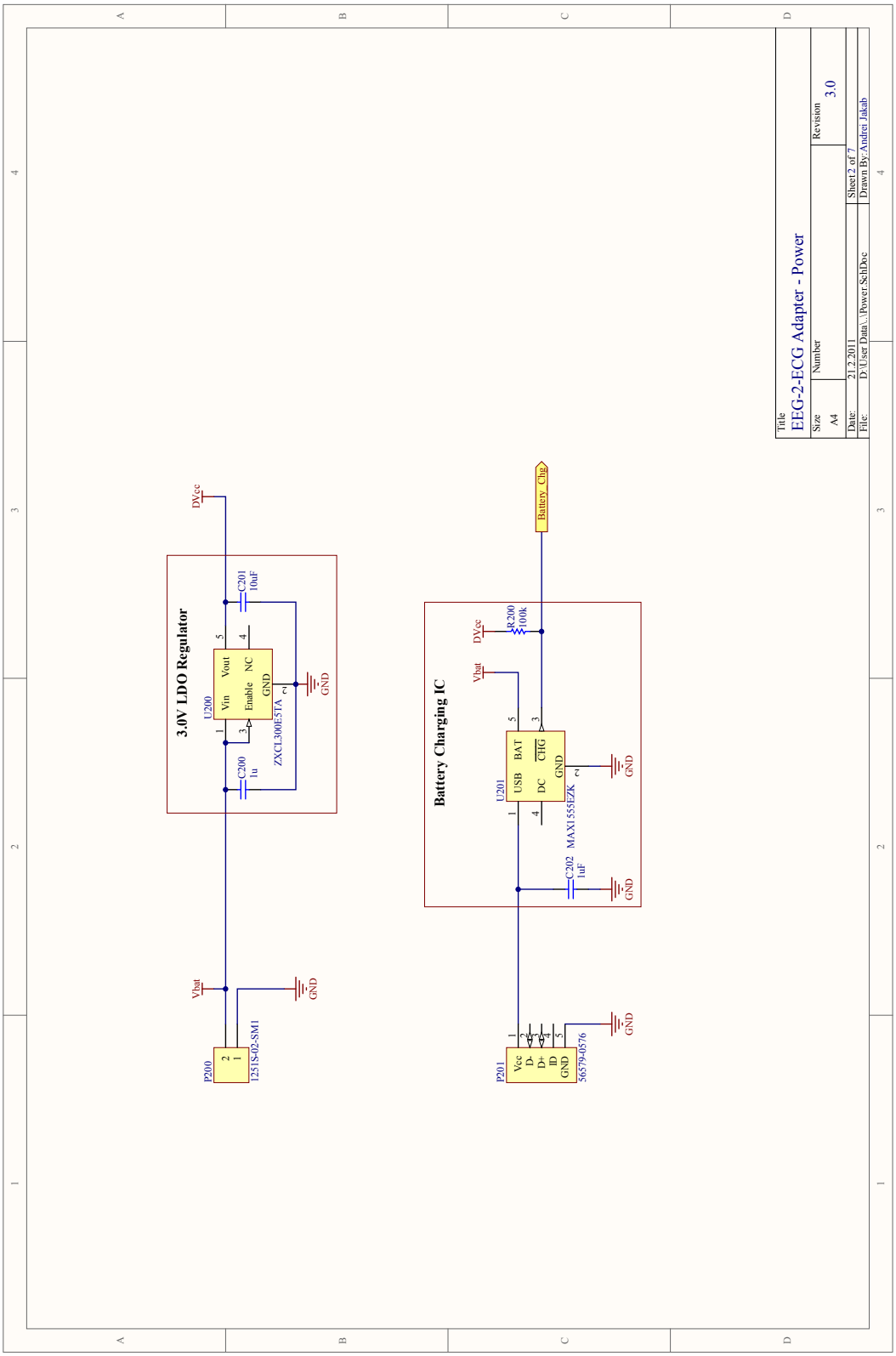
Title
EEG-2-ECG Adapter - Power
Size
A4
Number
Revision
3.0
Date:
21.2.2011
Sheet 2 of 7
File:
D:\User Data\..\Power.SchDoc
Drawn By: Andrei Jakab
3.0V LDO Regulator
DVcc
C201
10uF
U200
Vin
Vout
NC
Enable
GND
ZXCL300E5TA
C200
1u
GND
Vbat
GND
P200
2
1
1251S02-SM1
Battery Charging IC
Battery_Chip
DVcc
R200
100k
Vbat
U201
USB
BAT
DC
CHG
GND
MAX1555EZK
C202
1uF
GND
P201
Vcc
D-
D+
ID
GND
56579-0576
GND

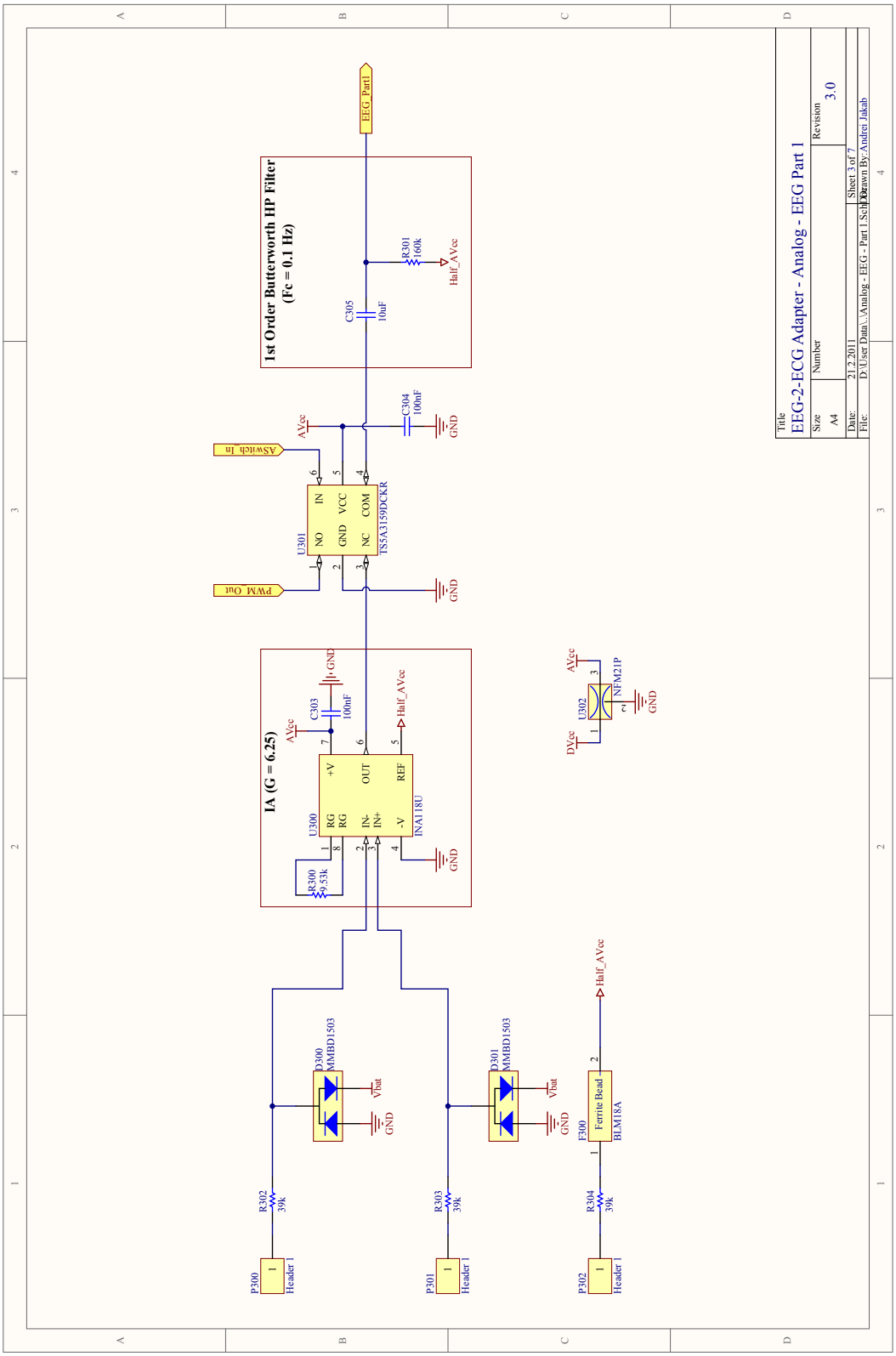
EEG_Part1
1st Order Butterworth HP Filter
(Fc = 0.1 Hz)
R301
160k
Half_AVcc
C305
10uF
C304
100nF
AVcc
GND
ASwitch_In
PWM_Out
U301
TS5A3159DCKR
IA (G = 6.25)
C303
100nF
R300
9.53k
U300
INA118U
D300
MMBD1503
D301
MMBD1503
Vbat
R302
39k
R303
39k
R304
39k
P300
P301
P302
Header 1
F300
Ferrite Bead
BLM18A
U302
NFM21P
DVcc
Title
EEG-2-ECG Adapter - Analog - EEG Part 1
Size
A4
Number
Revision
3.0
Date:
21.2.2011
Sheet 3 of 7
File:
D:\User Data\...\Analog - EEG - Part 1.SchDoc
Drawn By:
Andrei Jakab

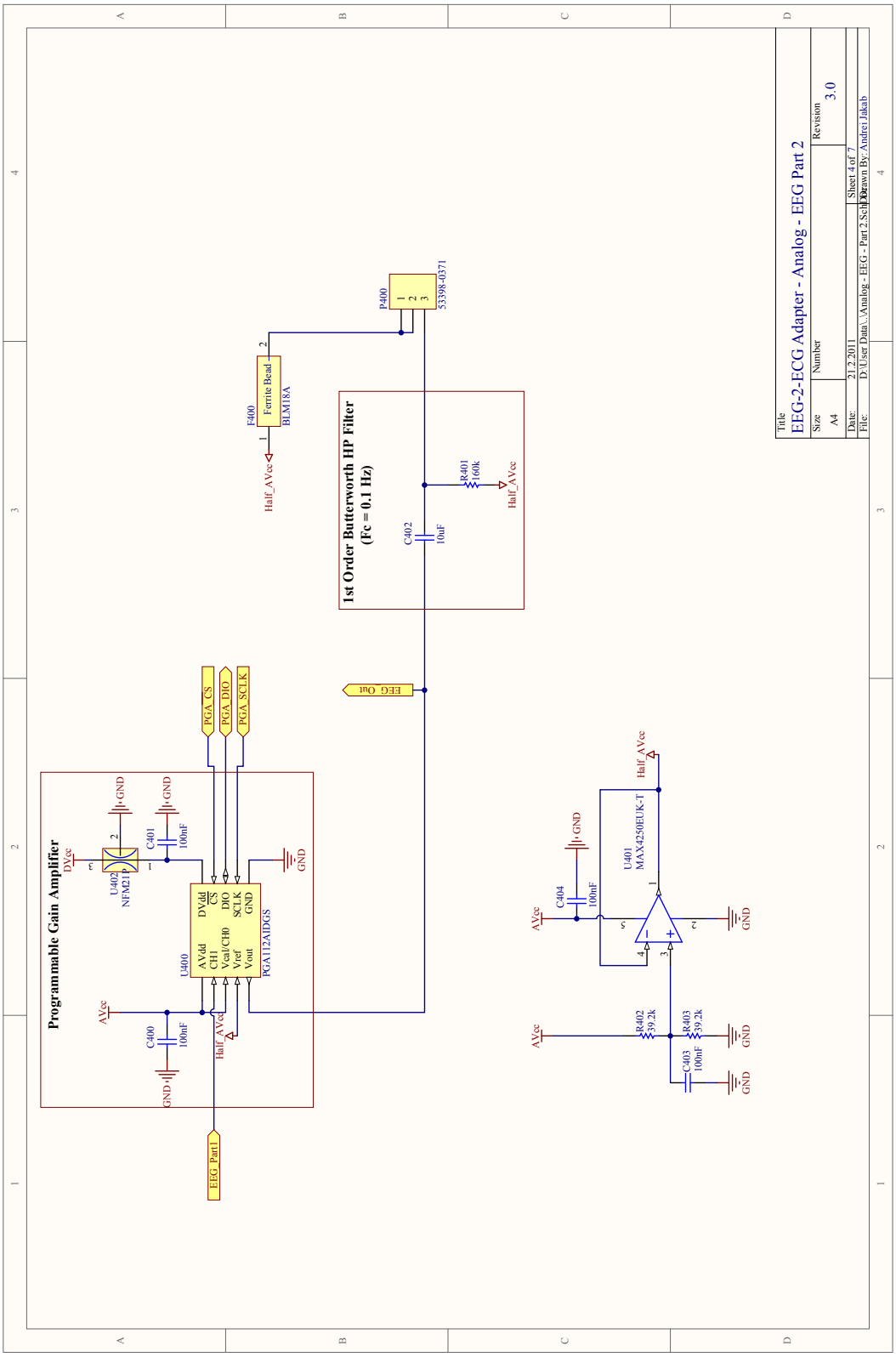
Title
EEG-2-ECG Adapter - Analog - EEG Part 2
Size
A4
Number
Revision
3.0
Date:
21.2.2011
Sheet 4 of 7
File:
D:\User Data\...\Analog - EEG - Part 2.SchDoc
Drawn By: Andrei Jakab
Programmable Gain Amplifier
1st Order Butterworth HP Filter
(Fc = 0.1 Hz)
P400
53398-0371
F400
Ferrite Bead
BLM18A
Half_AVcc
R401
160k
C402
10uF
EEG_Out
PGA_CS
PGA_DIO
PGA_SCLK
DVcc
U402
NFM21P
C401
100nF
GND
U400
DVdd
CS
DIO
SCLK
GND
AVdd
CH1
Vcal/CH0
Vref
Vout
PGA112AIDGS
AVcc
C400
100nF
EEG_Part1
U401
MAX4250EUK-T
C404
100nF
R402
39.2k
R403
39.2k
C403
100nF

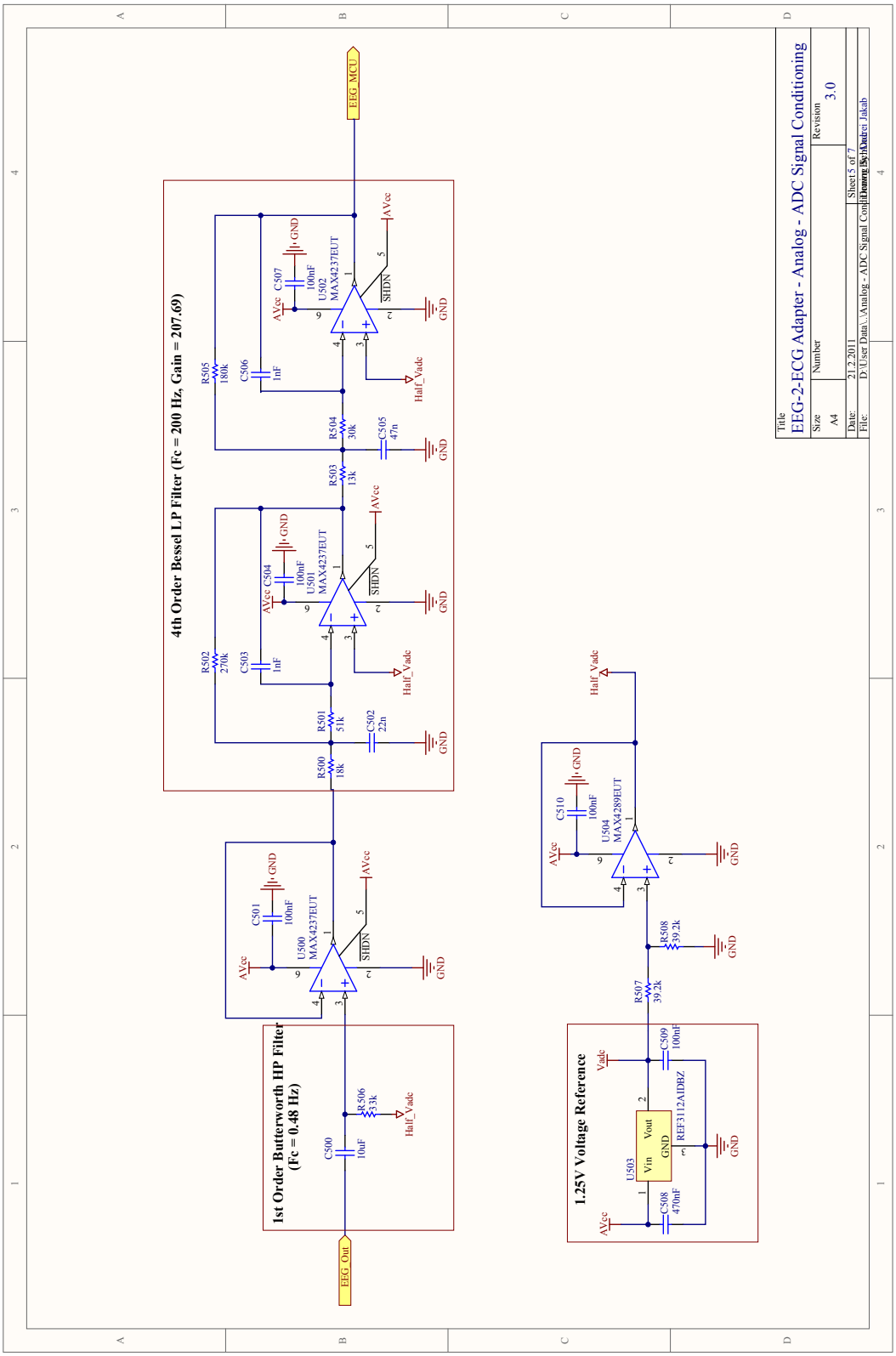
EEG_MCU
4th Order Bessel LP Filter (Fc = 200 Hz, Gain = 207.69)
1st Order Butterworth HP Filter (Fc = 0.48 Hz)
1.25V Voltage Reference
EEG_Out
Half_Vade
AVcc
GND
Vade
Title
EEG-2-ECG Adapter - Analog - ADC Signal Conditioning
Size
A4
Number
Revision
3.0
Date:
21.2.2011
Sheet 5 of 7
File:
D:\User Data\..\Analog - ADC Signal Cond
Drawn By:
Andrej Jakab

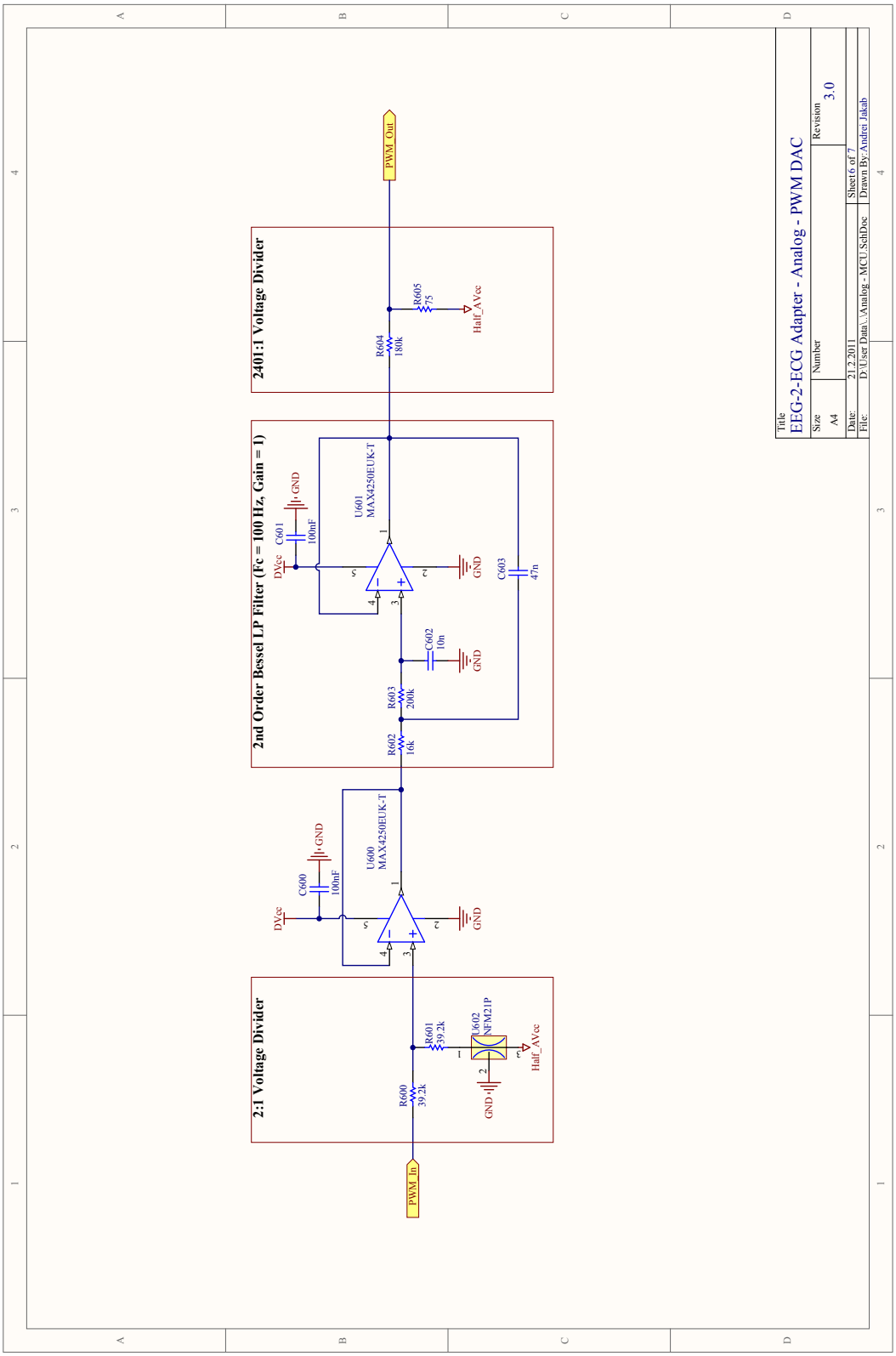
PWM_Out
2401:1 Voltage Divider
R605
75
Half_AVcc
R604
180k
2nd Order Bessel LP Filter (Fc = 100 Hz, Gain = 1)
U601
MAX4250EUK-T
C601
100nF
GND
DVcc
C603
47n
C602
10n
R603
200k
R602
16k
U600
MAX4250EUK-T
C600
100nF
2:1 Voltage Divider
R601
39.2k
U602
NFM21P
R600
39.2k
PWM_In
Title
EEG-2-ECG Adapter - Analog - PWM DAC
Size
A4
Number
Revision
3.0
Date:
21.2.2011
Sheet 6 of 7
File:
D:\User Data\..\Analog - MCU.SchDoc
Drawn By:
Andrei Jakab

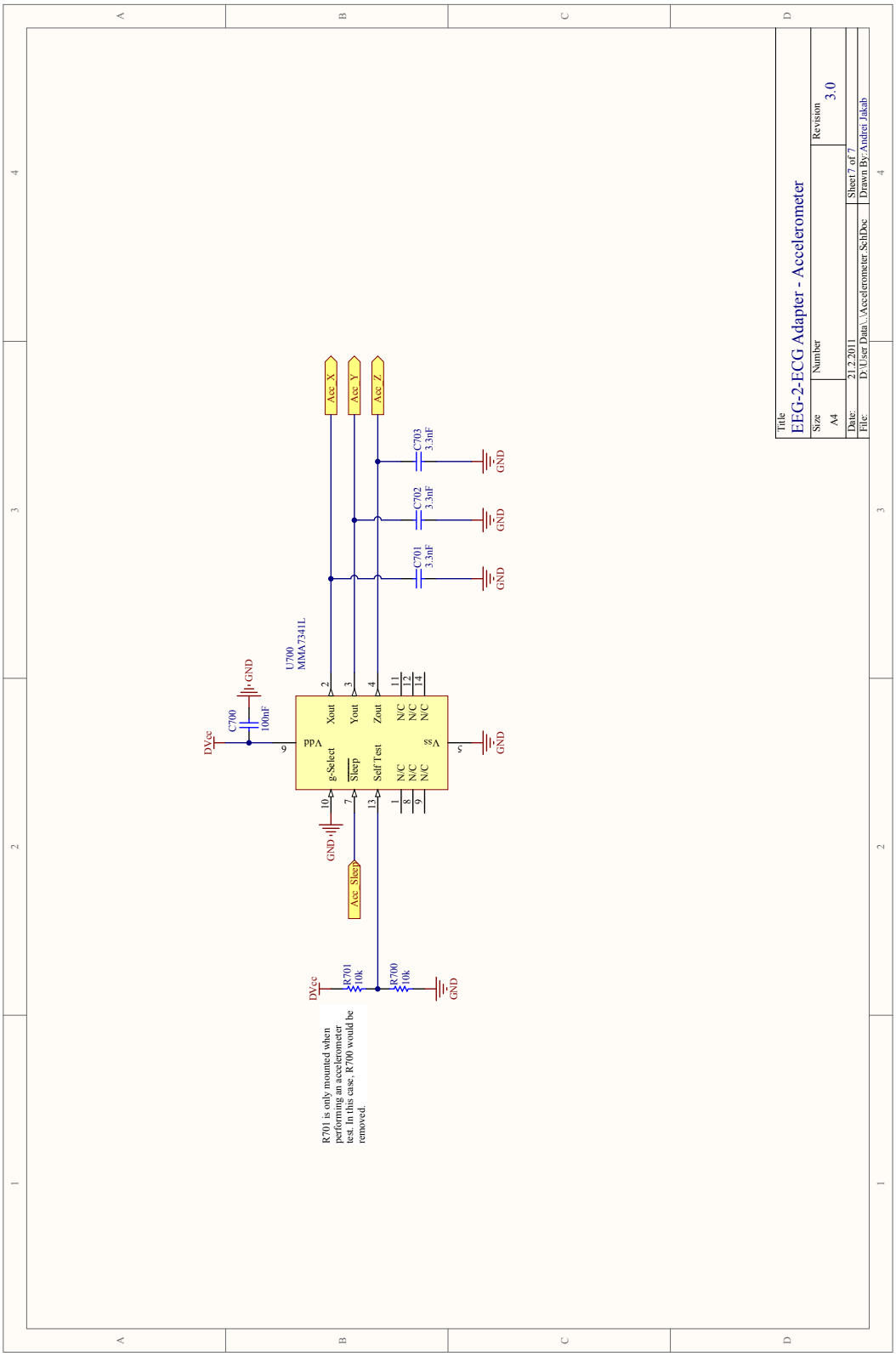
Title
EEG-2-ECG Adapter - Accelerometer
Size
A4
Number
Revision
3.0
Date:
21.2.2011
Sheet 7 of 7
File:
D:\User Data\...\Accelerometer.SchDoc
Drawn By: Andrei Jakab
U700
MMA7341L
Acc_X
Acc_Y
Acc_Z
Acc_Sleep
C700
100nF
C701
3.3nF
C702
3.3nF
C703
3.3nF
R700
10k
R701
10k
DVcc
GND
Xout
Yout
Zout
g-Select
Sleep
Self Test
N/C
R701 is only mounted when performing an accelerometer test. In this case, R700 would be removed.

A.2 Main Routine

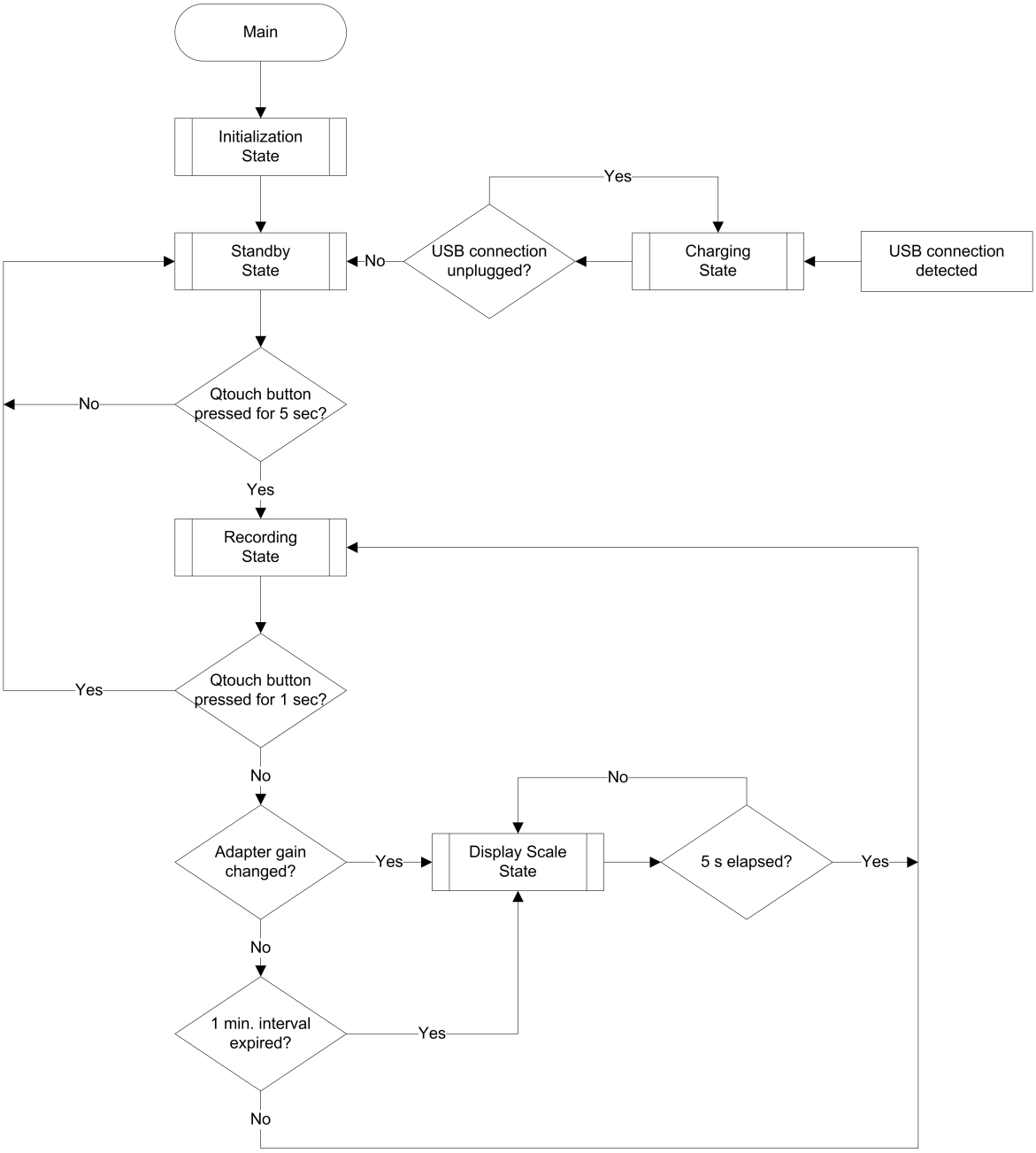

Appendix B

6-channel System

B.1 PMU Analog Frontend Schematics

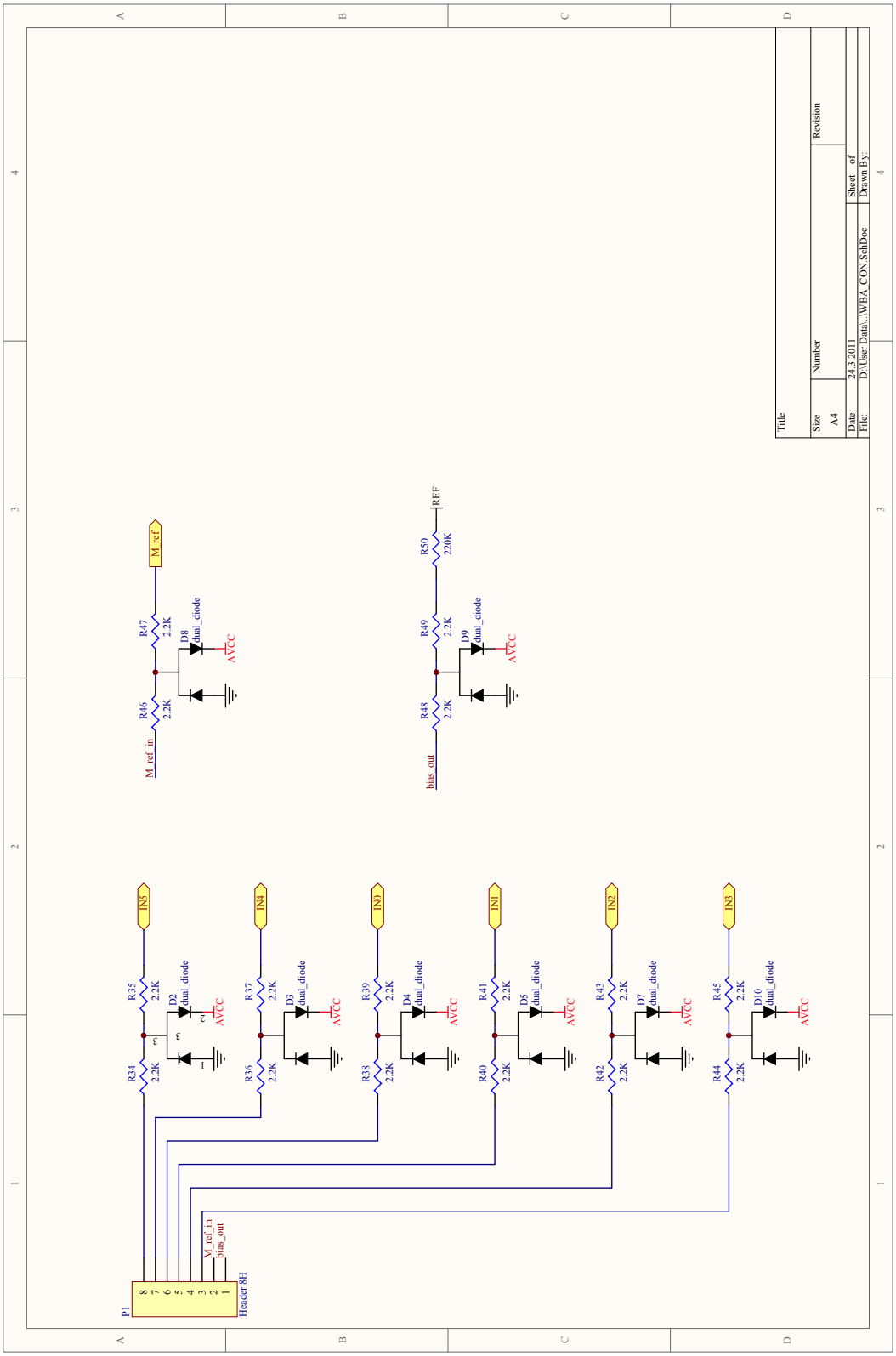

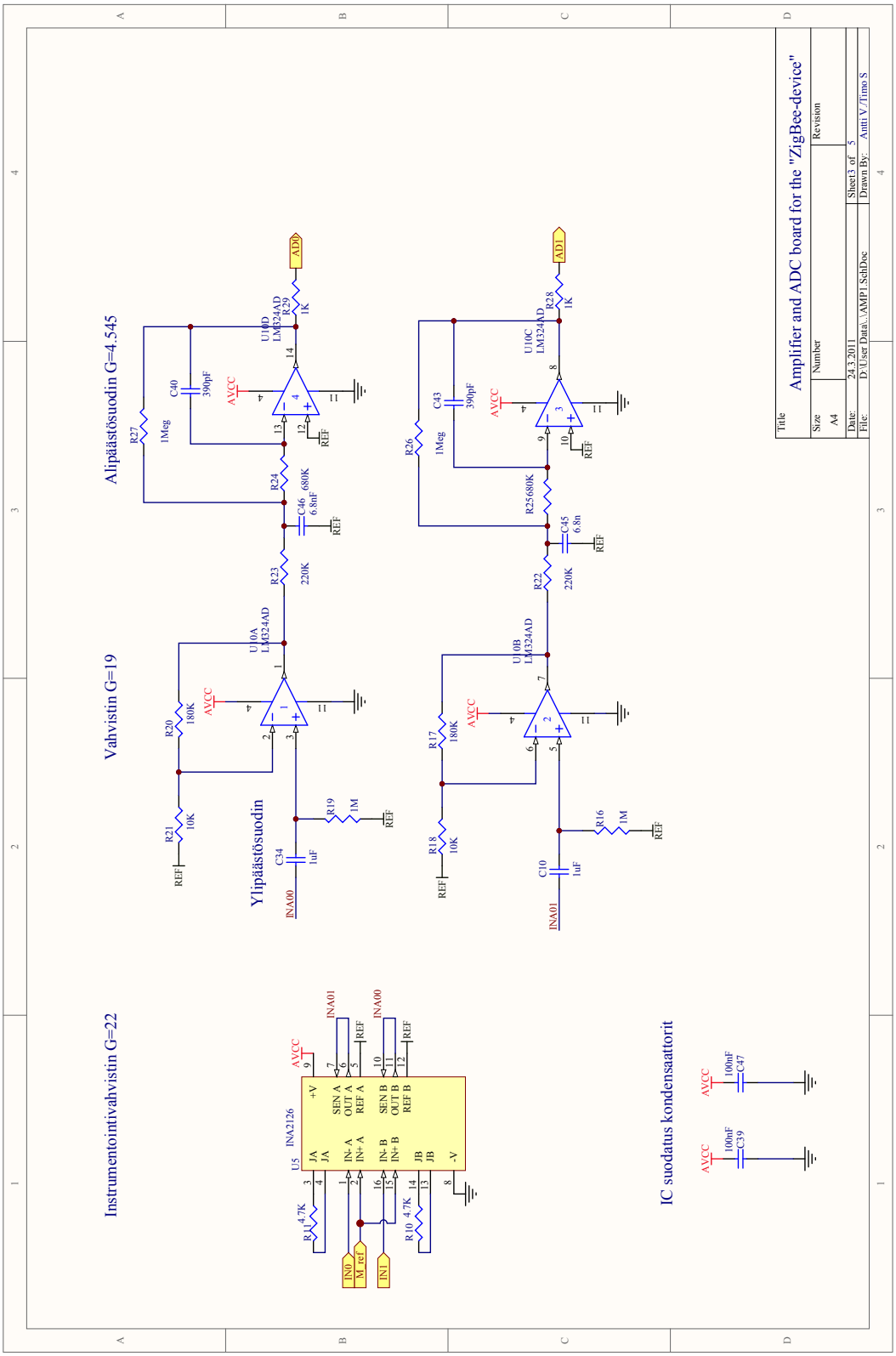
Instrumentointivahvistin G=22
Vahvistin G=19
Alipäästösuodin G=4.545
Ylipäästösuodin
IC suodatus kondensaattorit
Amplifier and ADC board for the "ZigBee-device"
Size A4
Number
Revision
Date: 24.3.2011
File: D:\User Data\..\AMP1.SchDoc
Sheet 3 of 5
Drawn By: Antti V./Timo S
U5 INA2126
U10A LM324AD
U10B LM324AD
U10C LM324AD
U10D LM324AD
AVCC
REF
AD0
AD1
INA00
INA01
IN0
IN1
M_ref
R20 180K
R21 10K
R19 1M
C24 1uF
R23 220K
R24 680K
C46 6.8nF
R27 1Meg
C40 390pF
R29 1K
R17 180K
R18 10K
R16 1M
C10 1uF
R22 220K
R25 680K
C45 6.8n
R26 1Meg
C43 390pF
R28 1K
R11 4.7K
R10 4.7K
100nF C47
100nF C39

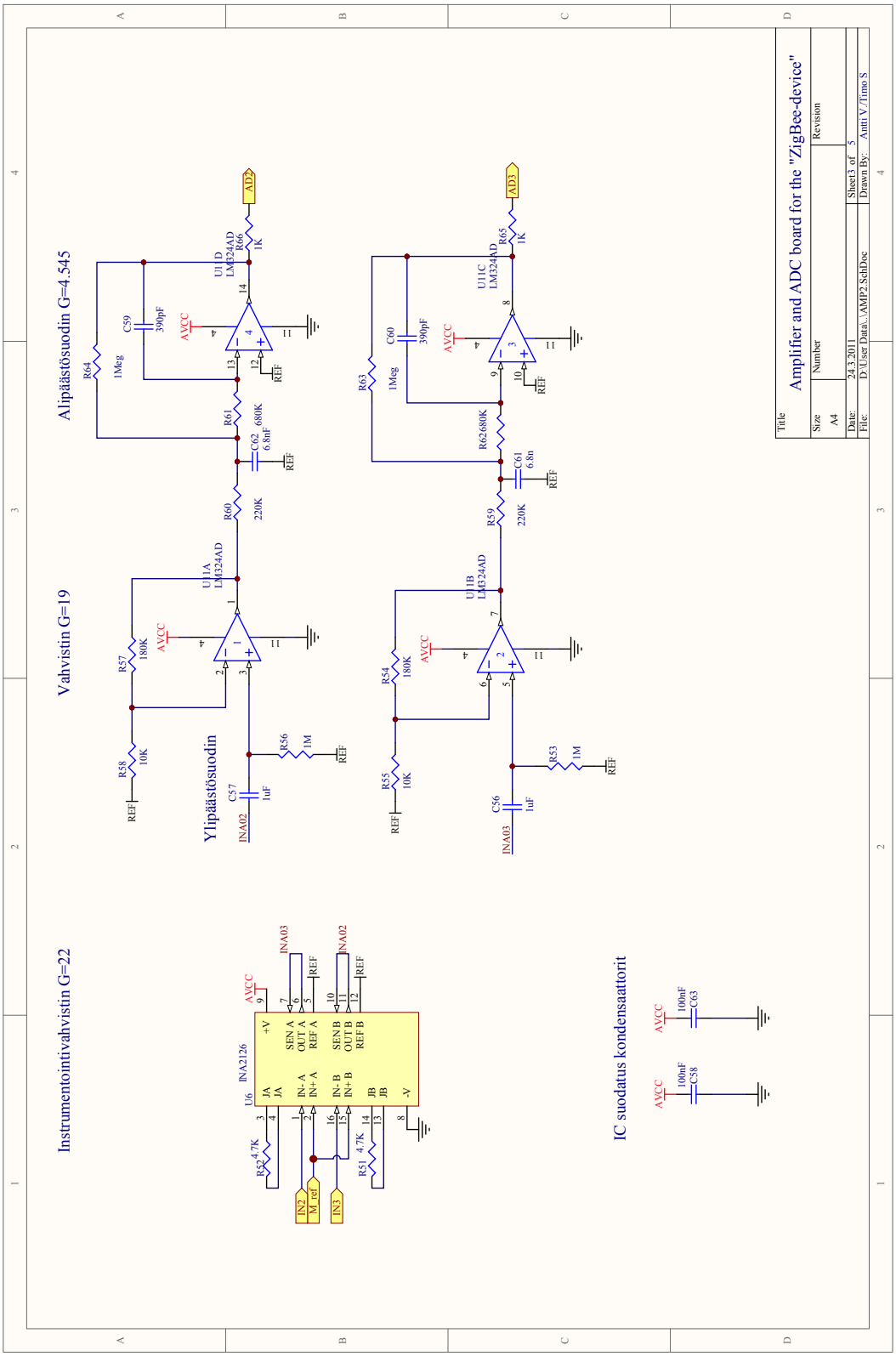
Alipäästösuodin G=4.545
Vahvistin G=19
Ylipäästösuodin
Instrumentointivahvistin G=22
IC suodatus kondensaattorit
Amplifier and ADC board for the "ZigBee-device"
U11A LM324AD
U11B LM324AD
U11C LM324AD
U11D LM324AD
INA2126
AVCC
REF
AD2
AD3
INA02
INA03
IN2
M_ref
IN3
Title
Size A4
Number
Revision
Date: 24.3.2011
File: D:\User Data\...\AMP2.SchDoc
Sheet 3 of 5
Drawn By: Antti V./Timo S

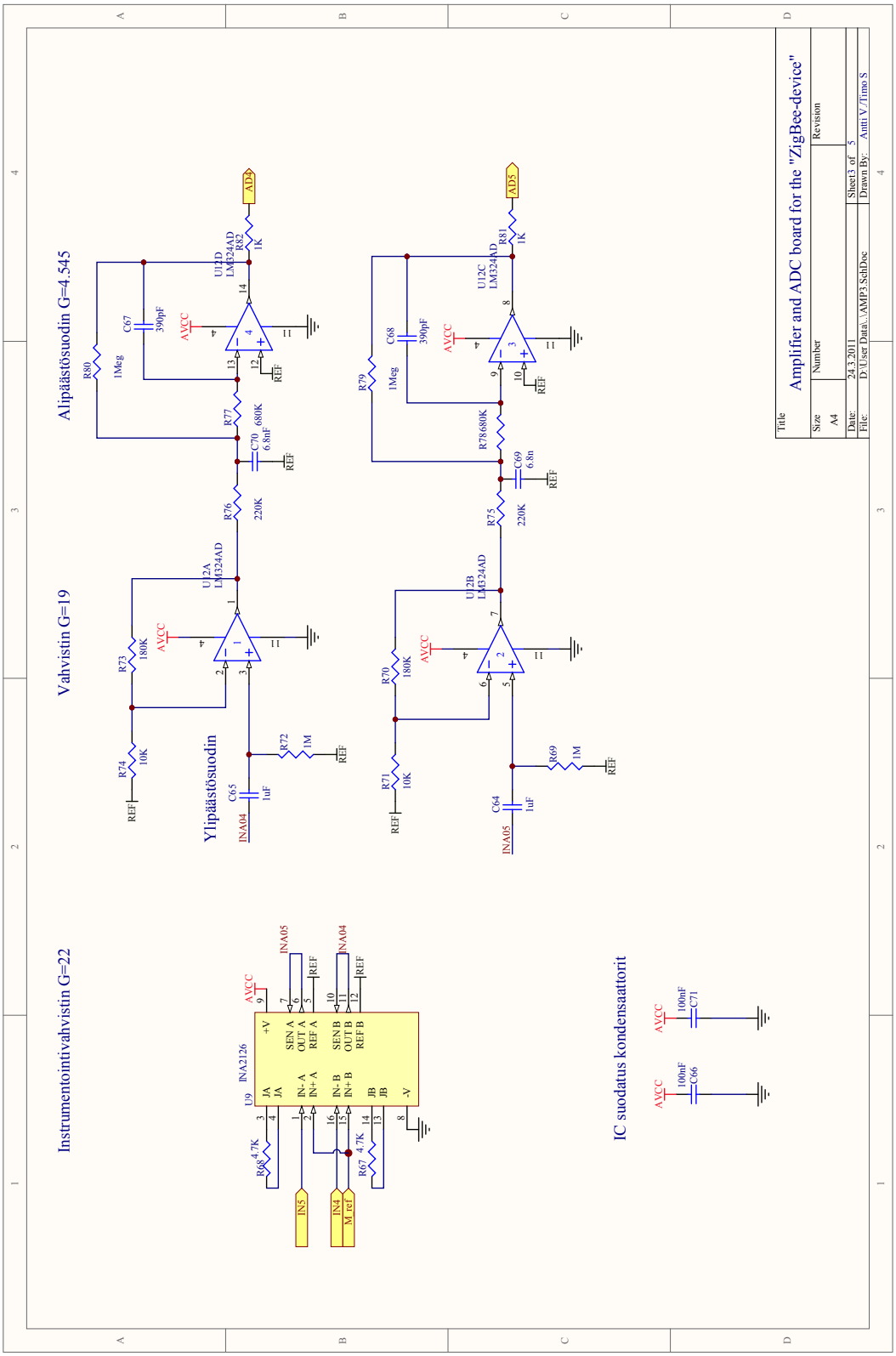
Alipäästösuodin G=4.545
Vahvistin G=19
Ylipäästösuodin
Instrumentointivahvistin G=22
IC suodatus kondensaattorit
Amplifier and ADC board for the "ZigBee-device"
U12D LM324AD
U12C LM324AD
U12A LM324AD
U12B LM324AD
INA2126
AD4
AD5
AVCC
REF
INA04
INA05
IN5
IN4
M_ref
Size A4
Number
Revision
Date: 24.3.2011
Sheet 3 of 5
File: D:\User Data\...\AMP3.SchDoc
Drawn By: Antti V./Timo S

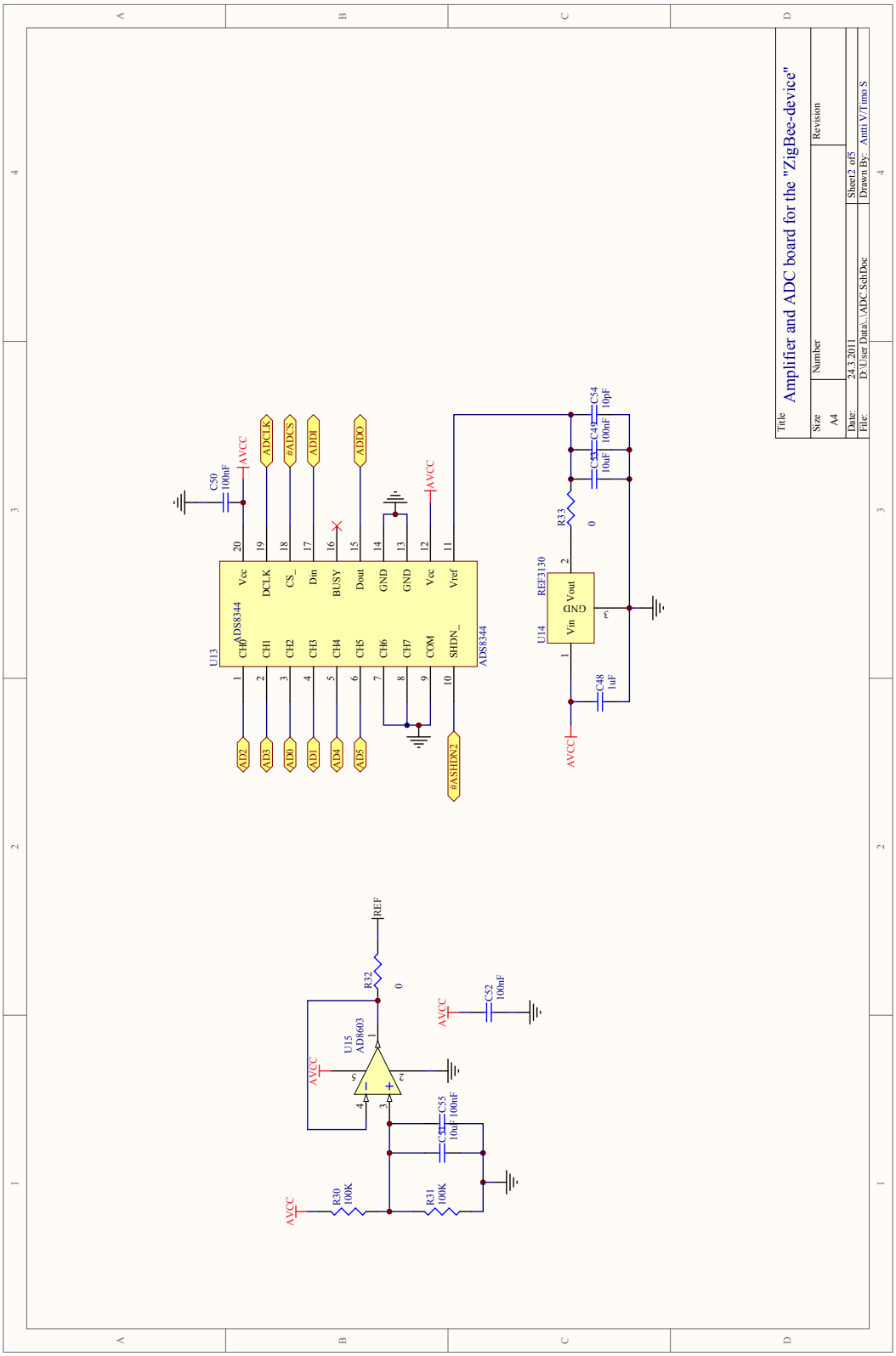
Title
Amplifier and ADC board for the "ZigBee-device"
Size
A4
Number
Revision
Date:
24.3.2011
Sheet2 of5
File:
D:\User Data\...\ADC.SchDoc
Drawn By:
Antti V/Timo S
U13
ADS8344
CH0
CH1
CH2
CH3
CH4
CH5
CH6
CH7
COM
SHDN_
Vcc
DCLK
CS_
Din
BUSY
Dout
GND
GND
Vcc
Vref
C50
100nF
AVCC
ADCLK
#ADCS
ADDI
ADDO
AD2
AD3
AD0
AD1
AD4
AD5
#ASHDN2
U14
REF3130
Vin
Vout
GND
R33
0
C54
10pF
C49
100nF
C53
10uF
C48
1uF
U15
AD8603
R32
REF
C52
100nF
C55
100nF
C51
10uF
R30
100K
R31
100K

B.2 CIU Schematics

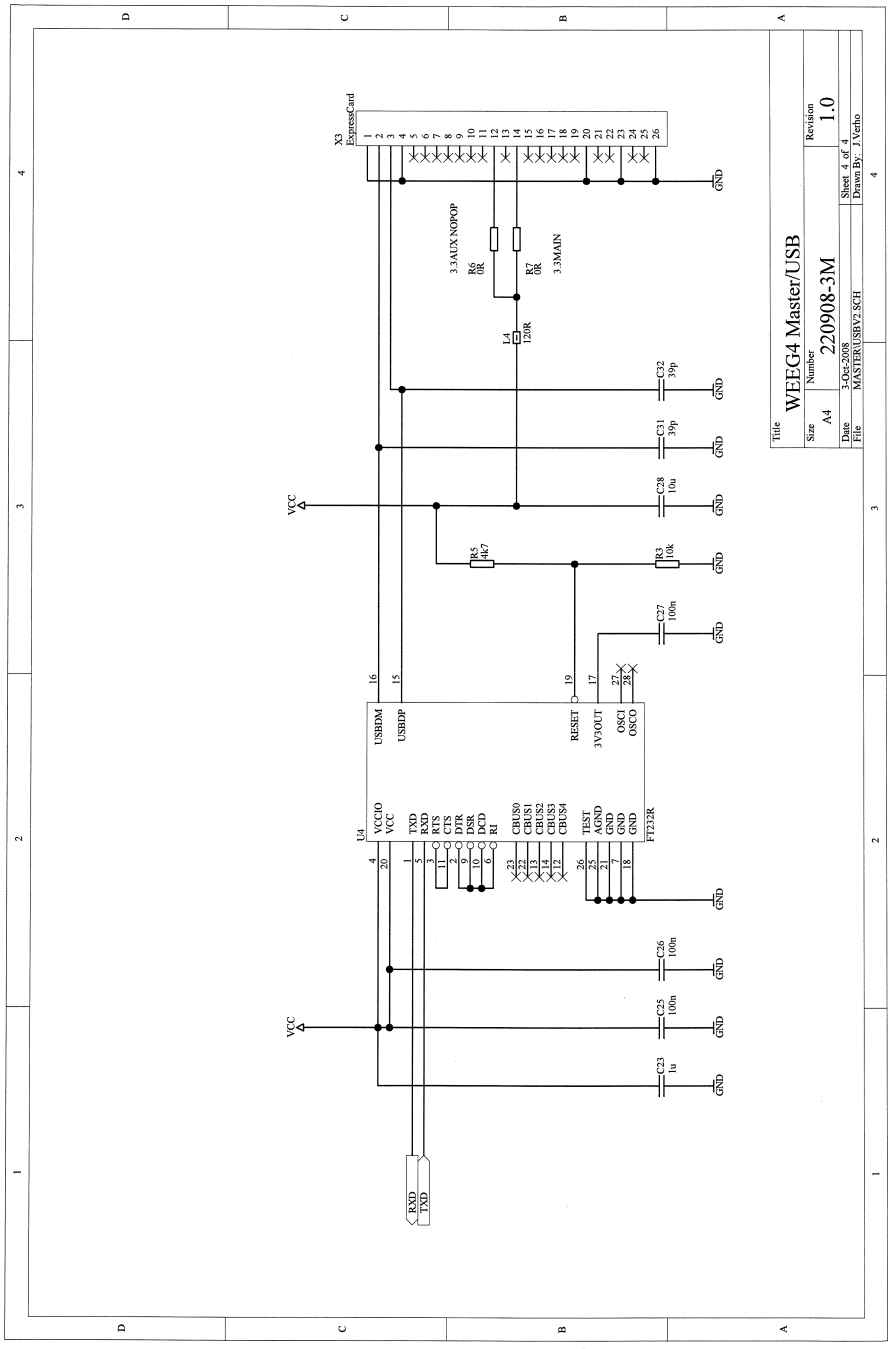

Appendix C

Digital Documents

The enclosed DVD contains the data sheets, the source code, and the schematics of both the 1-channel and 6-channel system.